Airborne and Ground-Based Geophysical Screening of Potential Brine Infiltration Sites, Runnels County, Texas

by

Jeffrey G. Paine, Alan R. Dutton, Martina U. Blüm, Erika M. Boghici,
Ianthe Nelson, Thomas A. Tremblay, and Steven W. Tweedy

Prepared for

The Railroad Commission of Texas
under Interagency Contract No. 96-0034

Bureau of Economic Geology
W. L. Fisher, Director *ad interim*
The University of Texas at Austin
Austin, Texas 78713-8924

1997

QAe7901

CONTENTS

Figures

Tables

EXECUTIVE SUMMARY

Salinization of soil, surface water, and ground water is a chronic environmental and agricultural problem in many parts of Texas. In this study of a 91 km^2 area near Ballinger in Runnels County, Texas, we integrated results from high-resolution airborne and ground-based geophysical surveys, water and soil sampling, and chemical analyses to locate near-surface concentrations of saline water and determine their origin. Possible salinity sources are upward movement of brine along natural conduits (faults, fractures, joints, and permeable stratigraphic units), downward migration from surface brine pits, leaking oil and gas wells, and evaporative concentration of shallow ground water as a result of agricultural practices. A prime goal of the study was to determine the effectiveness of the method in locating leaking wells and distinguishing them from other salinity sources. This project represents a coordinated and cooperative effort between the Railroad Commission of Texas (RRC), the Bureau of Economic Geology (BEG) and its airborne geophysical subcontractor Dighem I-Power, the Lower Colorado River Authority (LCRA), and the Colorado River Municipal Water District (CRMWD).

The geophysical instruments, both airborne and ground-based, measured (a) electrical conductivity increases in the ground that can be caused by high ionic concentrations in saline water, high moisture content, and high clay content, and (b) local perturbations in the earth's magnetic field caused by well casings and other large, ferrous objects. An airborne electromagnetic and magnetometer survey of the Hatchel study area, which encompasses more than 700 oil and gas wells that have been drilled since the 1920s, was flown at 100 m line spacing and 3 m sample spacing by Dighem in January 1996. Flight heights were 30 m for the electromagnetic sensors and 40 m for the magnetometer. During the helicopter flights, ground-truth surface water and ground water samples were collected and later analyzed by LCRA and CRMWD. Airborne results included maps of ground conductivity at three exploration depths, magnetic field maps, and selected conductivity cross sections. The maps, oil and gas well

locations, and soil and geology maps were imported into a geographic information system. The data were analyzed to select sites with an airborne geophysical signature consistent with that of a potential oilfield salinity source: a conductivity anomaly associated with either a known well location, a magnetic anomaly, or both. Airborne maps also guided ground-based geophysical surveys and soil and water sampling.

Combining airborne geophysical signatures with known well locations produced a list of 103 sites that are consistent with oilfield-related salinity sources. At 71 of these sites, an airborne conductivity anomaly coincides with both a magnetic anomaly and a known well location (type CMW sites). This signature implies infiltration of saline water near a known and detected well. At 14 sites, a conductivity anomaly coincides with a known well location but not a magnetic anomaly (type CW sites). These sites are where saline water has infiltrated the ground near a known well that either has no casing or was not detected by the airborne magnetometer. At 15 sites, a conductivity anomaly coincides with a magnetic anomaly but not a known well location (type CM sites). CM sites are those where saline water has infiltrated the ground near a ferrous object such as a tank battery or a mislocated or unknown well. At the remaining three sites, a conductivity anomaly has no associated well or magnetic anomaly (type C sites). This signature might be interpreted as a site where saline water entered the ground as a result of a spill or storage container leak or from an unknown and undetected or uncased well.

From the list of 103 sites, we chose 23 representative sites for on-the-ground geophysical investigations. These investigations included magnetometer surveys by RRC to pinpoint well locations, ground conductivity profiles across each site to establish the relationship between the conductivity anomaly and the well, multiple-frequency electromagnetic surveys to establish the lateral and vertical extent of highly conductive ground, and time-domain electromagnetic (TDEM) soundings to determine the thickness and depth of the salt water plume. TDEM soundings also helped us to understand patterns visible on the deepest sensing airborne conductivity map and to delineate a natural brine-bearing stratigraphic unit beneath the western part of the study area.

The ground-based geophysical surveys revealed that most of the conductivity anomalies detected by the airborne survey are not caused by leaking wells. Of the 23 representative sites (12 CMW, 4 CM, 5 CW, and 2 MW) investigated using ground-based methods, six are interpreted to be leaking wells and another two are possibly leaking. We used the results of the airborne and ground-based surveys to refine a geophysical "profile" of a site that might contain a leaking well: a site that (a) has a magnetic anomaly, or a known well location, or both and (b) has anomalously high ground conductivity on both the shallow-sensing 56,000 Hz airborne coils and the deeper sensing 7,200 Hz coils. Such a site might also have high conductivity measured by the deeply sensing 900 Hz coils. Conductivity anomalies that appear on the 56,000 Hz maps alone commonly are caused by features other than leaking wells. Because some known wells were not detected by the airborne magnetometer and because not all well locations are accurate, conductivity anomalies that have no associated magnetic anomalies should be examined in the field to ensure that there is no evidence of a nearby mislocated or undocumented well.

In the Hatchel study area, 46 of the 103 sites fit the refined airborne profile of a potentially leaking well. Ground-based geophysical surveys at 11 of the 46 profile-matching sites showed that most of these sites do have oilfield-related saltwater infiltration, but are not all leaking wells. For the 11 profile-matching sites investigated, ground-based survey results suggest that five are leaking wells, three are pits or surface spills, and three are sites where a likely source was not identified. The five profile-matching wells that are interpreted to be leaking are either CMW (four) or CW (one) sites. The two surveyed sites that had conductivity and magnetic anomalies but no known well location (a potentially leaking unknown well) proved to be tank or pit sites with no associated leaking well.

Ground-based geophysical surveys complement the airborne data and form a critical component in the understanding of ground conductivity changes in general and in the search for salinity sources in particular. Without the ground-based geophysical surveys, the specific causes of anomalies detected with airborne methods would be difficult to determine reliably. Without the airborne data, ground-based surveys can help determine whether known wells are likely to be

leaking and may find wide usage as a rapid and relatively inexpensive means of testing whether a well is leaking saline water into the shallow subsurface. However, unknown wells and wells not suspected to be leaking would likely be missed and conductivity profiles and soil and water samples would lack a regional ground conductivity context.

In relatively small areas (less than a few tens of square kilometers) where well locations are reliably known, ground-based surveys of prioritized wells constitute an effective technique for determining wells that should be plugged. At this scale, ground-based surveys represent a cost-effective alternative to the high mobilization and minimum survey costs for helicopter-based airborne surveys. Airborne surveys are most effective in typical oilfield-size areas of tens to hundreds of square kilometers where well locations are uncertain, multiple saline water sources are expected, and the extent of brine infiltration is poorly known. In these areas, airborne survey results both guide and improve the efficiency of labor-intensive ground investigations that are required to discern whether the salinity source is a leaking well, a brine pit, or leaking tank battery. Airborne surveys are generally not appropriate beyond the oilfield size because of the additional expense of acquiring tightly spaced flight data over areas that are not likely to have oilfield-related salinization.

INTRODUCTION

Infiltration of saline water into the shallow subsurface through natural geological conduits and oil-field sources can impact wildlife habitat, restrict or eliminate agricultural uses of land, and pollute aquifers and surface water bodies (Dutton and others, 1989; Richter and others, 1990). Agricultural landscaping practices can exacerbate the problem by locally raising water tables and increasing dissolved mineral concentration by evaporation. Public concern about the environmental effects of saline water has led to increasing interest in methods of determining whether oil-field brines have been introduced into the subsurface, where they have migrated, and whether they are the cause of specific problems on the land surface, in water wells, and in surface water bodies.

The purpose of this study was to evaluate the use of airborne and ground-based geophysical methods to (1) locate near-surface concentrations of saline water, and (2) discern the source of the saline water. A reconnaissance airborne electromagnetic and magnetometer survey of a 91 km^2 study area near Ballinger in Runnels County, Texas (fig. 1) was completed to locate areas that had a geophysical signature consistent with that of a well leaking brine. The electromagnetic survey was designed to locate conductive ground associated with the presence of saline water. The magnetometer survey was designed to locate magnetic anomalies caused by well casings. Airborne geophysical signatures that might indicate a leaking well included conductivity anomalies at one or more of the electromagnetic exploration depths and either an associated magnetic anomaly or a known well location.

On-the-ground investigations focused on representative sites identified from the airborne survey. These investigations included detailed geophysical surveys of sites and collection and chemical analysis of soil and water samples. Because ground conductivity is not simply a function of pore fluid chemistry but is also affected by soil type, rock type, and moisture content,

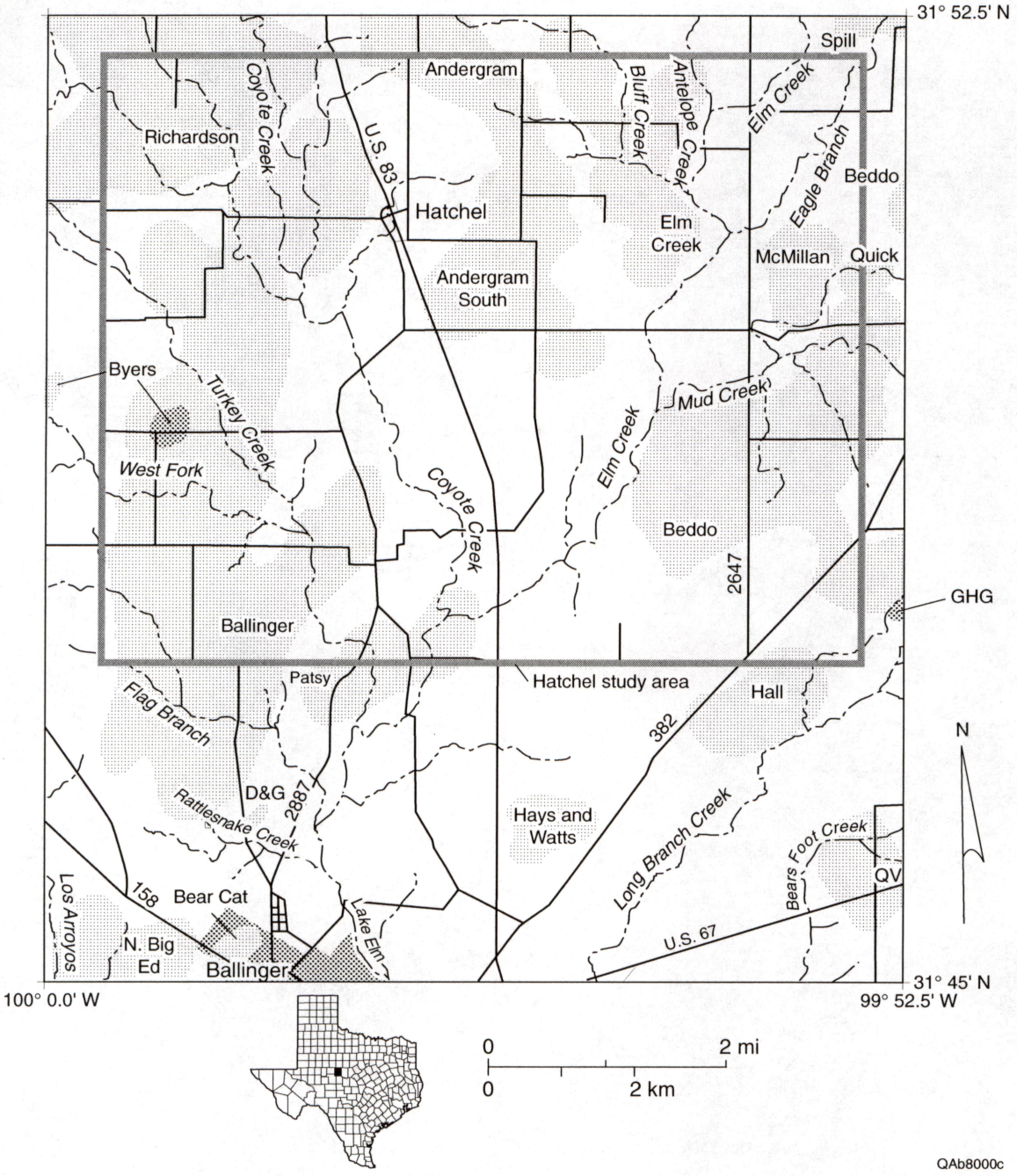

Figure 1. Map of the Hatchel, Texas, quadrangle. The airborne geophysical survey area is within the shaded rectangle. Shaded areas are oil and gas fields adapted from Abilene Geological Society (1992).

these factors were considered for each site as well. Once the data for a given site were analyzed, we interpreted the most likely cause of the ground conductivity anomaly at that site.

Geology and Soils

Rock and soil types can influence ground conductivity, but the effect of the host material on ground conductivity is generally smaller than that caused by ionic concentration in pore fluids. Soil and rock units that are high in clay content are generally more conductive than sandy units (McNeill, 1980a; Rhoades, 1981). Geologic units (Kier and others, 1976) within the exploration depth range of the geophysical equipment used in this study include (a) Quaternary alluvium (Qal, fig. 2 and table 1) that is generally sandy, has relatively high water content, and is found in topographic lows along streams, (b) thin Pleistocene surficial terrace deposits (Qu) that are composed of clay to gravel, are relatively dry, and are mapped at higher elevations along the central part of the study area, and (c) outcrop areas of Permian Clear Fork Group strata (Pcf) and the Lueders Formation (Pl) containing units of sandstone, limestone, shale, and marl. Permian stratigraphic units dip west-northwestward into the Permian basin.

The Coleman Junction Formation, a limestone and shale formation of the Permian Wichita-Albany Group (Kier and others, 1976), does not crop out in the study area. It is an artesian brine-bearing unit at depths of 200 to 300 m that is often cited as a principal source of near-surface brine in the study area (Richter and others, 1990).

Soils formed on these geologic units (fig. 3) can affect measured ground conductivities for the higher frequency, shallower penetrating conductivity instruments. Soils have been mapped in greater detail than have the geologic units for the study area (Wiedenfeld and others, 1970). On the lowlands, deep, loamy, relatively wet soils of the Spur-Colorado-Miles association are formed on Quaternary alluvium (figs. 2 and 3). These soils generally contain less clay than the residual upland soils, but may have higher ground conductivities because they are thicker, wetter, and in many places contain relatively conductive pore water. Soils on the uplands are generally the shallow, clayey to loamy, and relatively dry residual soils of the Portales-Potter-Mereta

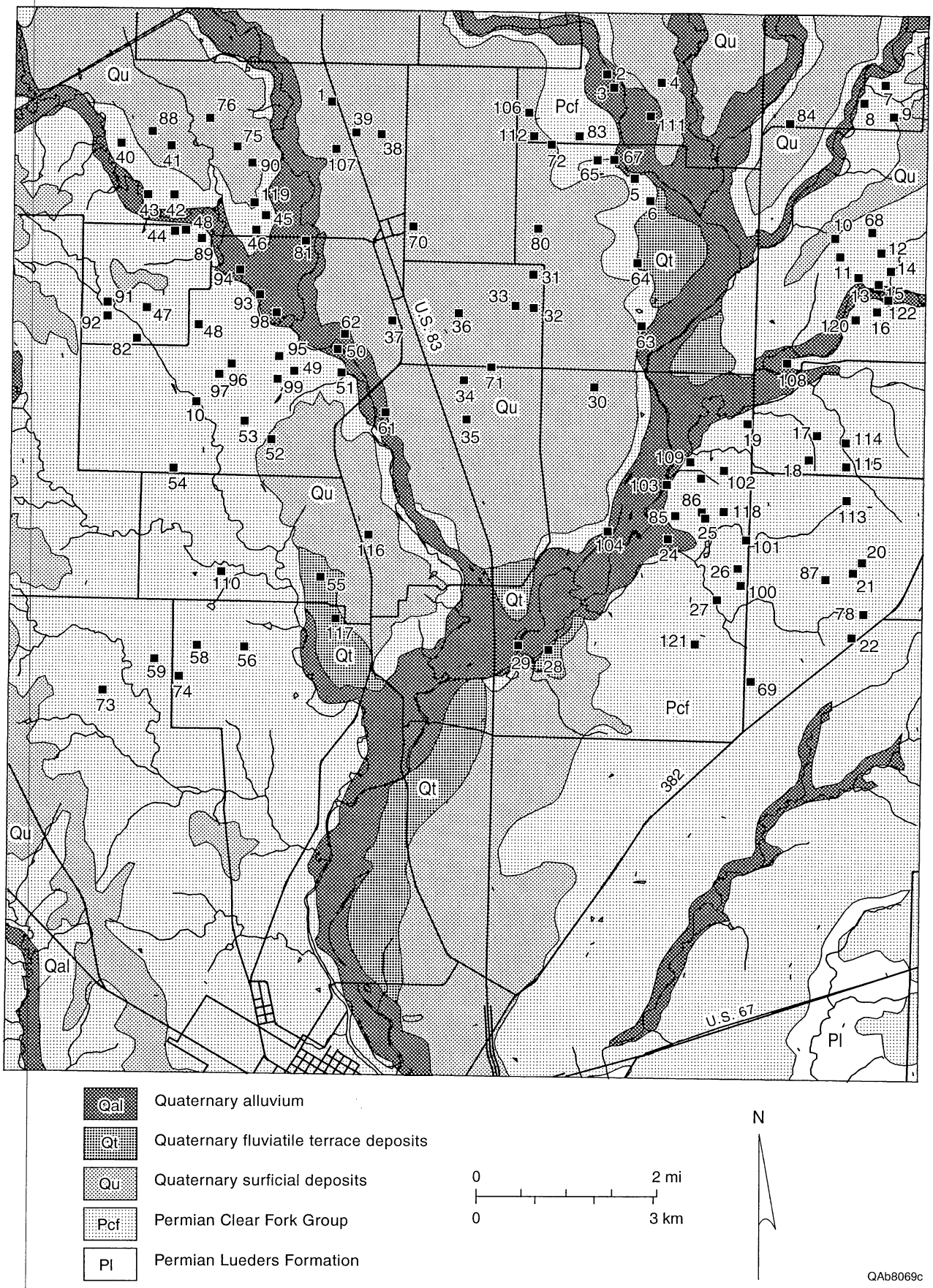

Figure 2. Generalized geologic map of the Hatchel quadrangle (adapted from Kier and others, 1976).

Table 1. Generalized stratigraphic chart for the Colorado River watershed. Modified from Brown and others (1972), American Association of Petroleum Geologists (1973), Eifler (1975), Lee (1986), and Richter and others (1990).

SYSTEM	SERIES	GROUP	FORMATION	LITHOLOGY
QUATERNARY	HOLOCENE			alluvium
	PLEISTOCENE		Leona	caliche and gravel
TERTIARY	PLIOCENE		Ogallala	gravel, sand, and caliche
	MIOCENE			
CRETACEOUS	COMANCHEAN	Washita	Buda	argillaceous limestone
		Fredericksburg	Edwards	limestone and dolomite
			Comanche Peak	limestone
			Walnut	limestone and clay
		Trinity	Antlers	sandstone and shale
TRIASSIC	UPPER	Dockum		sandstone and shale
PERMIAN	OCHOAN	Quartermaster		sandstone and gypsiferous shale
		Whitehorse		
	GUADALUPIAN	Pease River	San Andres (Blaine)	sandstone
			San Angelo	sandstone, gypsum, and dolomite
	LEONARDIAN	Clear Fork	Choza	sandstone and dolomitic limestone
			Vale	
			Arroyo	shale and marly limestone
		Wichita-Albany	Lueders	limestone and dolomite
			Talpa	limestone and shale
			Grape Creek	
			Bead Mountain	
			Jagger Bend-Valera	
			Elm Creek	
	WOLFCAMPIAN		Admiral	
			Coleman Junction	
PENNSYLVANIAN	VIRGILIAN	Cisco		limestone and shale
	MISSOURIAN	Canyon		
	DESMOINESIAN	Strawn		
	ATOKAN	Bend		sandstone, shale, and limestone
	MORROWAN			
ORDOVICIAN	CANADIAN	Ellenburger		dolomite
PRECAMBRIAN				granite and gneiss

QA 11656c

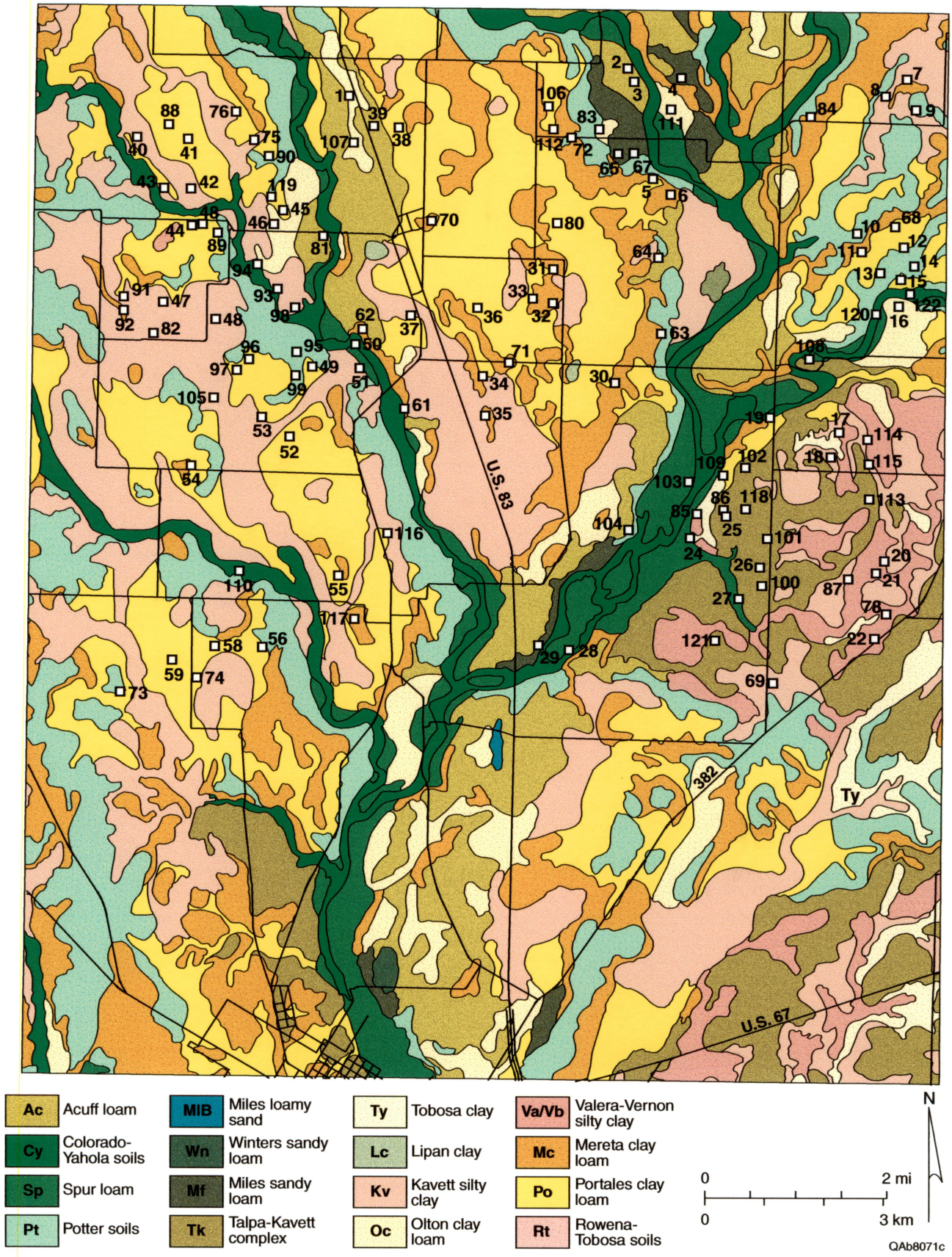

Figure 3. Soils map of the Hatchel quadrangle (adapted from Wiedenfeld and others, 1970). Numbered locations represent preliminary list of anomalous sites and other ground-based geophysical survey locations.

association that form on the Pleistocene terrace deposits and Permian Clear Fork Group strata (figs. 2 and 3). Despite their relatively high clay content, these soils have low measured conductivities due to their thinness and low moisture content.

Hydrogeologic Setting

The study area is located at the eastern side of the Southern Great Plains physiographic province, which slopes gently southeastward from eastern New Mexico to Central Texas, and at the southern end of the Rolling Plains. The informally named Southern Great Plains regional ground-water flow system includes diverse hydrostratigraphic units in Ordovician to Neogene rocks (Jorgensen and others, 1988). Physiographic features of the study area include gently rolling, dissected uplands and valleys formed by the southward-draining Elm and Coyote Creeks and their tributaries.

The Upper Permian rocks that contain fresh ground water at shallow depths beneath the study area contain brine and hydrocarbons only tens of kilometers to the west in the subsurface (McNeal, 1965; Core Laboratories, 1972). Oil and gas fields in the region occur at depths as shallow as 300 m in Permian formations to greater than 1,800 m in Pennsylvanian and Ordovician rocks (table 1). Brine is prevalent throughout the Paleozoic section except within 60 to 1,300 m of ground surface where it is displaced by locally recharged meteoric water. For example, salinity of subsurface water in the Guadalupian Series, which overlies the Clear Fork Group (table 1), varies from 50,000 mg/L just west of the outcrop to more than 200,000 mg/L westward in the Permian Basin (fig. 4).

Regional and local topographic relief have large effects on ground-water flow paths (Tóth, 1962). Potentiometric surfaces in the Southern Great Plains regional flow system (Jorgensen and others, 1988) are inclined toward the east, indicating the potential for eastward flow of subsurface brine in Paleozoic rocks toward formation outcrops in the study area (fig. 5). Eastward fluid flow probably influenced migration of hydrocarbons into reservoirs across the Eastern Shelf of the Permian Basin. Richter and Kreitler (1986) showed that brine at shallow

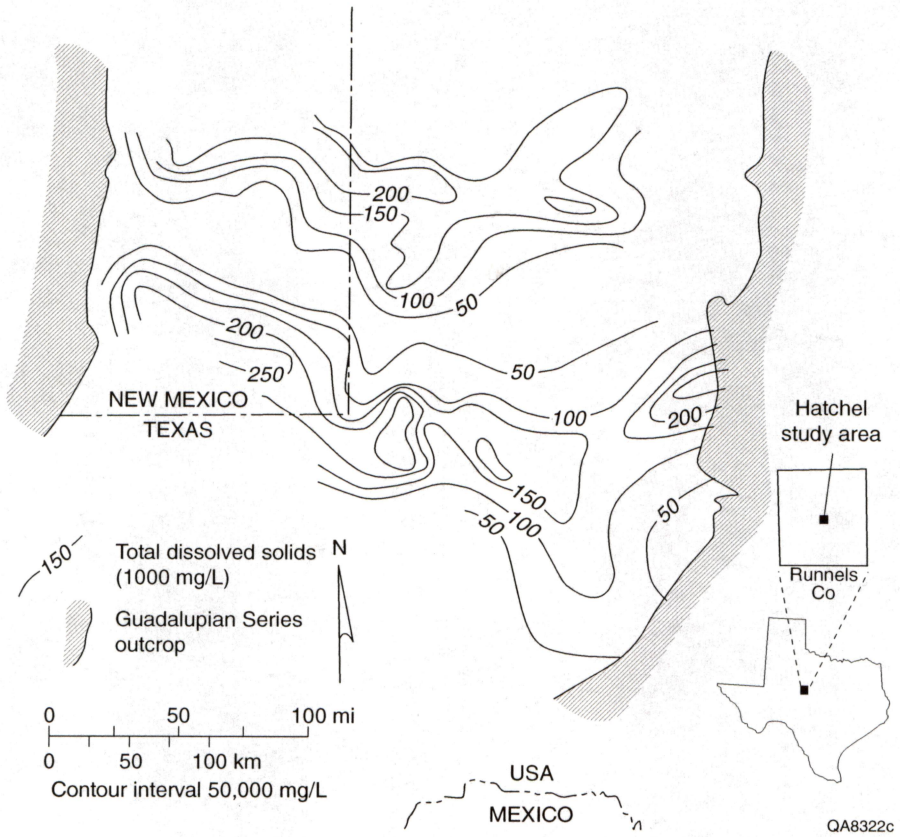

Figure 4. Total dissolved solids in brine from Guadalupian Series oil fields. Modified from McNeal (1965).

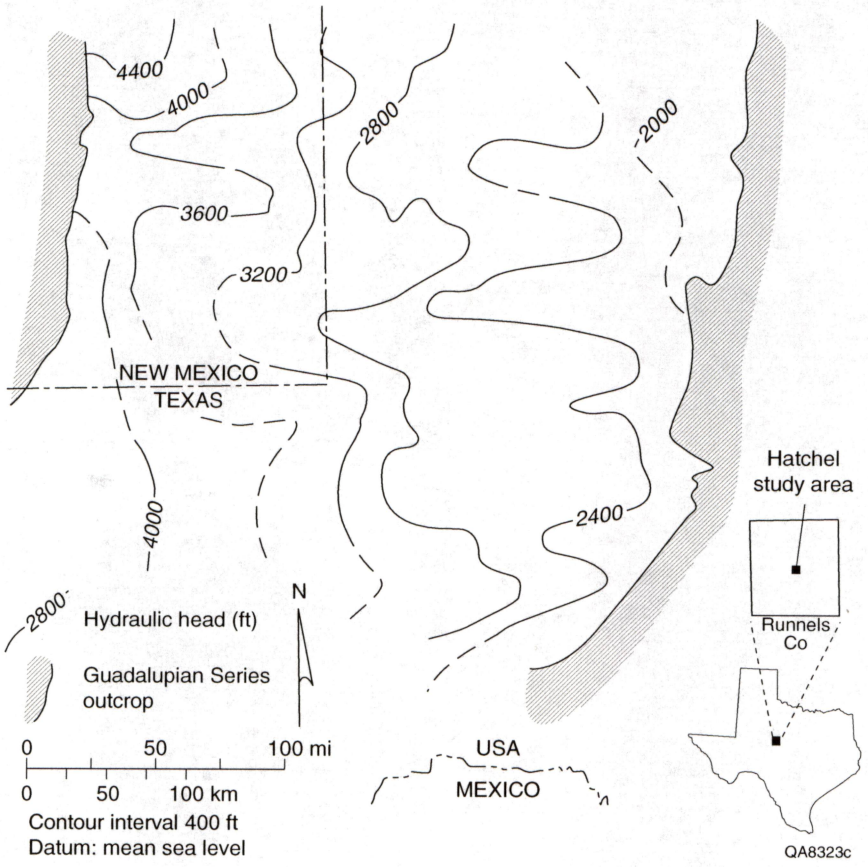

Figure 5. Potentiometric surface of brine in Guadalupian Series based on equivalent fresh-water hydraulic head. Modified from McNeal (1965).

(about 30 m) depths in the southern part of the Rolling Plains northwest of the study area is derived from deep parts of the regional flow system. Bein and Dutton (1993) mapped connate and meteoric water throughout the stratigraphic section across the Southern Great Plains and showed the eastward movement of saline waters into the Rolling Plains. Comparison of potentiometric surfaces of hydrostratigraphic units in Paleozoic rocks mapped by McNeal (1965) indicates that there is potential for upward movement of subsurface brine across confining layers if pathways such as fractures and unplugged boreholes exist. Potentiometric surfaces of subsurface brines beneath the valleys in the study area most likely are generally are close to, and in some Wolfcampian formations (for example, Coleman Junction) higher than ground surface.

Potentiometric surfaces of shallow ground water in different aquifer units most likely are inclined toward Elm and Coyote Creeks and their tributaries, reflecting topographic influence on recharge and discharge locations in the local ground-water flow system (Tóth, 1962). The upland areas probably are local recharge zones and ground-water discharge from local and regional flow systems most likely is focused in the valleys of Elm and Coyote Creeks.

Sources of Salinity

Salinization of soil and ground-water resources is a common problem in the central and southwestern United States (Dutton and others, 1989; Richter and others, 1990). Major potential causes of soil and water salinization in the study area include (1) natural discharge of subsurface brines through permeable units, fractures, or joints; (2) infiltration of produced brine beneath surface pits; (3) upward movement of brine across confining beds through oil and gas wells and deep, unplugged water wells; and (4) evaporative concentration of ground water from shallow water tables that have risen in response to agricultural landscaping and consequent increased ground-water recharge (fig. 6).

Oil and gas wells provide potential paths for brine to move to the near-surface environment. If brine is associated with the produced oil or gas, brine moves to the surface along with the hydrocarbons. Before 1969, when the no-pit order went into effect in Texas, produced brine was

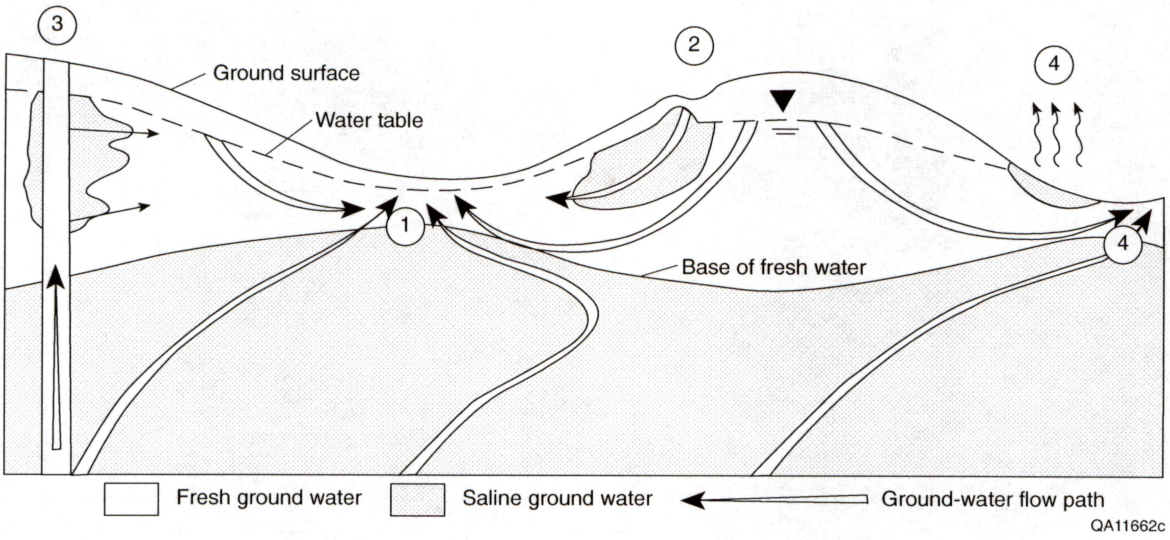

Figure 6. Conceptual model of salinity sources in the Hatchel area. Potential sources are: (1) natural discharge of brine through permeable stratigraphic units, fractures and joints, (2) infiltration of saline water beneath brine disposal pits, (3) upward flow of brine through inadequately plugged and leaky boreholes, and (4) evaporative concentration of shallow ground water (adapted from Richter and others, 1991).

often pumped into surface pits and left to evaporate or infiltrate the ground near the pit. Brine within non-producing geologic units such as the Coleman Junction Formation can also reach the near-surface environment through deep water wells and improperly plugged oil and gas wells that reach deeper targets.

Although increased salinity from any of the natural, oil-field related, and agriculture-related sources could cause similar increases in ground conductivity, each source may have a unique geophysical or chemical signature that would allow the sources to be distinguished. For example, ground conductivity that decreases with depth may indicate a surface salinity source such as a brine pit or evaporative concentration. Conductivities that increase downward may indicate deep salinity sources such as a leaking well or natural flow path. Areal conductivity patterns and magnetic data from airborne surveys may help further distinguish leaking wells (point sources with magnetic anomalies) from natural conduits (curvilinear features without magnetic anomalies).

Oil and Gas Activity

There are 18 named oil and gas fields that cover a substantial part of the Hatchel quadrangle (fig. 7). RRC records indicate that there are at least 963 wells in the quadrangle (718 in the study area) and that most of the drilling and production occurred before the no-pit order. The following summary was prepared from several sources, including Abilene Geological Society (1992), Fitzgerald (1952), and Gardner and Phifer (1953).

The McMillan Field, located in the northeast part of the Hatchel quadrangle (fig. 7), was discovered in August 1927 and was the first major oil discovery in the Hatchel area. Early production was from the Pennsylvanian Cisco Group. A less productive pay in the Canyon Group was discovered in 1942. The field was abandoned in the early 1940s.

Beddo Field (fig. 7), discovered in May 1928, was originally a gas field. A decade after the discovery of the field, oil was found in the Canyon and was produced from the Cisco in

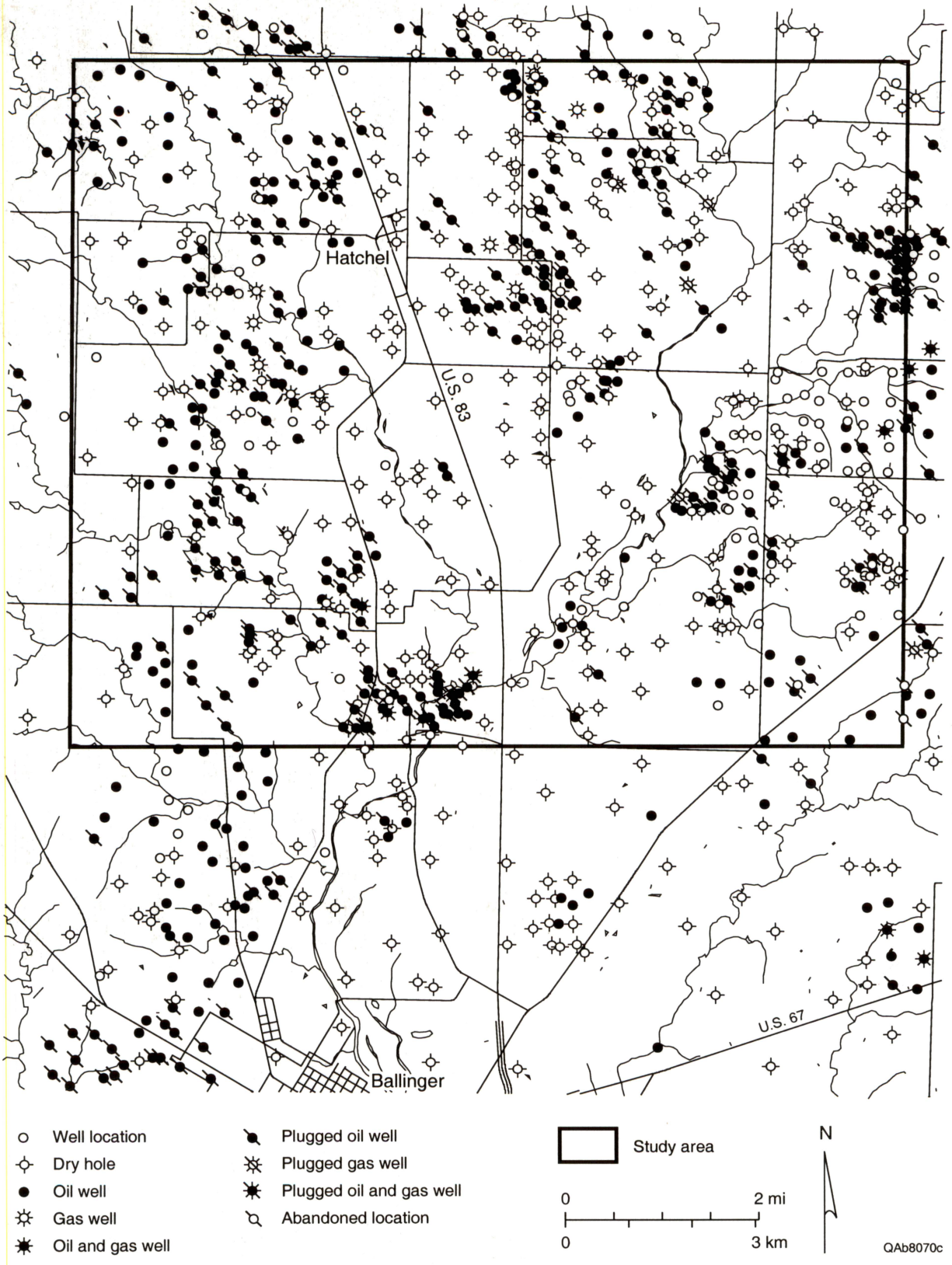

Figure 7. Oil and gas well locations in the Hatchel quadrangle. Well locations from Railroad Commission of Texas. Field locations shown on fig. 1.

subsequent years. Wells were also drilled in the late 1940s and produced from the Pennsylvanian Canyon and Strawn Groups. Eight small fields comprise the Beddo Field as it is known today.

The first well in Ballinger Field, located in the western part of the study area (fig. 7), was drilled in 1947 and completed in the Canyon Group. The Cisco and Canyon Groups were both produced in the Ballinger Field in the early 1950s. Production from the Strawn Group began in the mid-1950s. Current production in the Ballinger Field is from Canyon limestones and Strawn sandstones and conglomerates.

Elm Creek Field, located northeast of Hatchel (fig. 7), was discovered in 1950 and produced oil from Strawn Group sandstones. Additional producing intervals in Canyon limestones and Cisco sandstones and conglomerates were discovered in the 1950s and 1960s. Some wells in this field continue to produce oil from the Strawn and Canyon Groups.

The Patsy Field (fig. 7) was discovered in 1951. Oil production was from two zones within the Cisco Group, neither of which is currently producing. The Hays and Watts Field, discovered in 1951 in the southern part of the Hatchel quadrangle, was surrounded by failed exploration attempts. There the Cisco Group produced oil from a total of five wells, none of which are active today.

Oil was first produced from the Spill Field (fig. 7) in 1952. Production from a Canyon Group limestone was small, but it encouraged further drilling in the northeast part of the quadrangle. In 1958, a more productive limestone was discovered in the Canyon and two productive zones were soon discovered within the Strawn Group. Only the Strawn produces today.

Hall Field, located south of the larger Beddo Field (fig. 7), was discovered in 1953. It produced modest volumes of oil and some gas from Strawn Group clastic deposits. Of the six known wells drilled in this field, none are active today. The D. Richardson or Ballinger Northwest Field, discovered in 1957, covers the northwestern part of the Hatchel quadrangle and extends farther northward. There has been oil and gas production from Canyon and Strawn limestones and the field is presently active.

In late 1957, the Byers Field was discovered along the western boundary of the study area. Large volumes of gas and lesser amounts of oil were produced from the Strawn Group. In early 1958, additional oil was produced from the Canyon Group. The Strawn continues to produce, whereas the Canyon wells have ceased production.

Andergram Field, a large and productive oil and gas field located in the north central part of the Hatchel quadrangle (fig. 7), began production from three Strawn horizons and one Canyon horizon in 1958. In 1962, drillers discovered additional oil in the Cisco Group. The most recent Andergram discovery was in the Strawn in 1984. This zone still produces today, as does the Canyon. The Andergram Field was extended southward in 1959 (Andergram South) with further discoveries in the Cisco and Canyon Groups. The Canyon zone in Andergram South still produces oil and gas.

D & G Field, a small field located south of the Ballinger Field, was discovered in 1963. One well produced from the Canyon Group and was abandoned after producing 13,000 barrels of oil.

The first discovery in the Hatchel area during the 1980s oil boom was the QV Field in the southeast corner of the quadrangle (fig. 7). Five wells produced from the Strawn Group; these wells remain active today. In 1982, the QV field was extended with further production from the Strawn Group. The three wells producing from this zone also remain active.

Bear Cat Field is a small field that was discovered in 1981 near the southern boundary of the Hatchel quadrangle (fig. 7). It currently produces oil and gas from the Strawn Group. The North Big Ed Field, discovered in 1982, is more productive than the adjacent Bear Cat Field. Its seventeen wells still produce today.

The Quick oil and gas field, discovered in 1984, lies just north of the Beddo Field on the eastern edge of the study area (fig. 7). Its two active wells produce from a Strawn Group limestone. The GHG Field, located just south of the Beddo Field, was discovered in 1985 and currently produces from a Canyon Group limestone.

METHODS

Geophysical Methods

Electromagnetic induction methods (Parasnis, 1973; Frischknecht and others, 1991; West and Macnae, 1991) were used to measure apparent ground conductivity using airborne and ground-based instruments. Electromagnetic induction methods employ a changing primary magnetic field created around a transmitter coil to induce a current to flow in the ground, which in turn creates a secondary magnetic field that is sensed by the receiver coil. In general, the strength of the secondary field is proportional to the conductivity of the ground. An inherent assumption is that the near-surface environment consists of horizontal layers of infinite lateral extent; this is not strictly true in the Hatchel area, but the near-surface layers probably do have sufficient lateral extent to render this assumption valid at the scale of investigation.

Airborne Survey

Dighem surveyed the Hatchel study area with helicopter-based geophysical instruments between January 14 and 17, 1996 (Garrie, 1996). Principal instruments mounted in the Lama 315 helicopter were the multicoil, multifrequency DIGHEM^V electromagnetic induction system that is used to measure ground conductivity and a Scintrex Cesium vapor magnetometer for measuring magnetic field strength. The electromagnetic coils and the magnetometer were towed beneath the helicopter (fig. 8) at nominal heights of 30 m for the coils and 40 m for the magnetometer. The helicopter maintained a height of 60 m and flew at an average speed of 108 km/hr (Garrie, 1996). Supporting instruments included a differential GPS navigation system with locational accuracy to 5 m, a radar altimeter, and a video camera that recorded the ground along the flight lines.

Flight lines were oriented east-west, were spaced at 100 m intervals, and covered a total length 940 km within the 91 km^2 study area (fig. 1). Samples from the electromagnetic coils and

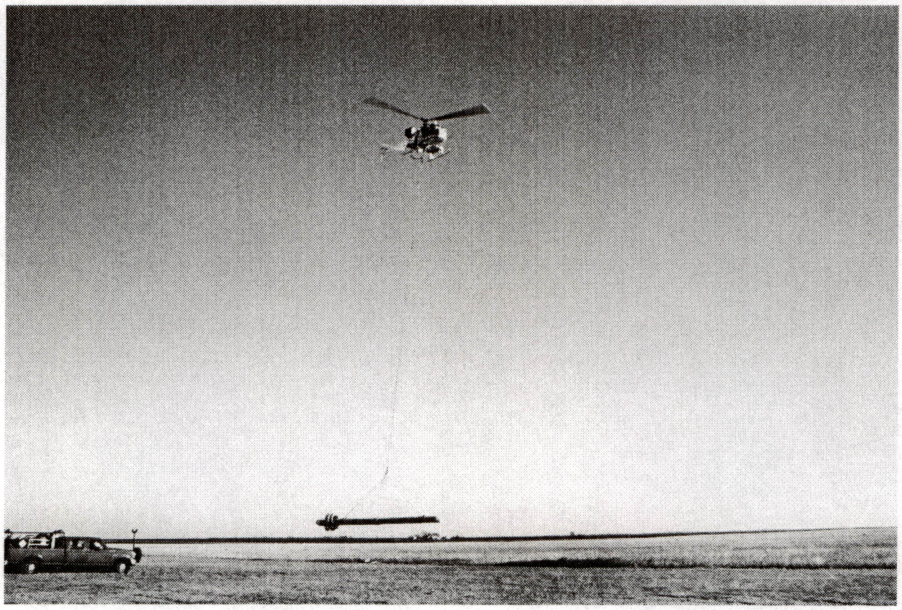

Figure 8. Lama 315 helicopter lifting Dighem magnetometer (upper bird) and electromagnetic induction coils (lower bird) in preparation for airborne geophysical survey.

the magnetometer were acquired at 0.1 s intervals, which corresponds to a sample spacing of about 3 m along each flight line. Lateral resolution was thus better by a factor of 33 in the east-west direction than in the north-south direction.

Raw electromagnetic and magnetometer data were recorded digitally and processed by Dighem I-Power in the months following the airborne survey (Garrie, 1996). Preliminary conductivity maps were supplied to BEG to enable us to select priority field sites and begin field investigations. Final products delivered by Dighem included maps of ground conductivity at three coil frequencies, maps of total and enhanced magnetic field strength, cross sections showing lateral and vertical conductivity changes along two east-west flight lines, a flight line track map and videotapes, and digital map images that were imported into a geographic information system database.

Ground-Based Surveys

Priority sites selected on the basis of their airborne geophysical signature were investigated by BEG staff using ground-based electromagnetic induction instruments. Frequency-domain electromagnetic techniques were used in a reconnaissance mode to screen sites for evidence of near-surface saline water and in multifrequency mode to more quantitatively delineate lateral and vertical extents of saline water plumes. Time-domain electromagnetic soundings were used to measure the thickness of the plumes and understand changes in ground conductivity deeper than depths reached by the airborne and ground-based, frequency-domain methods. RRC staff used a portable magnetometer to locate buried well casings and guide conductivity survey placement at the priority sites (fig. 9).

Reconnaissance Conductivity Profiling

Reconnaissance ground-conductivity surveys were completed at 23 sites in the Hatchel area to locate highly conductive ground that may be sites of brine leakage into the shallow subsurface.

Figure 9. Texas Railroad Commission employee using a portable magnetometer to look for an abandoned well.

In these surveys, a Geonics EM34-3 ground conductivity meter (fig. 10) was used to measure apparent conductivity (McNeill, 1980b). The EM34-3 supports a 10-, 20-, or 40-m transmitter and receiver coil separations (fig. 11) and two principal coil orientations (horizontal dipole and vertical dipole). A 20-m coil separation was used for reconnaissance surveys. This configuration has an exploration depth of 12 m for the horizontal dipole orientation and 25 m for the vertical dipole orientation. The conductivity values represent "bulk" conductivities, or an average conductivity of the sensed soil volume beneath the transmitter and receiver coils.

Conductivity measurements were taken as follows: (1) the transmitter coil was placed on the ground in the horizontal dipole orientation in an area of background conductivity levels at a chosen site; (2) the receiver coil was placed on the ground 20 m from the transmitter coil; (3) apparent conductivity was logged on a digital data logger; (4) both coils were realigned in the vertical dipole orientation at the same locations and coil separation; (5) apparent conductivity for the vertical dipole orientation was digitally logged; and (6) the transmitter and receiver coils were each moved forward 10 m. The entire process was repeated until the highly conductive area was crossed and background conductivity values were once again attained.

Multiple Frequency Profiling

Multiple frequency profiling, one of two ground-based techniques used to determine conductivity variations with depth during our field investigation, was completed at two sites using the Geonics EM34-3. Simple conductivity cross sections were constructed along the surveyed lines at each site by analyzing apparent conductivity data collected at multiple coil frequencies and configurations.

The effective penetration depth of the field generated by the EM34-3 increases with coil separation (and decreases with frequency) for a given coil orientation (fig. 11). Consequently, conductivities measured at different coil separations and orientations can be used to infer conductivity changes with depth beneath a site (McNeill, 1980b,c) if lateral conductivity variations are small.

Figure 10. BEG staff using Geonics EM34-3 ground conductivity meter to perform reconnaissance electromagnetic survey across abandoned Gardner #1 well at site 33. Transmitter coil is pictured.

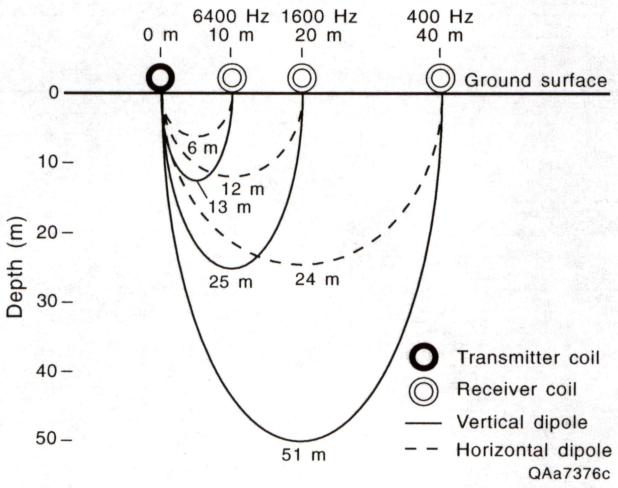

Figure 11. Effective penetration depth of various coil separations and coil orientations of the Geonics EM34-3.

At each of the two sites, apparent conductivities (in mS/m) were collected first at 10-m coil separation; these stations were used to determine the 10-m intervals between stations for the longer coil separations. After a line was completed using the 10-m coil separation, the 20-m coil separation was selected, the instrument was recalibrated, and horizontal and vertical dipole data were collected along the same line at the same 10-m station spacing. Finally, the 40-m separation was selected, the instrument was recalibrated, and apparent conductivities for both dipole orientations were measured at 10-m station spacings along the same line used for shorter coil separations.

EMIX34 Plus, a computer program published by Interpex, was used to process the data and produce simple models of lateral and vertical conductivity changes along each line. Horizontal and vertical dipole conductivities for each coil separation were entered in the program, a starting conductivity model (consisting of layer thicknesses and conductivities) was entered that qualitatively fit the observed data, and then the computer displayed both the observed conductivities and conductivities calculated from the chosen model. The model was then adjusted by the user to better fit the observed data. After reasonable agreement was obtained, the program adjusted layer thicknesses and conductivities to obtain the best fit. The program then performed equivalence analysis to determine the range of model thicknesses and conductivities that produced a nearly equivalent fit to the observed data.

Time-Domain Electromagnetic (TDEM) Soundings

In addition to the multiple-coil-separation soundings, time-domain, or transient, electromagnetic (TDEM) soundings (Kaufman and Keller, 1983; Spies and Frischknecht, 1991) were acquired with the Geonics PROTEM 47/S (fig. 12). These soundings gave a more detailed conductivity profile at several sites to a maximum depth of 75 to 100 m. Instead of using different frequencies and coil separations to vary exploration depth, the time-domain device measures the decay of a secondary electromagnetic field produced by the termination of an alternating primary electromagnetic field (fig. 13). The secondary field strength is measured by

Figure 12. Layout of Protem 47/S electromagnetic sounding instrument near abandoned Vancil #1 well at site 76.

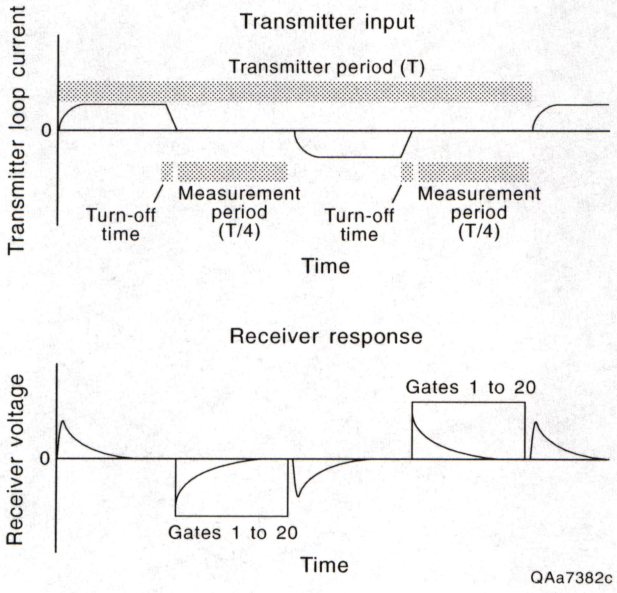

Figure 13. Protem 47/S transmitter input and receiver response. Adapted from Geonics Limited (1992).

the receiving coil at 20 moments in time (or "gates") following transmitter current termination. Secondary field strength at early times gives information about conductivity in the shallow subsurface; field strength at later times is related to conductivity at depth. The computer program TEMIX, by Interpex, was used to construct model conductivity profiles that best fit the observed transient decay for each site.

Thirteen TDEM soundings were conducted at 9 sites in April 1996. All time-domain soundings were collected with a 40 x 40 m transmitter loop with the receiver coil outside the transmitter loop (fig. 14). Whereas results of multiple coil-separation soundings are given in the conductivity unit mS/m, results of time-domain soundings are customarily given in the resistivity unit ohm-m. These units are the inverse of each other and are converted by the equation:

Conductivity (mS/m) = 1000/Resistivity (ohm-m)

Water and Soil Sampling

Sample Design

Ground water, surface water, and soil samples were collected to (1) evaluate how well the airborne geophysical data characterizes ground-water and soil salinity and (2) identify sources of salinity in the study area. Data collected by BEG were merged with data collected by the Lower Colorado River Authority (LCRA) and the Colorado Municipal Water District (CRMWD). Ground-water samples were obtained from six water wells by the BEG. Combined with the 19 wells sampled by LCRA-CRMWD (fig. 15), this was the majority of the available water wells in the study area and included areas of high and low conductivities mapped by the airborne geophysical survey. Locations of soil samples were paired with ground-water samples and chosen in areas of high and of low conductivity shown on the 56,000 Hz ground-conductivity map.

Surface-water samples obtained by LCRA-CRMWD were collected in January 1996. Four additional surface-water samples were collected in April 1996 by the BEG. In addition, water

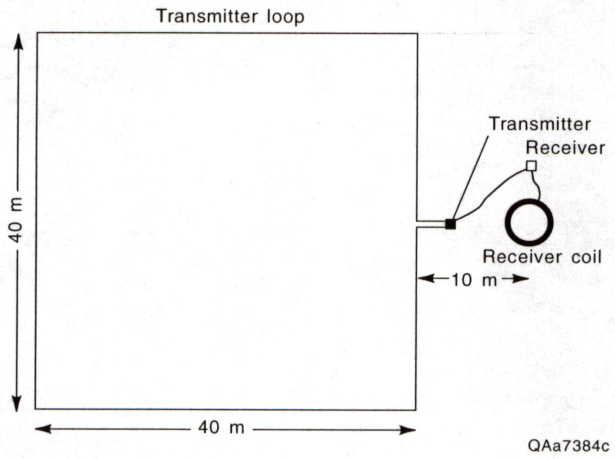

Figure 14. Instrument configuration of Protem 47/S sounding.

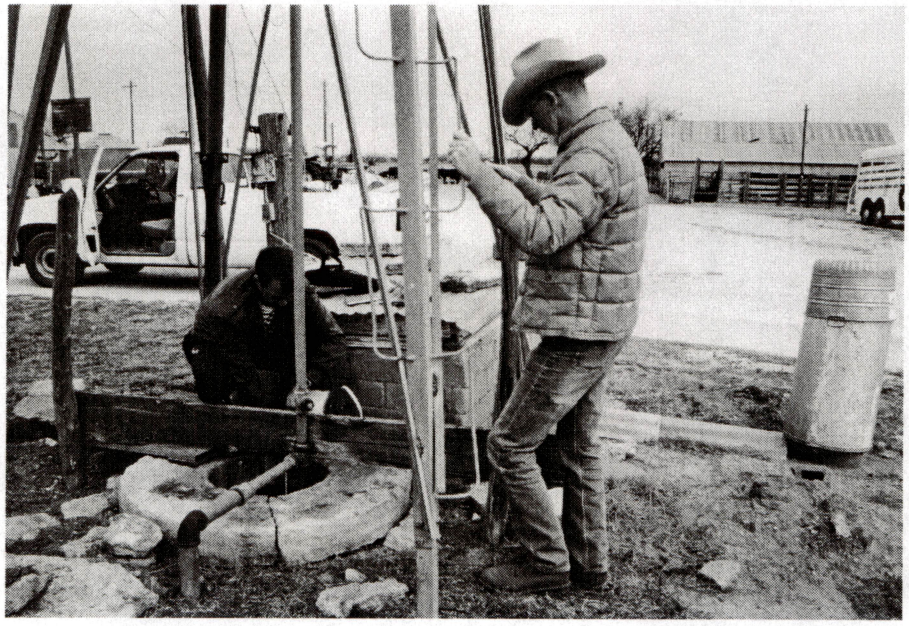

Figure 15. LCRA and CRMWD staff sampling the Vancil well during the airborne geophysical survey.

samples were collected at two abandoned oil wells being plugged by RRC and from a seep identified by RRC personnel as an unplugged core hole (fig. 16).

Sample Collection and Analysis

Ground-water samples were taken by BEG from abandoned and non-abandoned wells. Where a well was not equipped with a pump, BEG installed a temporary pump to purge the wellbore and obtain a sample. The BEG used a 1/3-hp submersible electric pump powered by a portable electric generator. Ground-water samples collected by the LCRA and CRMWD were from wells equipped with a functioning pump or from windmill wells. Three of the wells sampled by BEG were large-diameter dug wells holding 475 to 2,480 L in storage. The others were drilled wells holding much less water (less than 40 L) in storage.

Before taking our samples we monitored temperature, pH, and Eh in a flow cell connected to the water-discharge line from the sample pump. We collected samples after the values of temperature, pH, and Eh had stabilized. This process took approximately 30 to 45 min, during which time the water columns in the wells were drawn down as much as 80 percent. In other words, our 15 to 19 L/min pumping rate generally exceeded the rate of inflow of ground water, particularly in the shallow, hand-dug wells. Because of the high capacity and low yield of the hand-dug wells, multiple well-bore volumes in general were not purged before the water samples were taken. Nevertheless, the stabilized values of temperature, pH, and Eh suggest that the water that was sampled was being drawn into the wells largely from the formation and most likely is little affected by well-bore storage.

Water sampling followed standard techniques (Brown and others, 1970; Wood, 1976). Samples were passed through an in-line disposable 0.45-µm filter connected to the discharge line and collected in plastic 0.5-L narrow mouth bottles. Alkalinity was measured by titration of unfiltered samples with a standard H_2SO_4 solution within several hours of collection. Waters to be analyzed for major and minor cations were acidified in the field with 6N HNO_3; waters to be analyzed for anions were collected without treatment. Sample bottles were sealed with laboratory

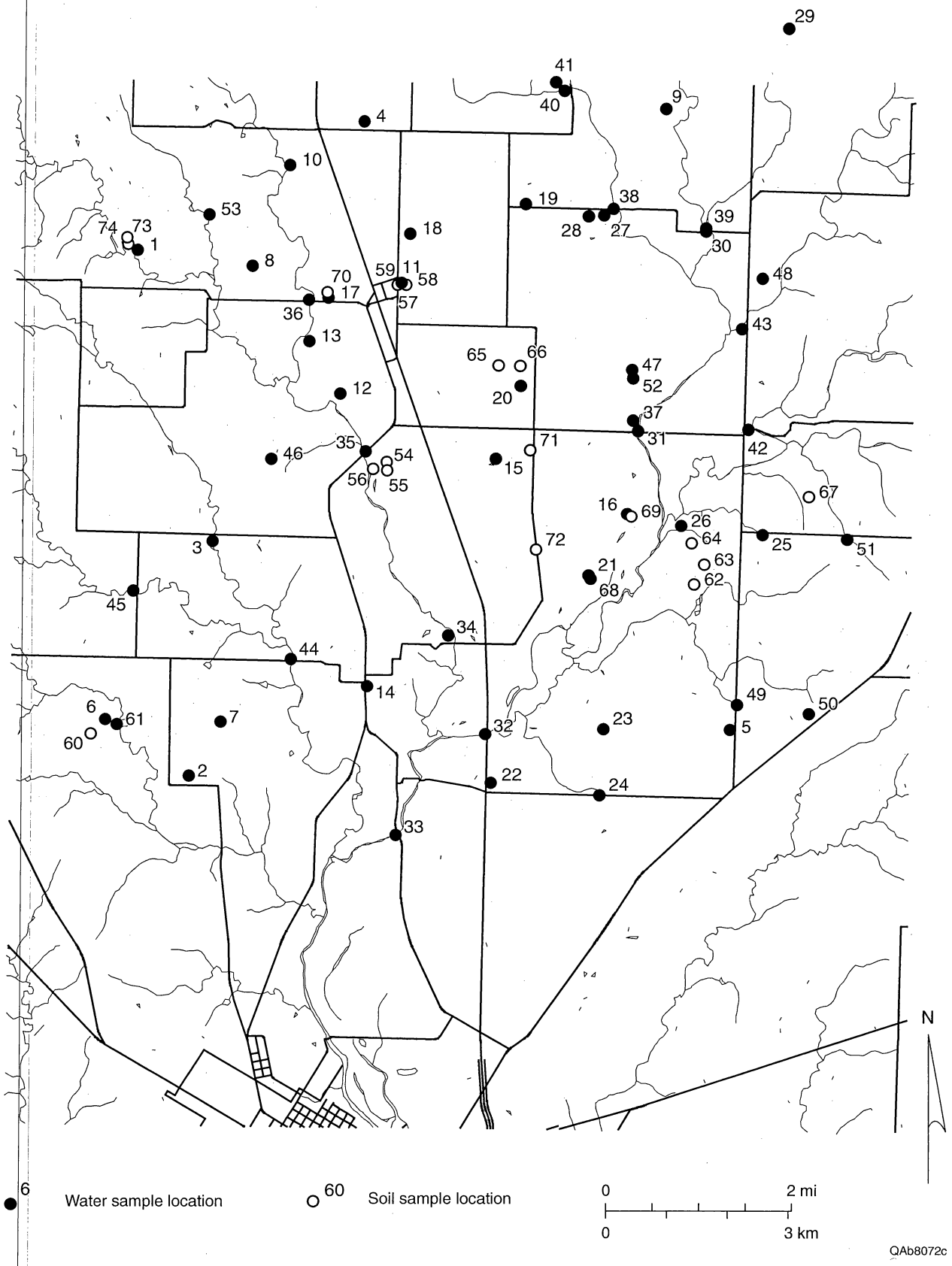

Figure 16. Location of water and soil samples collected by CRMWD, LCRA, and BEG.

parafilm and stored at 4°C prior to analysis. Cations were determined using ICP–OES (inductively-coupled plasma—optical emission spectroscopy). Fluoride, chloride, bromide, nitrate, and sulfate anions were determined by ion chromatography. Bicarbonate was determined by titration. Total dissolved solids (TDS) of the CRMWD samples was determined by gravimetric analysis of a filtered sample. TDS of the BEG samples was calculated as the sum of reported dissolved constituents (cations and anions and dissolved silica).

Samples at the abandoned oil wells were collected at the wellhead in a bucket and were then filtered. Fluid pressure in the wells allowed the wells to discharge at ground surface through the valve being used by RRC to control flow during the plugging operation. The liquid collected at the wellhead contained black suspended solids (pipe scale) and some oil. Samples were prefiltered by passing through glass wool in a funnel. The water samples then were drawn through an in-line 0.45-μm filter into a clear polycarbonate filter chamber. Water temperature was measured in the stream flowing from the wellhead into the collection pit and pH was measured in the filtered sample. The sample from the unplugged core hole was drawn into the filter chamber through a 0.45-μm filter. Analytical procedures were as described above.

The four surface-water samples collected by BEG were collected in a bucket. Each water sample was drawn through a 0.45-μm filter into the filter chamber and decanted into two 500-mL polyethylene bottles. Temperature was measured in the stream and pH was measured on site. Other sampling and analytical procedures were as described above.

Soil samples were collected with a hand auger and sealed in wide-mouth glass jars. In the laboratory the samples were air dried and then milled. Electrical conductivity and chloride measurements were performed on 1:1 extractions prepared at the BEG laboratory. Samples were mechanically shaken for 1 hr then centrifuged to obtain a particle-free liquid. Electrical conductivity (EC), which indicates the quantity of soluble salts in an aqueous sample, was determined on the supernatant using a direct-readout micro-conductivity cell and corrected to 25 °C. Chloride concentrations were determined by argentometric titration or ion chromatography.

RESULTS

We analyzed results from the airborne geophysical survey to determine whether the airborne method can reliably locate oil and gas wells and associated salt water plumes, distinguish oilfield-related salinization from other sources, and effectively guide ground-based geophysical, geological, and geochemical investigations of ground salinization.

Airborne Geophysical Survey

Dighem performed the airborne geophysical survey of the study area in January 1996 (Garrie, 1996). The principal instruments installed in the helicopter were a magnetometer to measure magnetic field variations and several pairs of induction coils to measure ground conductivity. One of the goals of the survey was to identify areas where conductive ground coincided with a magnetic anomaly. This geophysical signature, insofar as a magnetic anomaly can be produced by a well casing and a conductivity anomaly can be produced by subsurface brine, might indicate areas where salt water has entered the ground through a surface pit or a leaking oil or gas well. The products of the airborne survey, which included maps of magnetic field and ground conductivity, formed part of the dataset that was analyzed to identify priority sites for on-the-ground field investigations.

Magnetic Field Data

Total magnetic field data acquired during the airborne survey show abundant local magnetic anomalies superimposed on a regional gradient (fig. 17). Magnetic field strength increases along the regional gradient from the lowest value of 50,186 nT in the southwest corner of the study area to the highest value of 50,382 nT in the northeast corner (Garrie, 1996). These results are consistent with regional maps of magnetic field strength (G. R. Keller, unpublished data).

Linear and oval magnetic anomalies are superimposed on the regional gradient (fig. 17). The anomalies are weak relative to the total field strength (as much as 30 nT, or about 0.06%), but are well above the stated 0.01 nT sensitivity of the magnetometer. The linear features, some

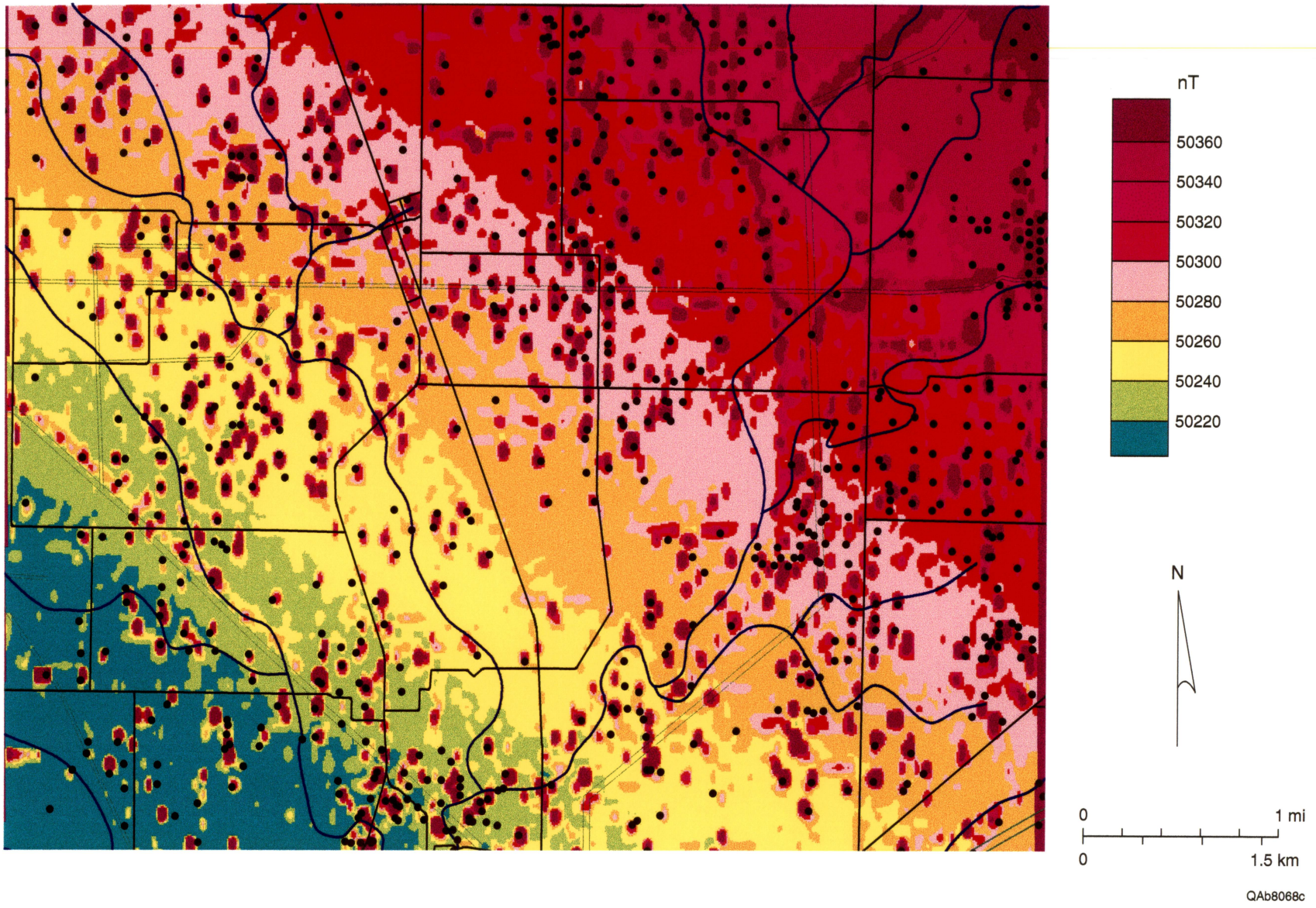

Figure 17. Map of enhanced total magnetic field strength. Black dots are oil and gas well locations from RRC. Green lines represent pipelines.

of which extend completely across the study area, are generally 150 to 200 m wide. Their locations correspond with those of known pipelines. Two of the more obvious anomalies, the northwest-southeast trending line in the southwest corner and the north-south trending line on the east side that bends to the northeast, are both known (and slightly mislocated) Comyn Crude pipelines (fig. 17). There are also known pipelines in the study area that are not visible on the magnetic field map.

Most of the oval anomalies are about 160 m across, although they range from 80 to 200 m. These are anomaly dimensions in an east-west direction (along the flight lines), where magnetometer measurements were acquired at 3 m intervals, rather than north-south (across the flight lines), where measurements were 100 m apart. The oval anomalies are well distributed over the study area. Most of the oval magnetic anomalies coincide with known well locations (fig. 17) and are interpreted to be local magnetic field perturbations caused by magnetic elements of the well (casing and pump jack). Other magnetic anomalies coincide with structures containing significant magnetically-susceptible material, such as some homes, metal barns, and windmills. The presence of oil and gas wells (known both from RRC well records and ground surveys completed during this study) in areas where no magnetic anomalies are mapped confirms that not all wells were detected during the airborne survey.

Typical oval anomaly diameters of 80 to 200 m suggest that the chosen flight line spacing was a good compromise between anomaly detection and survey cost. Line spacing of 100 m used in this survey probably missed some wells that produce small anomalies. Line spacings of 200 m tested during processing by Dighem showed a reduction in the number of detected magnetic anomalies.

Electromagnetic Data

Ground conductivity maps of the study area were produced by Dighem after processing electromagnetic data acquired during the airborne survey (Garrie, 1996). Maps were made from horizontal coplanar coils operating at 56,000 Hz (fig. 18), 7,200 Hz (fig. 19), and 900 Hz

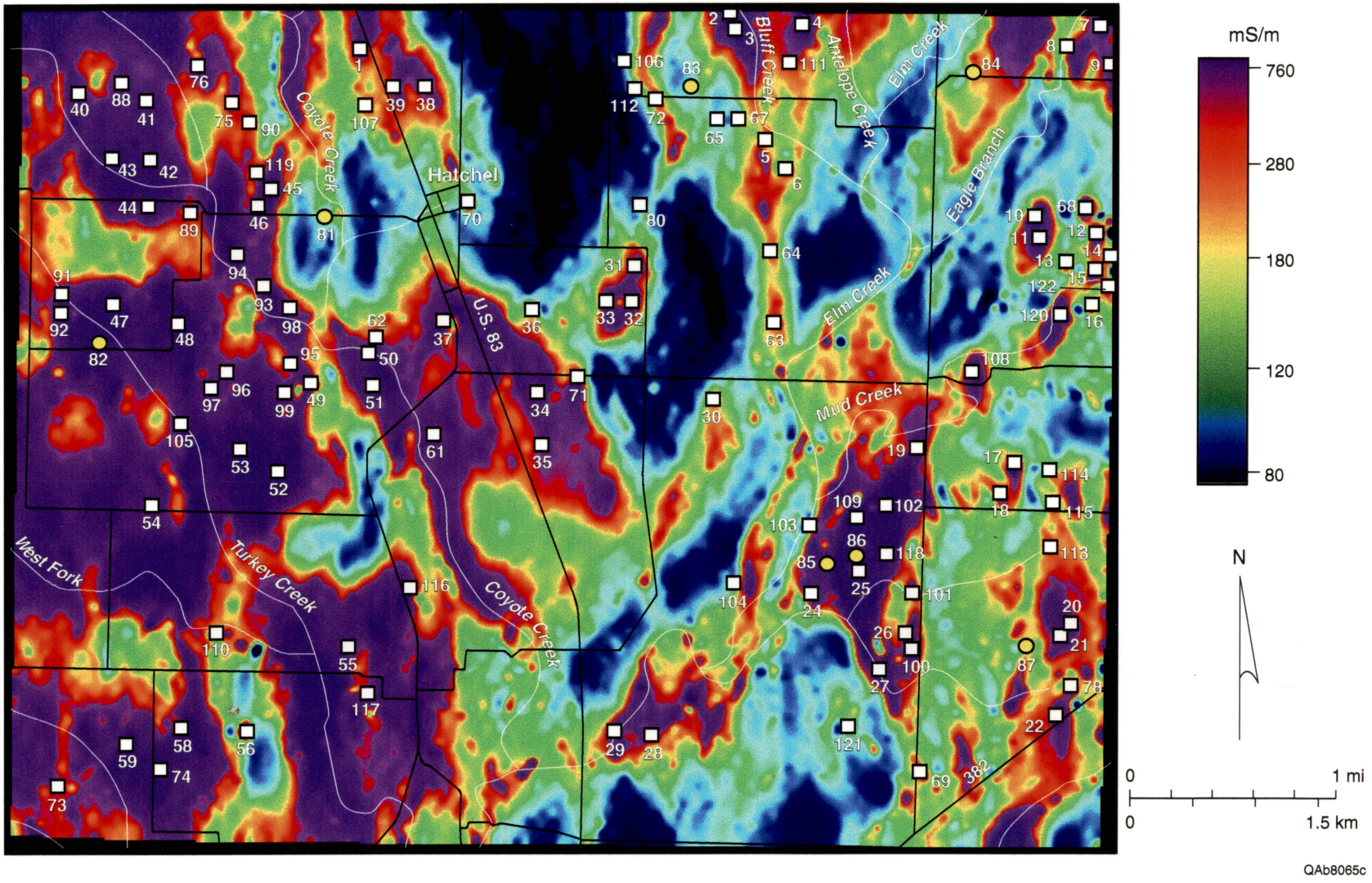

Figure 18. Map of shallow ground conductivity at 56,000 Hz using vertical dipole coil orientation. Numbered locations represent preliminary list of anomalous sites and other ground-based geophysical survey locations.

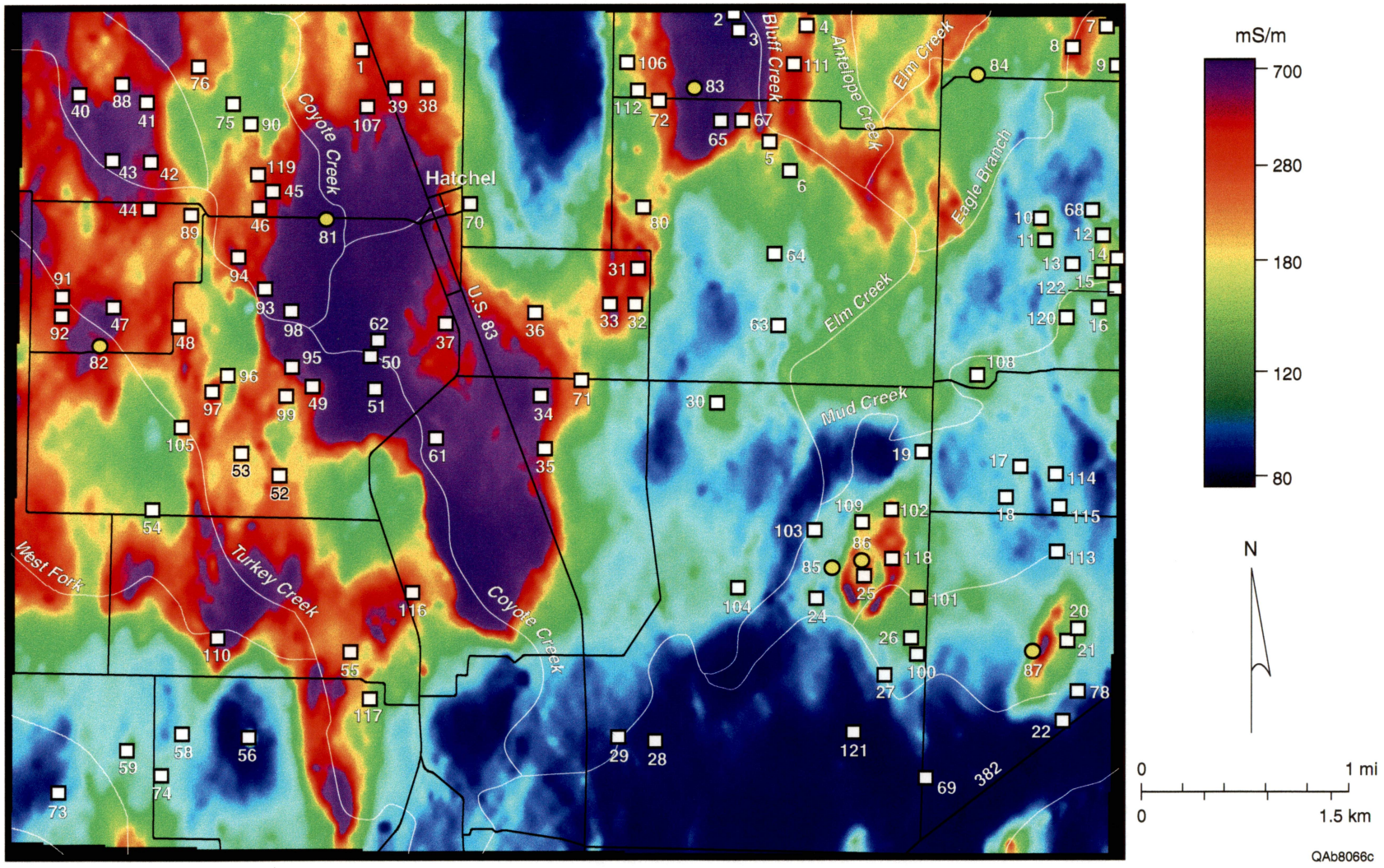

Figure 19. Map of moderately deep ground conductivity at 7,200 Hz using vertical dipole coil orientation.

(fig. 20). Because exploration depth depends on both frequency and ground conductivity, deeper exploration depths were attained at lower coil frequencies and, for a given coil frequency, less conductive ground (fig. 21).

56,000 Hz Horizontal Coplanar Data

Ground conductivities measured by the 56,000 Hz coils, the shallowest exploration depth frequency, showed good contrast between the lowest observed values of about 60 to the highest values of 730 mS/m (fig. 18). Maximum exploration depths for this frequency deepen from 2.5 m over highly conductive ground to as much as 9 m over ground with the lowest observed conductivities (fig. 21). This depth range is the one that is most affected by near-surface changes in many factors that control ground conductivity, such as soil type (clay soils are more conductive than sandy soils), moisture content (wet soils are more conductive than dry soils), and water chemistry (saline water is more conductive than fresh water).

Highly conductive areas visible on the 56,000 Hz map include numerous small ovals that are generally 80 to 250 m across, curvilinear features that are a few hundred meters wide and hundreds of meters long, and large, irregularly-shaped features covering many square kilometers (fig. 18).

Significant curvilinear features include (a) a zone about 200 m wide and more than 2 km long located along an east-facing bluff west of Bluff Creek in the northern part of the study area, (b) a segment about 400 m wide along Coyote Creek that extends from the northern edge of the study area to near the southern edge, (c) a 200-m wide zone along an east-facing bluff west of Elm Creek, and (d) a short segment of Elm Creek just downstream from its confluence with Eagle Branch (fig. 18).

The most significant of the large, irregular areas of high conductivity are (a) the western third of the study area, (b) an area south of Hatchel and east of Coyote Creek, and (c) the area just east of Elm Creek south of its confluence with Mud Creek (fig. 18).

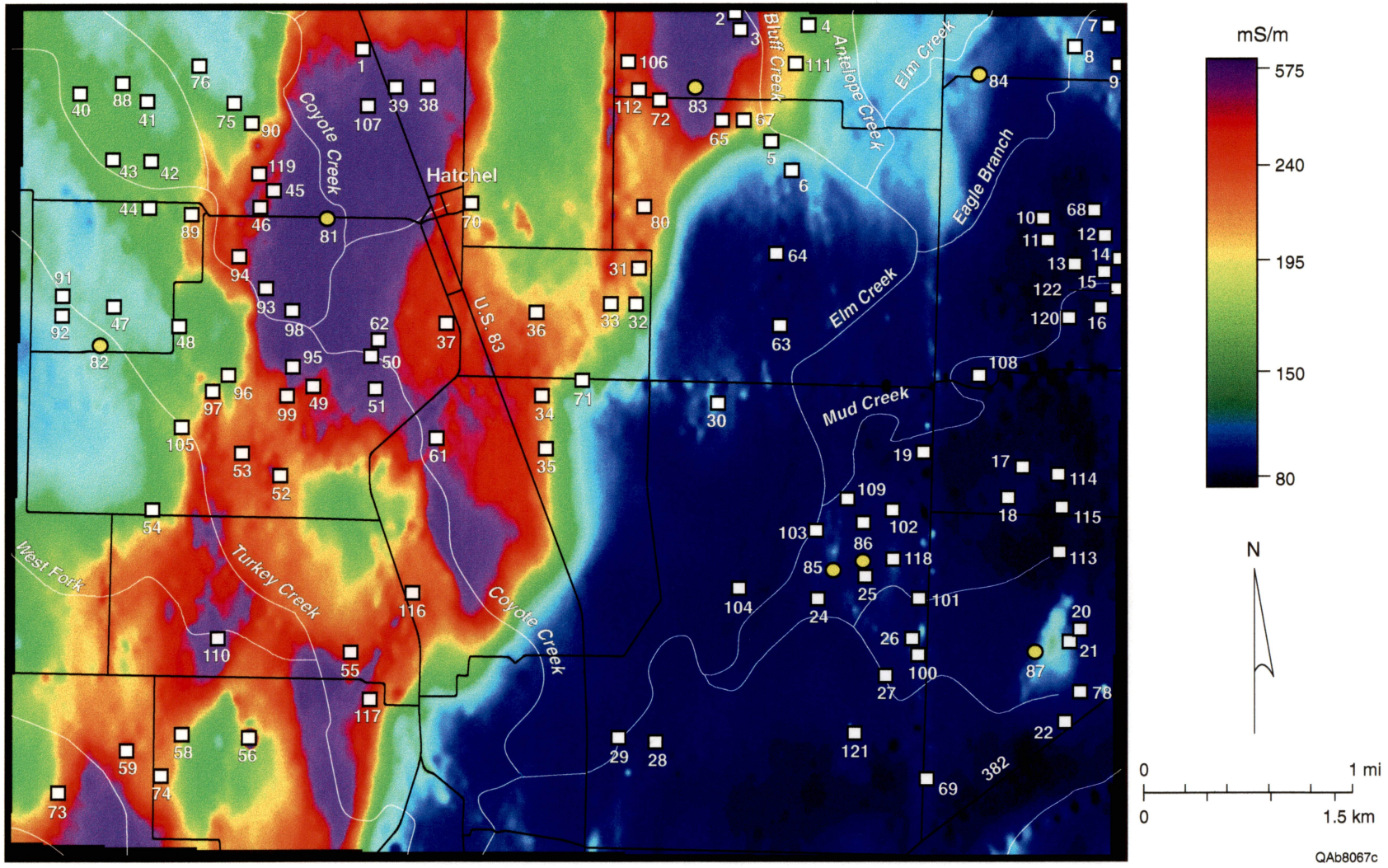

Figure 20. Map of deep ground conductivity at 900 Hz using vertical dipole coil orientation.

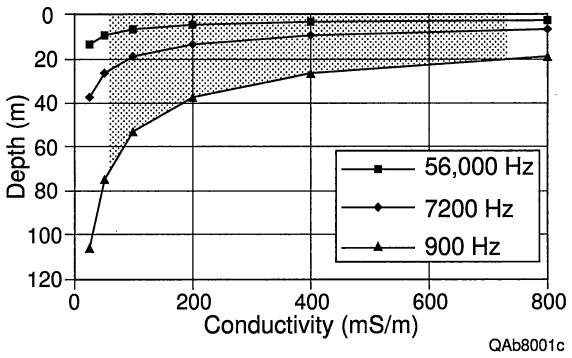

Figure 21. Changes in estimated exploration depth (skin depth) with ground conductivity for 900 Hz, 7,200 Hz, and 56,000 Hz coil configurations. Values calculated from formula given for Dighem equipment by C. Nind (pers. comm.). Shaded area indicates conductivity range observed in the Hatchel area.

Sites were chosen for detailed ground investigation largely from the smaller, oval-shaped anomalies because of the limited lateral distance that salt water plumes can move from brine pits and potentially leaking wells. These features may also include small patches of conductive soil, springs, and stock tanks. The curvilinear conductivity highs located at similar elevations along a bluff or hill slope probably mark the location of ground water seeps where the land surface has intersected a water-bearing unit. Curvilinear features along the creeks most likely represent areas where higher salinity water flows in the creek or associated alluvium. The large, irregularly-shaped features are too extensive to be caused by individual leaking wells, but some may be located where there are numerous closely spaced salt water sources. Most of these large features are probably not oilfield-related, but instead are located in areas where soils or shallow geologic units have more clay, are wetter, or contain water with higher dissolved mineral content.

7,200 Hz Horizontal Coplanar Data

Ground conductivity as sensed by the 7,200 Hz airborne coils ranges from 60 to more than 700 mS/m, only slightly lower than the range observed for the higher frequency coils (fig. 19). Consequently, exploration depths with the 7,200 Hz coils are deeper and range from about 24 m for the least conductive ground to about 7 m for the most conductive ground (fig. 21).

There is less highly conductive area on the 7,200 Hz map than on the 56,000 Hz map, which suggests that many of the conductivity anomalies visible on the 56,000 Hz map represent features within a few meters of the land surface. Local, oval-shaped anomalies that are ubiquitous on the higher frequency map are less common on the 7,200 Hz map. They are concentrated along the upper reaches of Mud Creek, east of Elm Creek and south of its confluence with Mud Creek, and east and northeast of Hatchel, and a few more are scattered across the study area (fig. 19). Large areas of anomalously high conductivities are found along and east of Turkey Creek, along and west of Bluff Creek upstream from its confluence with Elm Creek, and over the entire west-northwest section of the study area. The strongest large anomalies are along Turkey Creek and Bluff Creek. Linear and curvilinear features such as those

evident on the 56,000 Hz map are absent at 7,200 Hz except along some roads. These are likely to be power line artifacts.

Most of the sites investigated using ground-based geophysical surveys were the small, oval-shaped anomalies visible on the 56,000 and 7,200 Hz conductivity maps. These sites are discussed in a subsequent section of this report.

900 Hz Horizontal Coplanar Data

Highly conductive ground, as measured by the 900 Hz airborne coils, covers less total area than that detected by the 7,200 Hz coils (fig. 20). Total range in conductivity values is also lower for the 900 Hz coils: most of the measurements fall between 60 and 400 mS/m. Maximum exploration depths are 68 m for the least conductive ground and 27 m for the most conductive ground (fig. 21).

Few local conductivity anomalies are visible in the 900 Hz data. The principal features are three areas of similar ground conductivity (fig. 20). The smallest is an area of low to moderate conductivity (100 to 150 mS/m) in the northwest part of the study area. This northwest low conductivity zone is bordered to the southeast by a 4 to 5 km wide band of highly conductive ground that trends north-northeast across the study area. Conductivities within this zone typically range from 150 to 400 mS/m. Bordering this zone to the southeast is an extensive area of low conductivity (60 to 120 mS/m).

The north-northeasterly trend of the conductive band matches the strike of Permian geologic units in the area (Kier and others, 1976). These units dip gently to the west-northwest into the Permian Basin. The 900 Hz coils, which sense the upper 30 to 40 m in the conductive zone, are probably detecting a brine-bearing unit that is more conductive than units above and below it and is shallowing to the east-southeast. It is probably too deep to be detected in the northwest corner of the study area and has been removed by land surface erosion in the southeast part of the area. Deeper-exploring time domain electromagnetic soundings that were acquired to help understand

the conductivity patterns visible on the 900 Hz map are discussed in a subsequent section of this report.

Ground-Based Geophysical Surveys

Before the airborne survey was completed, we recognized that highly conductive ground could be caused by several natural and cultural effects. For example, we could not be certain from airborne geophysical data alone whether a given conductivity anomaly represented a leaking well, an abandoned brine pit, a natural saline spring, clay-rich or wet soil, an outcrop of a conductive geologic unit, or some other conductive feature. Field investigations that included soil sampling, water sampling, and ground-based geophysical surveying were completed at a number of sites in the study area that represent the variety of sites that would be encountered in a future geophysical search for leaking wells. Soil type, geologic unit, and topographic setting were established for each of these sites to examine their potential effects on the geophysical signature. We did not attempt to investigate every well or every geophysical anomaly visible in the airborne survey.

Site Selection

Ground-based geophysical investigations were carried out at 23 locations in the study area. Field sites were a representative subset chosen from a list of 103 preliminary sites (table 2 and appendix A) identified from the airborne magnetic and electromagnetic data. These sites were classified into three common airborne signature types: CMW, CM, and CW. Type CMW sites are those that have high conductivity anomalies on the 56,000 Hz map, have magnetic anomalies, and have known wells nearby. Of the 103 preliminary sites, 71 are type CMW and represent known wells where oilfield-related salt water might have infiltrated the ground. Type CM sites are those that have high 56,000 Hz conductivity anomalies and magnetic anomalies, but have no known wells nearby. There are 15 of these sites, which might represent salt water infiltration

Table 2. Summary statistics for Hatchel area airborne and ground-based geophysical sites (figs. 18, 19, and 20). Type CMW sites are those that have a conductivity anomaly, a magnetic anomaly, and a known well. Type CM sites have a conductivity anomaly and a magnetic anomaly, but no known well. Type CW sites have a conductivity anomaly and a known well, but no magnetic anomaly. Type C sites have a conductivity anomaly, but neither a known well nor a magnetic anomaly. Attributes of individual geophysical sites are listed in Appendix A.

Total geophysical sites	113	
Type CMW, CM, CW, and C sites	103	
Type MW sites	2	
TDEM sounding-only sites	7	
Other (corehole)	1	
Mapped conductivity anomalies	103	46 fit profile[1]
CMW sites	71	33 fit profile
CM sites	15	6 fit profile
CW sites	14	7 fit profile
C only sites	3	0 fit profile
Conductivity anomalies, 56,000 Hz	94	
Conductivity anomalies, 7,200 Hz	54	20 are weak anomalies
Conductivity anomalies, 56,000 and 7,200 Hz	46	20 are weak anomalies
Conductivity anomalies, 56000, 7200, and 900 Hz	9	
Reconnaissance sites	23	
CMW	12	6 fit profile; 4 sources
CM	4	2 fit profile; 2 sources
CW	5	3 fit profile; 2 sources
C	0	0 fit profile
MW	2	0 fit profile; 2 sources

Reconnaissance results at sites fitting profile[1]

Site	Anomaly type	Inferred salinity source
14	CMW (56,000+7,200)	Pit or Leak
46	CMW (56,000+weak 7,200)	Source not found
56	CMW (56,000+7,200+900)	Leak
59	CMW (56,000+weak 7,200+900)	Leak?
74	CMW (56,000+weak 7,200)	Source not found
76	CMW (56,000+7,200)	Leak
25	CM (56,000+7,200)	Tanks or pit
71	CM (56,000+v. weak 7,200)	Tanks
12	CW (56,000+7,200)	Pit
16	CW (56,000+weak 7,200)	Leak or pit
70	CW (56,000+weak 7,200)	Source not found

[1] Sites that fit a profile of a potentially leaking well are those that show conductivity anomalies measured by both the 56,000 Hz and 7,200 airborne coils and have either a known well location, a magnetic anomaly, or both.

near leaking tank batteries or near wells that are either mislocated or not presently inventoried. Type CW sites, of which there were 14, represent locations where there is a 56,000 Hz conductivity anomaly and a known well, but no magnetic anomaly. These sites might indicate salt water infiltration at known wells that were undetected by the airborne magnetometer or at old wells that have no casing and are thus more likely to be leaking brine. The remaining three preliminary sites had a conductivity anomaly but no well or magnetic anomaly (type C), which might be interpreted as salt water infiltration near an unknown well that was not detected by the airborne magnetometer. In addition to the investigations at the conductivity anomalies, we visited two sites that had magnetic anomalies associated with known wells, but no conductivity anomaly (type MW).

Ground-based geophysical investigations consisted of (a) 36 reconnaissance conductivity profiles across 23 preliminary sites, (b) four surveyed conductivity profiles using multiple exploration depths and six transient electromagnetic soundings at two sites, and (c) seven additional transient electromagnetic soundings at background locations across the study area.

Type CMW Sites

Type CMW sites, where a conductivity anomaly (C), a magnetic anomaly (M), and a known well location (W) coincide, were the most common of the 103 preliminary sites identified from the airborne geophysical data (table 2 and appendix A). Ground-based geophysical methods were employed at 12 of these sites, 11 of which are discussed individually below.

Site 76

Site 76, located in the northwest part of the study area, appears as an anomalously conductive area on the shallow (56,000 Hz) and moderately deep (7,200 Hz) airborne conductivity maps, but not on the 900 Hz map (figs. 18, 19, 20). The conductivity anomaly measures about 120 m east-west and 200 m north-south on the 56,000 Hz map and coincides

with a magnetic anomaly that is similar in size (fig. 17). The site encompasses the abandoned Vancil #1 well (fig. 22), which was drilled and completed in 1966 and plugged in 1975. Thin Quaternary surficial deposits cover Permian Clear Fork strata (fig. 2); soil is not cultivated and is mapped as Portales clay loam (fig. 3).

Ground investigations at site 76 consisted of a reconnaissance conductivity profile and two multiple-coil-separation conductivity profiles centered on the well and three TDEM soundings at and near the well (fig. 12). The reconnaissance profile, line 76A (fig. 23), reveals that elevated ground conductivities extend about 130 m across the site from east to west for the 20 m coil separation. This distance is similar to that measured from the airborne survey maps. High conductivities for the horizontal dipole mode (above 100 mS/m) are found near the well, with highest values located 20 m west of the well.

Multiple-coil-separation profiles (fig. 24) were acquired along an east-west line and a north-south line across the well to determine vertical and lateral ground conductivity patterns. Vertical dipole data were erratic, but horizontal dipole measurements show well-defined conductivity peaks on both lines (fig. 24a and b). Highest ground conductivities on line 76B, the east-west line, are found for the 10- and 20-m coil separations (fig. 24a). This indicates that the upper 6 to 12 m (the exploration depths for the 10- and 20-m separations) is more conductive than the 12- to 24-m depth range.

The highest conductivity for the 10-m coil separation on line 76B is 10 m west of the abandoned well. For the 20-m separation, the peak is 10 m farther west. Highest conductivities for the 40-m separation are lower than those for the shorter separations, but cover a broader area and are also centered about 20 m west of the well (the downslope direction). East and west of the peak, conductivities increase with coil separation from 50 to 60 mS/m at 10 m separation, to 70 to 80 mS/m at 20 mS/m, to 80 to 90 mS/m at 40 m separation. This suggests that, away from the peak, conductivity increases with depth within the upper 20 m.

Similar trends are visible on the north-south line 76C (fig. 24b). Peaks at each of the three separations have similar conductivities (about 100 mS/m) and are all centered within 5 m of the

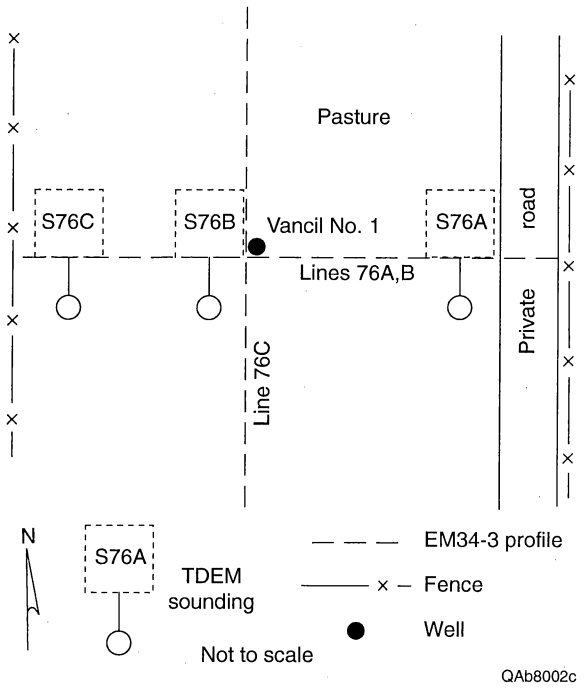

Figure 22. Sketch map of site 76. One reconnaissance conductivity profile (76A), two multiple-coil-separation profiles (76B and 76C), and three time-domain electromagnetic soundings (S76A, S76B, and S76C) were acquired near the abandoned Vancil #1 well.

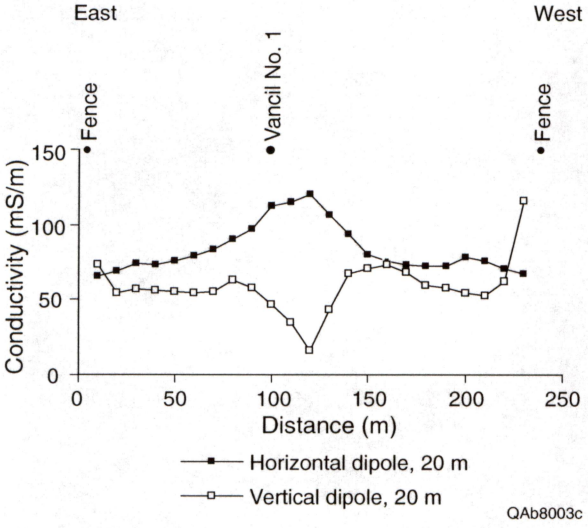

Figure 23. Apparent ground conductivity at site 76 using 20 m coil separation and horizontal and vertical dipole orientations. Line 76A crosses the abandoned Vancil #1 well from east to west.

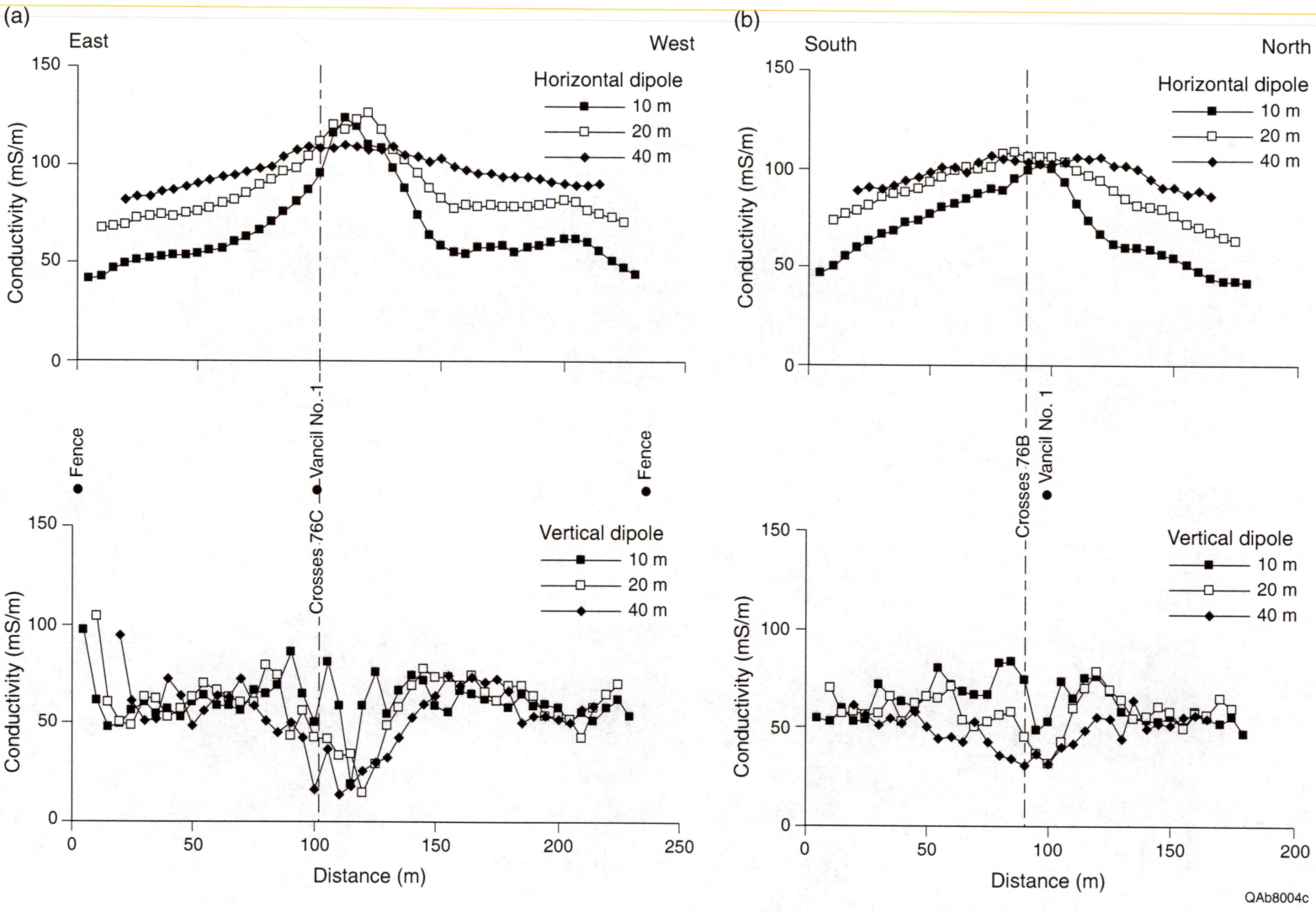

Figure 24. Apparent ground conductivity at site 76 using multiple coil separations (10, 20, and 40 m) and horizontal dipole (upper plot) and vertical dipole (lower plot) orientations. Line 76B (a) crosses the abandoned Vancil #1 well from east to west. Line 76C (b) crosses the well from south to north.

well. Peaks drop off more quickly north of the well (the upslope direction) for the 10 and 20 m coil separations than they do south of the well.

Horizontal dipole data were used to construct two layer conductivity models along lines 76B and 76C (fig. 25). On line 76B, a low conductivity layer (23 to 90 mS/m) overlies a layer with higher conductivities (144 to 211 mS/m) on the eastern and western flanks of the abandoned well at about 100 m (fig. 25a). The surface low conductivity layer thins from about 4 m at each end of the line to less than 1 m thick near the well. At the well, the low conductivity layer is replaced by a layer that is 2 to 4 m thick and is more conductive than the layer below it. Two-layer models constructed along north-south line 76C (fig. 25b) exhibit a similar pattern: a poorly conductive surface layer overlies a more conductive layer and is a few meters thick away from the well, thins toward the well, and is replaced at the well by a layer that is 1 to 2 m thick and is more conductive than the underlying layer. The conductive surface layer is present along a distance of about 30 m on the east-west line and about 15 m on the north-south line.

TDEM soundings were located at three sites along line 76B (fig. 22) to examine deeper variations in ground conductivity. Transients for each of the soundings show decreasing apparent resistivity with time (fig. 26), which suggests that conductivities increase with depth. Four layer conductivity models were calculated that provide good fits to the observed transient decays. These models (fig. 26) confirm that resistivities decrease (or conductivities increase) in general with depth and differ significantly only in the upper 10 m of the subsurface.

Each of the models shows a decrease in resistivity from about 10 ohm-m to 2 to 3 ohm-m near 40 m depth. A thin surface layer that is more conductive than underlying units thickens from less than 5 m at the most upslope sounding (S76A, fig. 26a) to 7 or 8 m at the sounding closest to the well (S76B, fig. 26b) and at the sounding downslope from the well (S76C, fig. 26c). This high conductivity surface layer probably correlates with the lower conductive layer detected on the multiple-coil-separation profiles.

Despite a lack of surface evidence of brine leakage (no barren zone or brine at the surface), this plugged well is probably leaking. Evidence suggesting a recent or ongoing leak includes

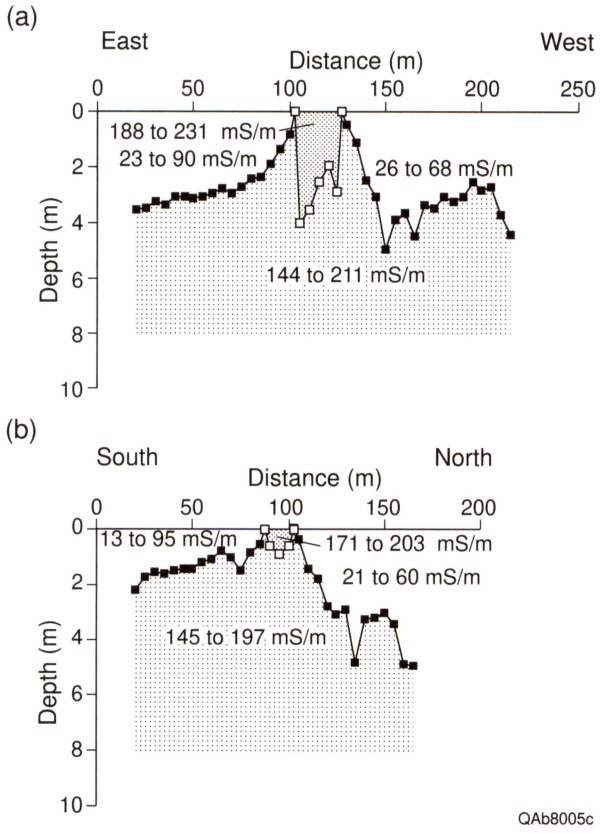

Figure 25. Two-layer conductivity models that fit multiple-coil-separation data for east-west line 76B (a) and north-south line 76C (b) at site 76. Vancil #1 well is located at 100 m on line 76B and at 90 m on line 76C.

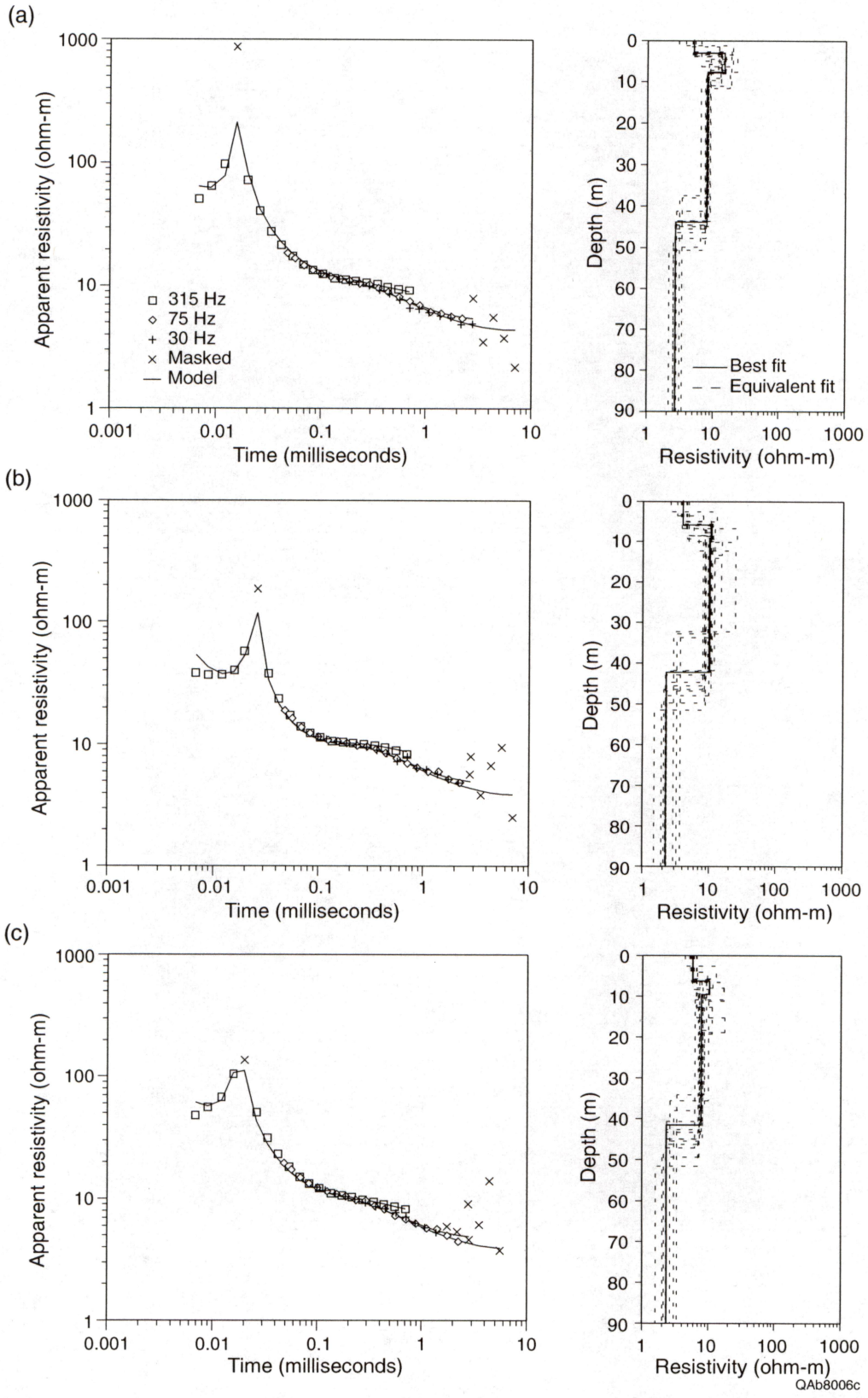

Figure 26. Transient decay curve (left) and resistivity models (right) at TDEM sounding sites S76A (a), S76B (b), and S76C (c).

conductivity anomalies visible on 56,000 and 7,200 Hz airborne conductivity maps, conductivity peaks centered near the abandoned well for the 10 m, 20 m, and 40 m EM34 coil separations, a modeled conductive layer that shallows near the well, and the presence of a near-surface high conductivity zone downslope from the well. The most likely cause of elevated ground conductivity near the well is the presence of brine from the well. Background conductivity levels are reached within about 50 m of the well, suggesting that little brine has migrated farther than that distance.

Site 14

Site 14 is situated near a tributary of Mud Creek in the northeast part of the study area (fig. 18), where a few cm of Potter clay loam soil grade downward into Permian Clear Fork Group strata (figs. 2 and 3). Site 14 consists of conductivity anomalies on 56,000 Hz and 7,200 Hz maps, but no anomaly is apparent on the deeper 900 Hz map (figs. 18, 19, and 20). Two abandoned wells are located within the area of anomalous ground conductivity. The northern of the two, the Brevard #1-B well, was drilled in 1934 and plugged with state funds in 1991. The #6-A well is located 75 m south of the #1-B well.

Two reconnaissance conductivity profiles were acquired across site 14. Line 14A, oriented east-west across well #1-B (fig. 27), shows a slight increase in ground conductivity (horizontal dipole orientation) from background values of 50 mS/m to about 60 mS/m near the well (fig. 28a). This slight increase at the #1-B well is not evident on the north-south line 14B (fig. 28b). Line 14B does show a more substantial increase in ground conductivity near the #6-A well, where horizontal dipole values are as high as 90 to 100 mS/m. The zone of elevated ground conductivity near well #6-A is at least 100 m wide and has higher conductivities on the south side of the well (downslope toward the Mud Creek tributary) than at equivalent distances from the well on the north side of the well.

It is unlikely that the #1-B well is a significant source of salt water. Slightly elevated apparent conductivities at this well may be caused by nearby metallic debris or by small amounts

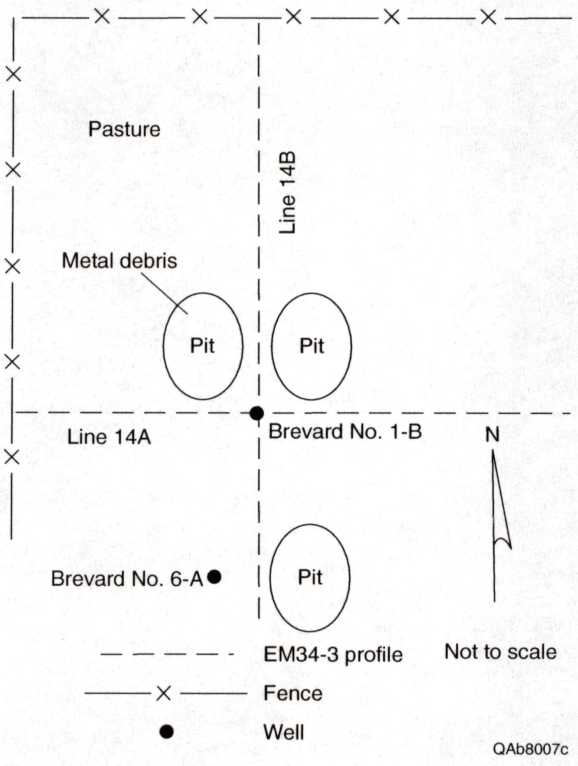

Figure 27. Sketch map of site 14. Reconnaissance conductivity profiles 14A and 14B cross the abandoned Brevard #1-B and #6-A wells.

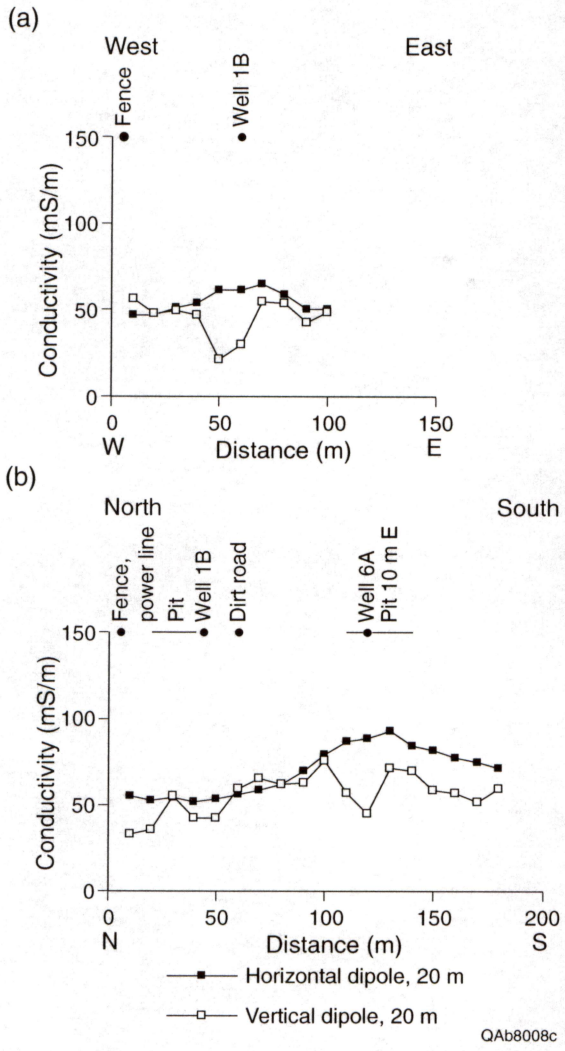

Figure 28. Apparent ground conductivity at site 14 using 20 m coil separation and horizontal and vertical dipole orientations. Line 14A (a) crosses abandoned Brevard #1-B well from west to east and line 14B (b) crosses the Brevard #1-B and Brevard #6-A wells from north to south.

of brine introduced during drilling or production. More salt water is likely to be present in the subsurface near the #6-A well. Brine has probably infiltrated the shallow subsurface at this site either through a well leak or by brine disposal in a pit 10 m east of the well. Because this well was recently plugged by RRC, the source of this brine has probably been eliminated.

Site 33

Site 33 is located southeast of Hatchel (fig. 18) and encompasses two abandoned wells. Mapped soils (fig. 3) are the Mereta clay loam, which is a shallow soil over hardened caliche, and the Portales clay loam, which is similar to the Mereta soil but is thicker. These soils have formed on Quaternary surficial deposits that mantle Clear Fork Group strata (fig. 2). The northern part of the site is cultivated, whereas the southern part is currently neither cultivated nor grazed. The Gardner #1 well, located in the northeast part of the site, was drilled in 1967, served as a salt water disposal well, and was plugged in 1980. A barren area remains visible at this well (fig. 10). At the southwestern part of the site is the Caudle #1 well, which was drilled in 1953 and plugged in 1963.

Site 33 has an airborne signature consisting of anomalously high conductivity on the 56,000 Hz map (fig. 18) and a magnetic anomaly near the Caudle well but not the Gardner well (fig. 17). Conductivity indicated on the 7,200 and 900 Hz maps is high, but not anomalously higher than the adjacent area (figs. 19 and 20). One surface conductivity profile, acquired in a northeast-southwest direction across the two well locations (fig. 29), shows slightly elevated ground conductivities as high as 80 mS/m in the horizontal dipole orientation at the Gardner well (fig. 30). Higher horizontal dipole conductivity values of 80 to 90 mS/m were measured between the Caudle #1 well and its associated pit; one measurement of 160 mS/m was recorded directly beneath the pit. Erratically varying horizontal and vertical dipole conductivities were measured at the northeast end of the line where pipelines are buried.

It is unlikely that either of these wells is currently leaking. Slightly elevated conductivities near the Gardner well are probably related to past salt water disposal activities, as is the barren

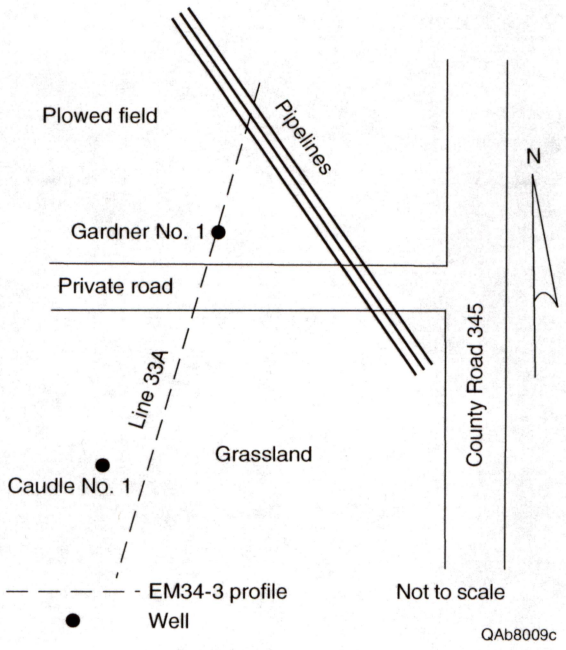

Figure 29. Sketch map of site 33. Reconnaissance conductivity profile 33A crosses the abandoned Gardner #1 and Caudle #1 wells.

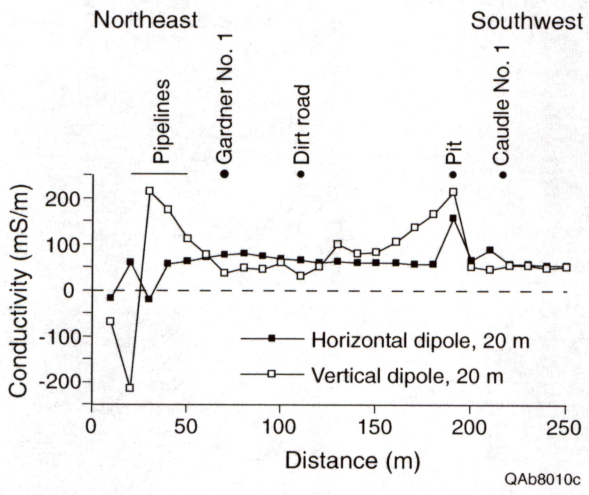

Figure 30. Apparent ground conductivity at site 33 using 20 m coil separation and horizontal and vertical dipole orientations. Line 33A crosses the abandoned Gardner #1 and Caudle #1 wells from northeast to southwest.

area surrounding the well. Ground conductivities near the Caudle well are highest beneath the pit, which suggests that brine has infiltrated the shallow subsurface from the pit.

Site 34

This site is located south-southeast of Hatchel (fig. 18) on a cultivated and terraced field. Thicker Portales clay loam soil grades westward into thinner Mereta clay loam soil across the site (fig. 3). Caliche fragments are present at the surface where the clay loam is thinnest. These soils are formed on thin Quaternary surficial deposits that overlie Clear Fork Group rocks (fig. 2). The site includes the location of the abandoned Waller #1 well, a dry hole that was drilled and plugged in 1977.

On maps produced from the airborne data, site 34 has a weak magnetic anomaly (fig. 17) and anomalously high conductivity on the 56,000 Hz map (fig. 18). Conductivity is high on the 7,200 and 900 Hz maps, but is no higher than adjacent areas (figs. 19 and 20). A reconnaissance east-west conductivity profile acquired across the site (fig. 31) shows relatively low ground conductivities in both the horizontal and vertical dipole orientations (fig. 32). There is no conductivity peak evident at the Waller well, but ground conductivities in the horizontal dipole mode do gradually increase from near 55 mS/m at the east end of line 34A to 75 mS/m at the west end of the line. This gradual westward increase is also indicated on the 7,200 and 900 Hz conductivity maps (figs. 19 and 20).

Absence of high ground conductivities near the Waller well suggest that it is not leaking. The gradual westward increase in ground conductivity coincides with a westward decrease in elevation, an observation that supports an interpretation of increasing conductivity related to a reduction in depth to saline ground water.

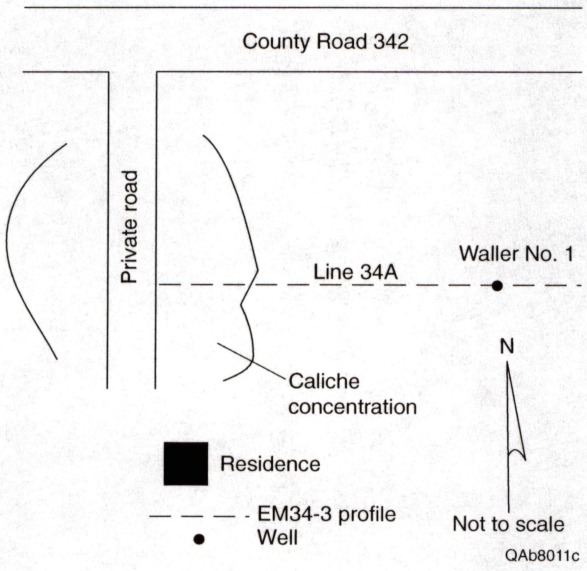

Figure 31. Sketch map of site 34. Reconnaissance conductivity profile 34A crosses the Waller #1 dry hole.

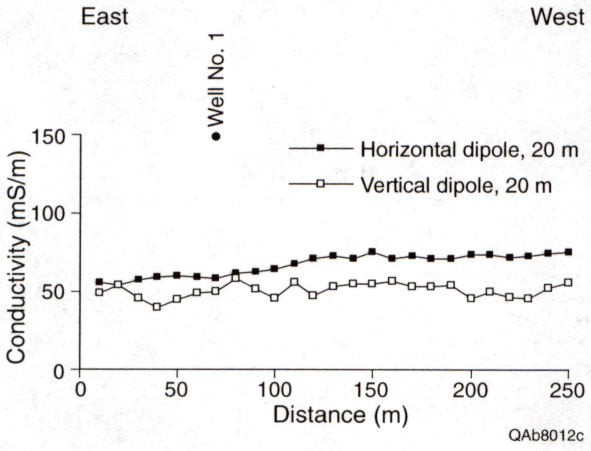

Figure 32. Apparent ground conductivity at site 34 using 20 m coil separation and horizontal and vertical dipole orientations. Line 34A crosses the abandoned Waller #1 well from east to west.

Site 43

Site 43 is located in the northwest part of the study area near a tributary to Coyote Creek. The airborne survey reveals a shallow conductivity anomaly (fig. 18) that coincides with a magnetic anomaly (fig. 17) and is near a known well. The conductivity anomaly does not appear on the deeper-exploring 7,200 and 900 Hz maps (figs. 19 and 20).

The site lies in rangeland that straddles the boundary between alluvial deposits of the Coyote Creek tributary and Clear Fork Group strata (fig. 2). Soil is classified as moderately deep Portales clay loam (fig. 3). A reconnaissance conductivity profile (line 43A, fig. 33) was acquired across an elongate area that is barren of vegetation. This barren area was reported by the landowner to occasionally flow salt water that runs off into the tributary. The landowner reported that there was once a well located near the barren area. Aerial photographs taken in 1940 do show road access to the site and a disturbed area that could be the well. A buried wellhead was not located during a magnetometer survey of the barren area by RRC staff.

Line 43A shows a distinct horizontal dipole conductivity peak centered on the barren area (fig. 34). The broad peak, which is nearly 150 m wide, has conductivities as high as 135 mS/m. These values are significantly higher than background conductivities of 70 to 80 mS/m.

Two possible interpretations of the geophysical data at this site are that (a) there is an abandoned well at or near the barren area that is leaking brine into the shallow subsurface, or (b) there is a natural saline spring that periodically discharges at the site. The broad conductivity peak on the ground-based data, the presence of a conductivity anomaly on the shallow airborne data, surface evidence of brine leakage, aerial photographic evidence of oil field roads, and landowner reports of an abandoned well suggest that there is a leaking well at the site.

Site 46

This site is located in a cultivated field west of Hatchel (fig. 18) where the abandoned Vancil D #1 well was drilled in 1955 and plugged in 1974. Soil is mapped as the Olton clay

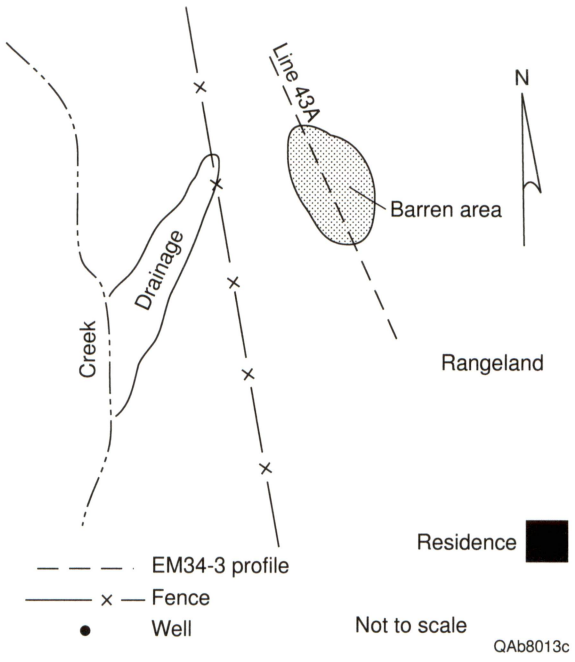

Figure 33. Sketch map of site 43. Reconnaissance conductivity profile 43A crosses a barren area on rangeland.

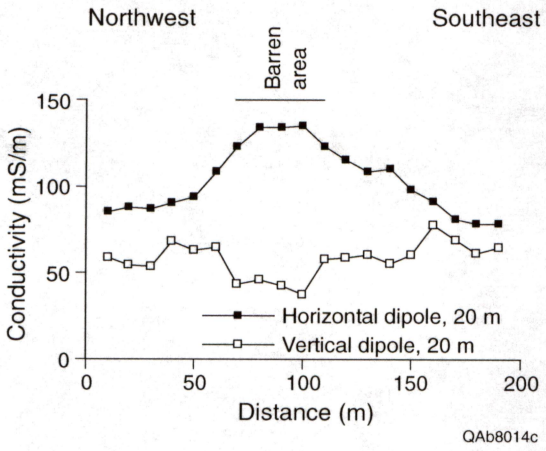

Figure 34. Apparent ground conductivity at site 43 using 20 m coil separation and horizontal and vertical dipole orientations. Line 43A crosses a barren area in a pasture from northwest to southeast.

loam, a relatively thick (to 1 m depth), noncalcareous soil in old alluvium (fig. 3). The mapped bedrock unit is the Clear Fork Group (fig. 2).

The well coincides with a magnetic anomaly (fig. 17) and a conductivity anomaly on the 56,000 Hz map (fig. 18). At the more deeply penetrating frequencies, there is a small conductivity high on the 7,200 Hz map (fig. 19) and no apparent anomaly on the 900 Hz map (fig. 20). A reconnaissance conductivity profile that crosses the well in an east-west direction (fig. 35) shows relatively low ground conductivities (fig. 36). There is no conductivity peak at the well, but horizontal dipole conductivity does gradually increase eastward (downslope toward Coyote Creek) from 65 mS/m at the west end of the line to 80 mS/m at the east end of the line.

Gradual increases in ground conductivity downslope without a peak near the abandoned well suggest that the well is not leaking and that the loss of elevation is decreasing the depth to saline water.

Site 51

Site 51 is located south of Hatchel (fig. 18) on an alluvial terrace on the west side of Coyote Creek. The active Cederholm B #2 well was drilled and completed on the terrace in 1994. Deep, clay loam to clay Rowena and Tobosa soils grade eastward across the site into deep Spur loam on the floodplain west of Coyote Creek (fig. 3). Beneath the thick surficial alluvial and eolian deposits are Clear Fork Group strata (fig. 2).

A magnetic anomaly is visible at the well site on the magnetic field map (fig. 17). Conductivities at the site are high on the 56,000 Hz, 7,200 Hz, and 900 Hz maps (figs. 18, 19, and 20), but are higher than nearby areas only on the 56,000 Hz map. Conductivities for the deeper penetrating 900 Hz data are uniform at the site, whereas the 7,200 Hz map shows increasing conductivities eastward.

Reconnaissance profile 51A extends northeastward from higher to lower floodplain elevations (fig. 37). This profile crosses over a barren area adjacent to the well that was probably disturbed during recent well drilling and completion activities. Horizontal dipole ground

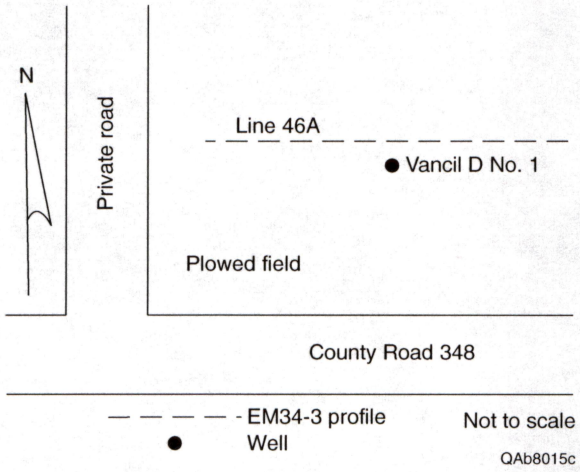

Figure 35. Sketch map of site 46. Reconnaissance conductivity profile 46A crosses the abandoned Vancil D #1 well.

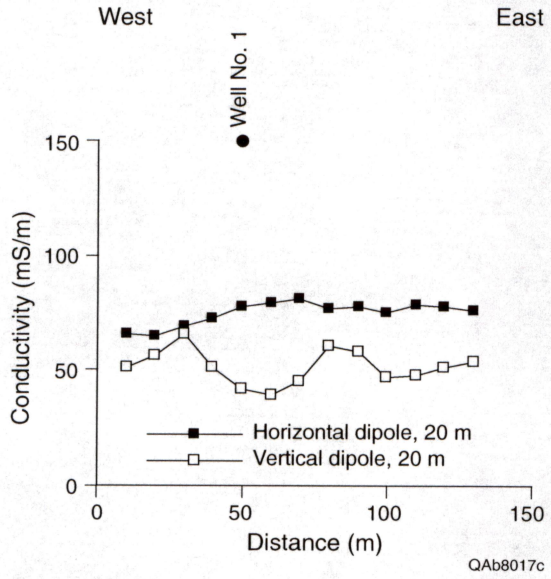

Figure 36. Apparent ground conductivity at site 46 using 20 m coil separation and horizontal and vertical dipole orientations. Line 46A crosses the abandoned Vancil D #1 well from west to east.

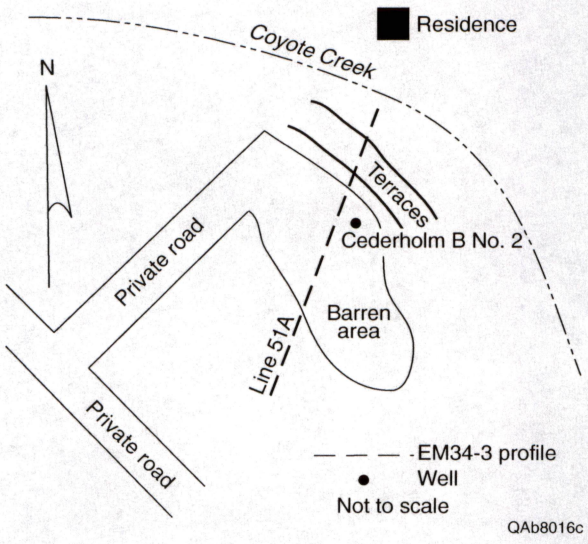

Figure 37. Sketch map of site 51. Reconnaissance conductivity profile 51A crosses the active Cederholm B #2 well and an adjacent barren area.

conductivities are relatively high at this site, but show no peak at either the barren area or the well (fig. 38). Conductivities decrease slightly from the upslope, southwest end of the line to the downslope, northeast end. This trend is similar to that observed in the 7,200 Hz airborne data (fig. 19).

Ground-based geophysical measurements suggest that this well is not leaking. The slight and gradual decrease in conductivity along line 46A toward Coyote Creek is best explained as an effect of decreasing clay content from the thick Rowena and Tobosa clay and clay loam soils at the southwestern end of the line to the thick, loamy Spur soils lower on the Coyote Creek floodplain at the northeastern end of the line.

Site 56

This site, located in the southwest part of the study area (fig. 18), was chosen based on its prominent airborne signature on the magnetic anomaly map (fig. 17) and the ground conductivity maps for all three frequencies (figs. 18, 19, and 20). The highly conductive area encloses the locations of two known wells: the Campbell #1, which was drilled and plugged in 1952, and the Campbell C #3, which was drilled in 1950 and plugged in 1962. Soil at the site are classified as moderately deep Portales clay loam (fig. 3), which grades downward into Clear Fork Group bedrock (fig. 2).

The airborne magnetic and conductivity anomalies at site 56 are oval-shaped and elongate in a north-south direction. The size of the conductivity anomalies decreases with increasing penetration depth and ranges from 160 by 240 m on the 56,000 Hz map (fig. 18) to 120 by 200 m on the 900 Hz map (fig. 20). Reconnaissance conductivity profile 56A was acquired at the plugged Campbell C #3 well within the anomalously conductive area (fig. 39). This profile indicates the presence of a broad conductive zone where horizontal dipole conductivities increase from 50 mS/m to more than 100 mS/m (fig. 40). Highest conductivities are observed about 10 m southwest of the C #3 well. Lower horizontal dipole values and higher vertical dipole values on

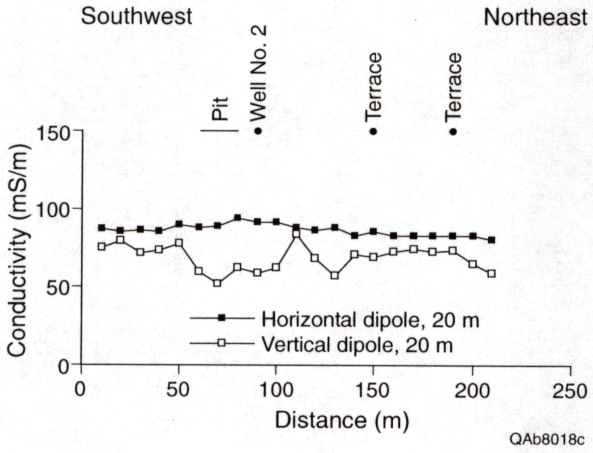

Figure 38. Apparent ground conductivity at site 51 using 20 m coil separation and horizontal and vertical dipole orientations. Line 51A crosses active #2 well from southwest to northeast.

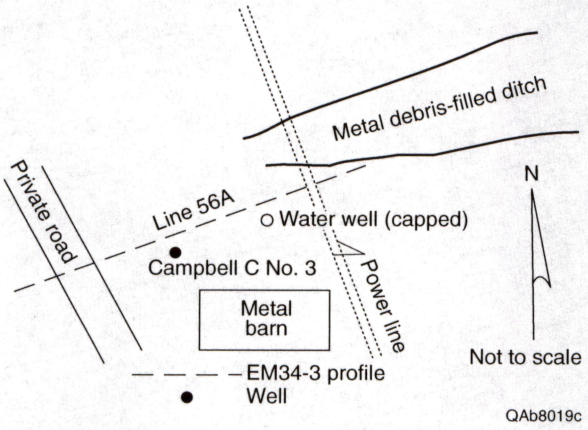

Figure 39. Sketch map of site 56. Reconnaissance conductivity profile 56A crosses the abandoned Campbell C #3 well and a nearby capped water well.

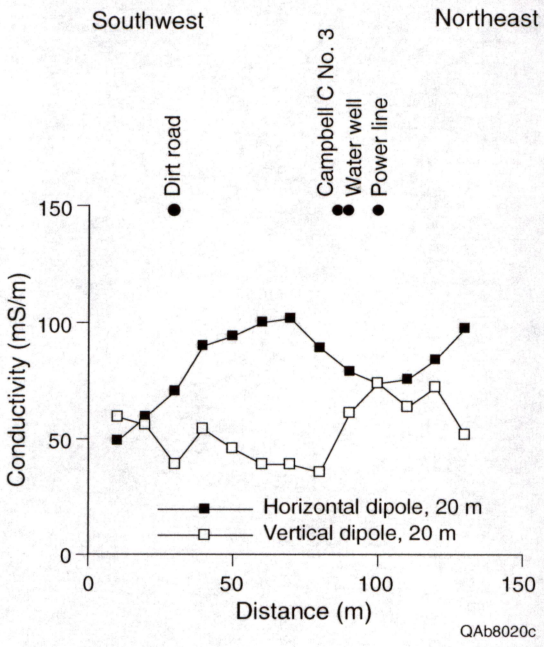

Figure 40. Apparent ground conductivity at site 56 using 20 m coil separation and horizontal and vertical dipole orientations. Line 56A crosses capped well Campbell C#3 and a capped water well from southwest to northeast.

the northeastern part of the profile are affected by an overhead power line. Actual ground conductivities in this area are likely to be as high or higher than those southwest of the C #3 well.

The presence of a large metal stock barn at this site probably enhanced both the magnetic and electromagnetic response in the airborne survey. Nevertheless, high conductivities detected in the ground-based survey near the C #3 well and the presence of a shallow water well that was recently capped because of high dissolved mineral content suggest that this well is leaking brine into the shallow subsurface.

Site 59

Site 59, located in the southwest part of the study area (fig. 18), is a short distance upslope from the Flag Branch of Elm Creek. The active Byler A-1 well, completed in 1980, falls within the airborne conductivity anomaly that defines the site. Soil is moderately deep Portales clay loam that is currently under cultivation (fig. 3). The Portales soil grades downward into Clear Fork Group strata (fig. 2).

The airborne survey detected a strong magnetic anomaly at the well site (fig. 17). Anomalously high conductivities are also present, particularly on the shallower (56,000 Hz) and deeper (900 Hz) conductivity maps (figs. 18 and 20), where the anomalies cover an area about 140 m wide. High conductivities are not as well expressed on the 7,200 Hz map (fig. 19).

Two ground-based conductivity profiles, lines 59A and 59B (fig. 41), pass near the A-1 well. Horizontal dipole ground conductivities on line 59A increase toward the well from background values of 60 mS/m about 60 m west of the well to more than 100 mS/m at the well (fig. 42a). The zone of elevated conductivity is about 110 m wide, similar to the width of the anomaly observed on the airborne maps. An operating pumpjack and a nearby power line disturb the vertical dipole readings near those features. Line 59B, oriented northwest-southeast, passes west of the well (fig. 42b). This line shows no sharp peak in the horizontal dipole mode at the well, but the vertical dipole data suggest the presence of a buried pipeline that may influence the

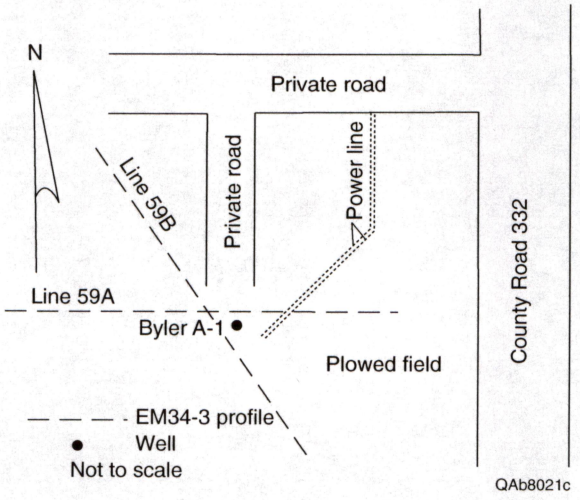

Figure 41. Sketch map of site 59. Reconnaissance conductivity profiles 59A and 59B cross the active Byler A-1 well in a cultivated field.

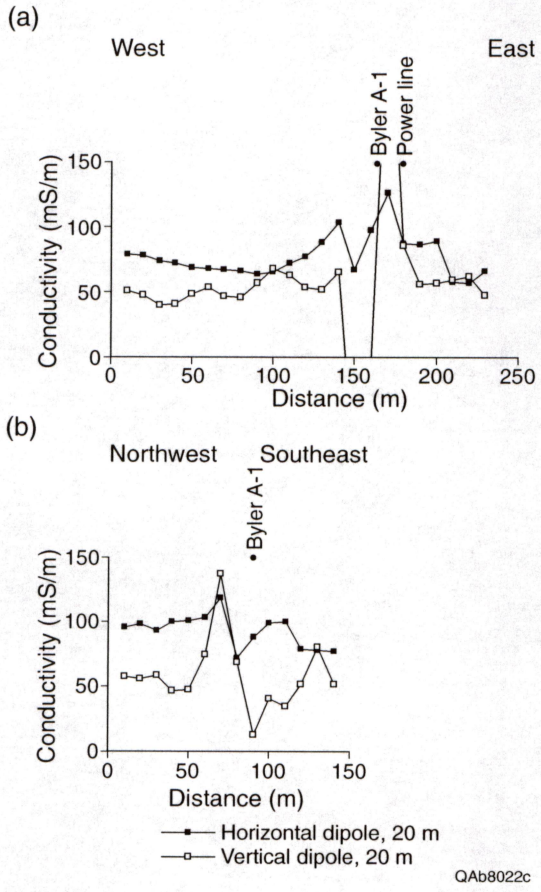

Figure 42. Apparent ground conductivity at site 59 using 20 m coil separation and horizontal and vertical dipole orientations. Line 59A (a) crosses the active Byler A-1 well from west to east and line 59B (b) crosses A-1 well from northwest to southeast.

results. Ground conductivities are higher near the well than background values at the southeastern end of line 59B or the western end of line 59A (fig. 42a and b).

Conductivity peaks at site 59 on the shallow- and deep-focus airborne data and a broadly-defined conductivity peak centered on the well on line 59A suggest that brine is entering or has recently entered the shallow subsurface at the Byler A-1 well. Conversely, the lack of a definite anomaly on the moderate-depth 7,200 Hz map and the presence of cultural noise (operating pump jack and overhead power lines) suggest that the well may not be leaking. This well should be considered a suspect well that may or may not be leaking brine.

Site 74

This site is located in a cultivated field in the southwest part of the study area where moderately deep Portales clay loam grades downward into Clear Fork Group strata (figs. 2 and 3). The site is defined by a marked conductivity anomaly on the 56,000 Hz map (fig. 18) that coincides with a minor magnetic anomaly (fig. 17). Slightly elevated conductivities are also observed at the site on the deeper 7,200 Hz and 900 Hz conductivity maps (figs. 19 and 20). There is no RRC record of a well having been drilled at this site, but a plugged well that may be mislocated is shown east of site 74.

A portable magnetometer survey of the site by RRC staff located a buried well casing and an adjacent mud pit in the field (fig. 43). Aerial photographs of the site taken in 1970 also show the well. Reconnaissance conductivity profiles acquired across the well site and mud pit indicated moderate ground conductivities of 70 to 80 mS/m that decrease gradually to the east on line 74A (fig. 44a) and to the north on line 74B (fig. 44b), but no peak is apparent at the well or the pit.

Conductivity anomalies that decrease in intensity downward on airborne maps and the lack of elevated ground conductivities that peak near the well imply that this well is probably not leaking. Elevated conductivities evident on the shallow 56,000 Hz map may be related to brine discharged into the pit during well drilling.

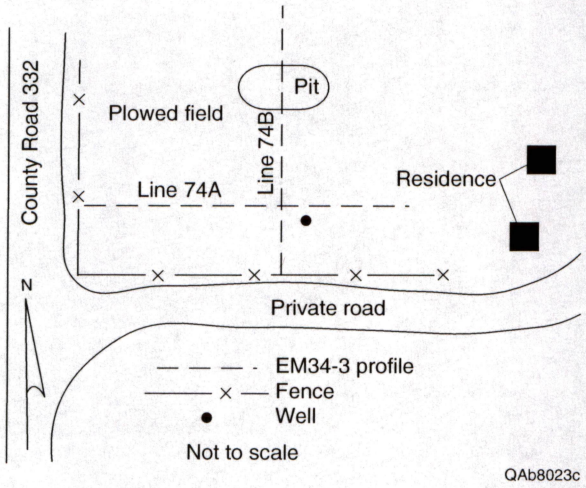

Figure 43. Sketch map of site 74. Reconnaissance conductivity profiles 74A and 74B cross an abandoned well site and mud pit in a cultivated field.

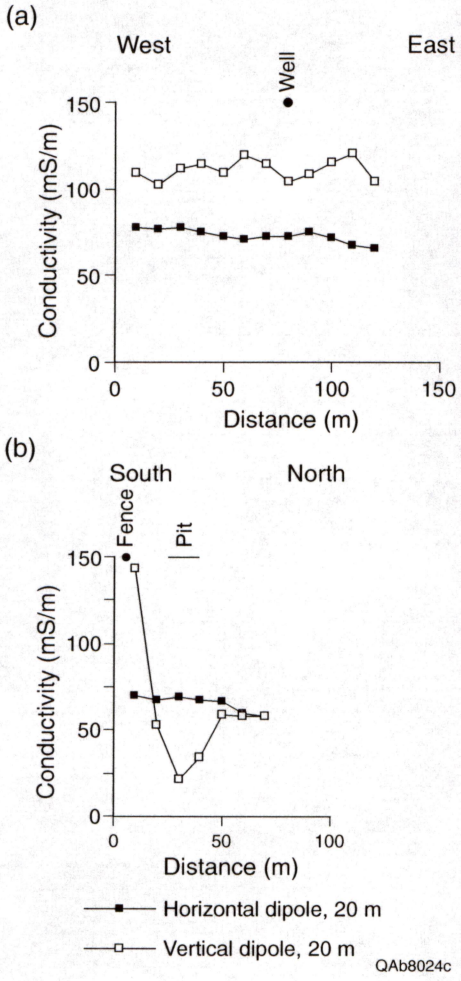

Figure 44. Apparent ground conductivity at site 74 using 20 m coil separation and horizontal and vertical dipole orientations. Line 74A (a) crosses an abandoned well from west to east. Line 74B (b) crosses a surface pit from south to north about 20 m west of well.

Site 75

This site is located on rangeland in the northwest part of the study area and is defined by a weak anomaly visible on the 56,000 Hz conductivity map (fig. 18). The Vancil B #1 well, which was drilled in 1968 and plugged in 1982, and the pipe stacked at the well site are the apparent source of a magnetic anomaly (fig. 17) at the site. Thin soils classified as Mereta clay loam grade downward into thin Quaternary surficial deposits atop Clear Fork bedrock (figs. 2 and 3).

No anomaly is visible on the deeper conductivity maps (figs. 19 and 20). One ground-based conductivity profile, line 75A, crosses the abandoned well site from west to east (fig. 45). Ground conductivities at and adjacent to the well are between 60 and 70 mS/m (fig. 46), which is within the background range observed at other sites.

Lack of elevated ground conductivities near the well and the presence of relatively low conductivities on the deeper conductivity maps allow us to conclude that this well is not leaking. Elevated conductivities near the well in the shallow subsurface may be related to brine discharged at the surface during drilling or operation of the well.

Type CM Sites

Type CM sites are those where a conductivity anomaly (C) and a magnetic anomaly (M) coincide, but there is no mapped well. These sites are important because their airborne signature alone could be interpreted to represent unknown or mislocated oil or gas wells that are leaking brine. Ground-based geophysical methods (reconnaissance conductivity profiles, multiple-coil-separation profiles, or time-domain soundings) were employed at 4 of the 15 CM sites identified to determine the cause of the airborne signatures.

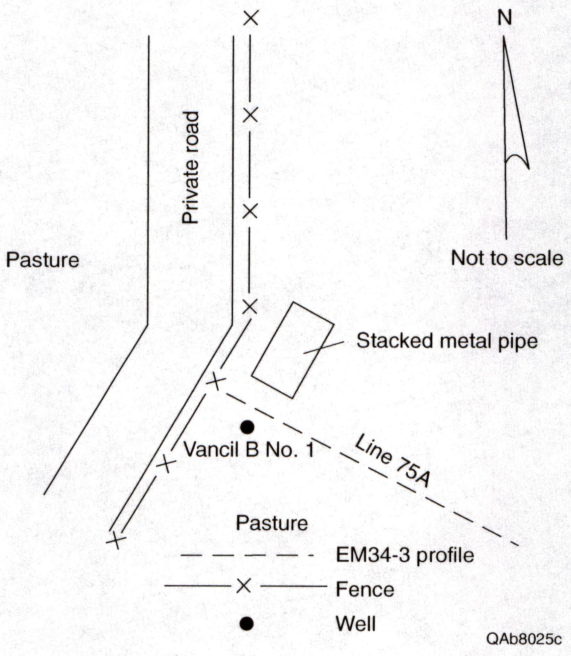

Figure 45. Sketch map of site 75. Reconnaissance conductivity profile 75A crosses the abandoned Vancil B #1 well.

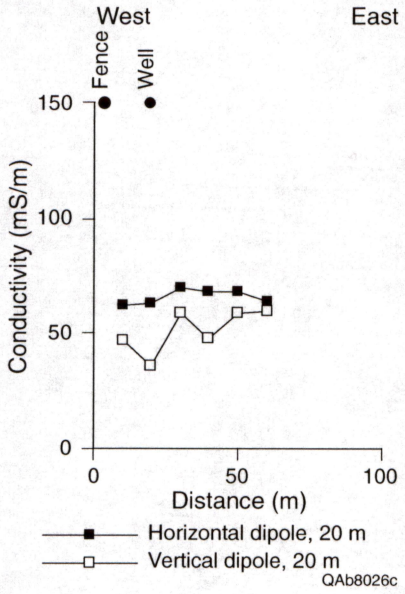

Figure 46. Apparent ground conductivity at site 75 using 20 m coil separation and horizontal and vertical dipole orientations. Line 75A crosses abandoned well #1B from west to east.

Site 17

This site (and the adjacent site 18) is located on the east side of the study area along a tributary of Mud Creek and is defined by a large conductivity anomaly on the 56,000 Hz map (fig. 18). The conductivity anomaly is elongate in a northwest-southeast direction and measures about 200 m by 400 m. There is a coincident magnetic anomaly (fig. 17), but conductivities on the deeper 7,200 Hz and 900 Hz maps are not anomalously high (figs. 19 and 20).

Aerial photographs and site visits revealed that the conductivity anomaly extends northwestward from an abandoned surface pit near the active Williams #1 well. Adjacent to the pit to the northwest (downslope toward the creek) is an area that is barren of vegetation (fig. 47). Soils within the boundaries of site 18 are classified as either the moderately deep Valera silty clay, the shallow Kavett silty clay, or the moderately deep Tobosa clay (fig. 3). These soils all overlie Clear Fork Group limestone (fig. 2).

Ground-based geophysical investigations at this site consisted of two reconnaissance profiles, two multiple-coil-separation profiles, and three TDEM soundings (fig. 48). The reconnaissance profiles (lines 17A and 17B, fig. 49) confirmed the presence of a conductivity peak centered on the brine pit and adjacent barren zone. Horizontal dipole conductivities increased from background levels of 50 to 60 mS/m at distances of 100 m northwest of the pit to 150 mS/m at the pit (fig. 49a). Line 17B, which crosses the barren area west of the pit and extends southward to the active well at site 18, indicates lower peak horizontal dipole conductivities (110 mS/m) and a broader zone of elevated conductivity (fig. 49b). The total width of the conductive zone is greater than 140 m northwest-southeast and is about 200 m north-south.

As coil separation (and thus exploration depth) increases, multiple-coil-separation profiles 17C (fig. 50a) and 17D (fig. 50b) show that ground conductivity decreases for the horizontal dipole mode. Conductivity reaches a peak of 220 mS/m for the 10-m coil separation (6 m exploration depth), 160 mS/m for the 20-m coil separation (12 m exploration depth), and

Figure 47. Vegetation kill area adjacent to abandoned surface brine disposal pit, site 17.

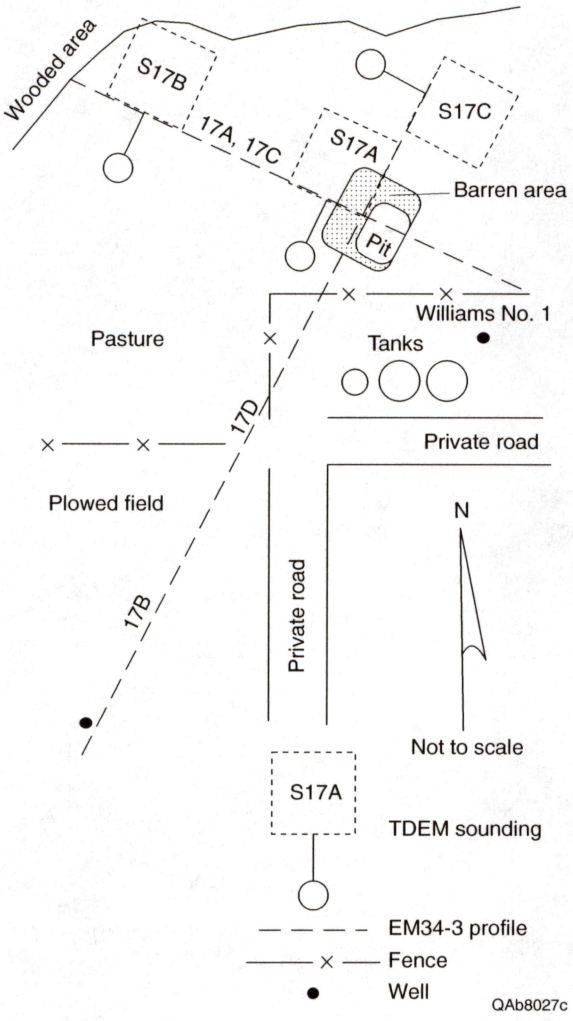

Figure 48. Sketch map of sites 17 and 18. Site 17 includes the surface pit on the northern part of the map; site 18 includes the well on the southern part of the map. Two reconnaissance conductivity profiles (17A and 17B), two multiple-coil-separation profiles (17C and 17D), and three time-domain electromagnetic soundings (S17A, S17B, and S17C) were acquired near the surface pit.

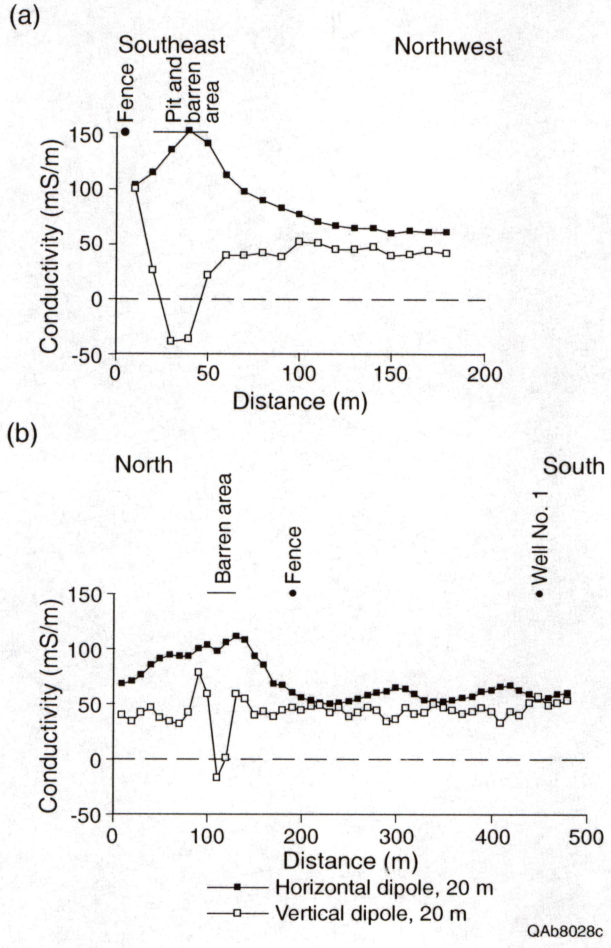

Figure 49. Apparent ground conductivity at sites 17 and 18 using 20 m coil separation and horizontal and vertical dipole orientations. Line 17A (a) crosses an inactive pit and adjacent barren area from southeast to northwest and line 17B (b) crosses the barren area from north to south and extends southward to the Edmondson #1 well.

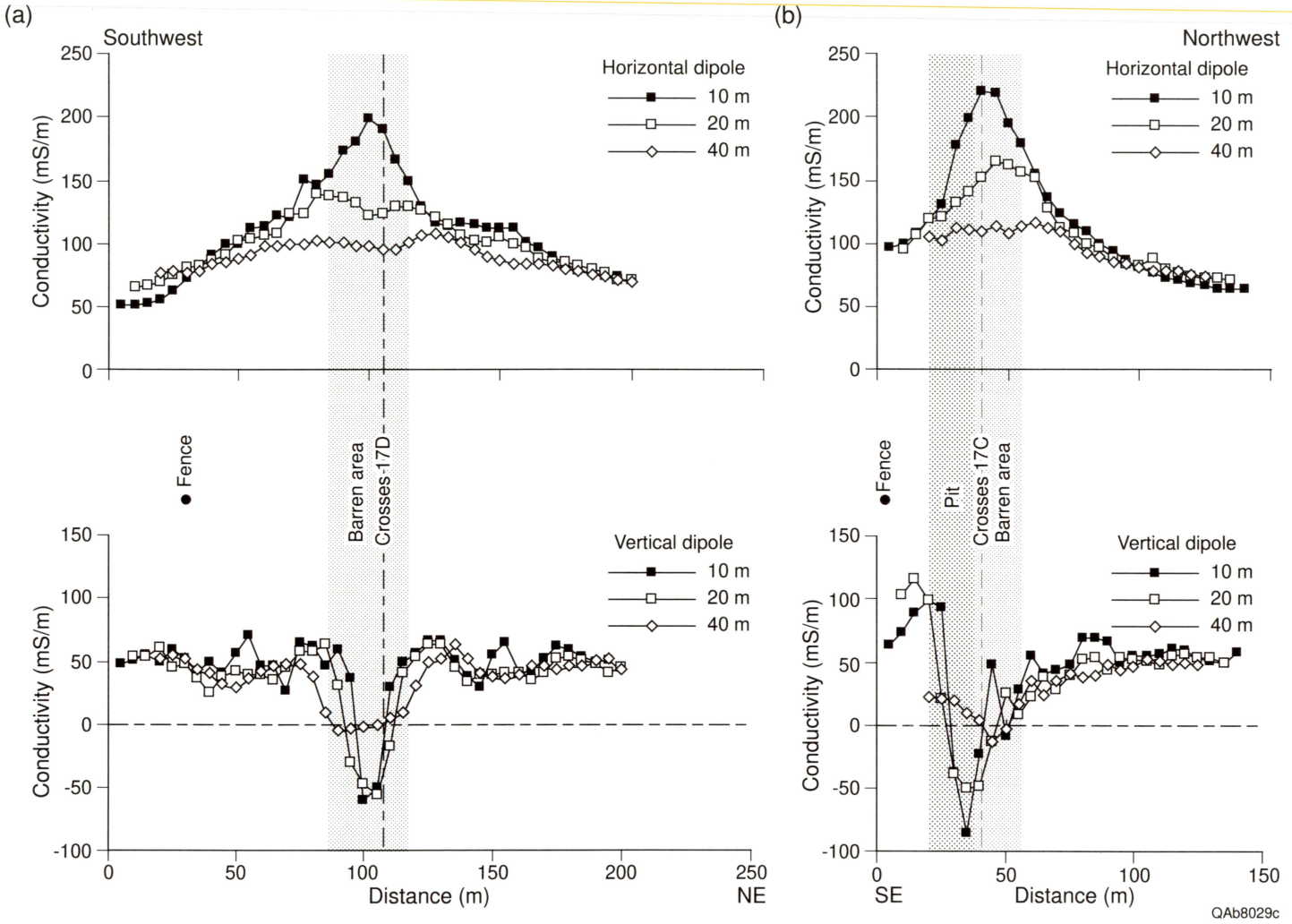

Figure 50. Apparent ground conductivity at site 17 using multiple coil separations (10, 20, and 40 m) and horizontal dipole (upper plot) and vertical dipole (lower plot) orientations. Line 17C (a) crosses barren area adjacent to surface pit from southwest to northeast. Line 17D (b) crosses pit and barren area from southeast to northwest.

110 mS/m for the 40-m coil separation (24 m exploration depth). Peak conductivities on line 17D, which crosses the pit and the barren area from southeast to northwest, are offset to the northwest (downslope) of the pit. Ground conductivities away from the peaks on both lines show little variation with increasing coil separation.

Decreasing ground conductivities accompany increasing coil separation and imply that ground conductivities decrease with depth near the surface pit. Support for this observation is provided by three TDEM soundings acquired at and near the pit. These soundings have transient decay shapes that are generally similar (fig. 51), but differ the most at early times (or shallow depths). Deeper than 10 to 20 m below the surface, resistivities are about 10 ohm-m at the three sites. Closer to the surface, thin conductive layers overlie a more resistive layer. The conductive layers are thickest (7 m) and least resistive (2 to 7 ohm-m) at S17A (fig. 51a), which was acquired closest to the brine pit and barren area. Thicknesses of the surface conductive layer decrease to about 5 m and resistivities increase to the 5 to 7 ohm-m range at soundings S17B (fig. 51b) and S17C (fig. 51c), which are located farther from the brine pit.

Airborne data and on-the-ground geophysical surveys and visual observations support the interpretation that brine has infiltrated the shallow subsurface at site 17 and is migrating northwestward (downslope). Infiltration depths are probably 5 to 7 m. Decreasing conductivities with depth imply a surface brine source. The presence of a surface pit with an adjacent barren area that coincides with a ground conductivity peak suggests that brine has been discharged to the pit and subsequently infiltrated the shallow subsurface.

Site 25

Site 25 lies on the southern edge of a larger area of anomalously high ground conductivity in the southeastern part of the study area (fig. 18). The anomalously conductive area is most extensive on the 56,000 Hz conductivity map, where it is elongate in a north-northeasterly direction and measures 2.4 km long by 0.8 km wide. The area is also anomalously conductive on the 7,200 Hz map (fig. 19), but covers a smaller area that is 1.4 km long and 0.6 km wide.

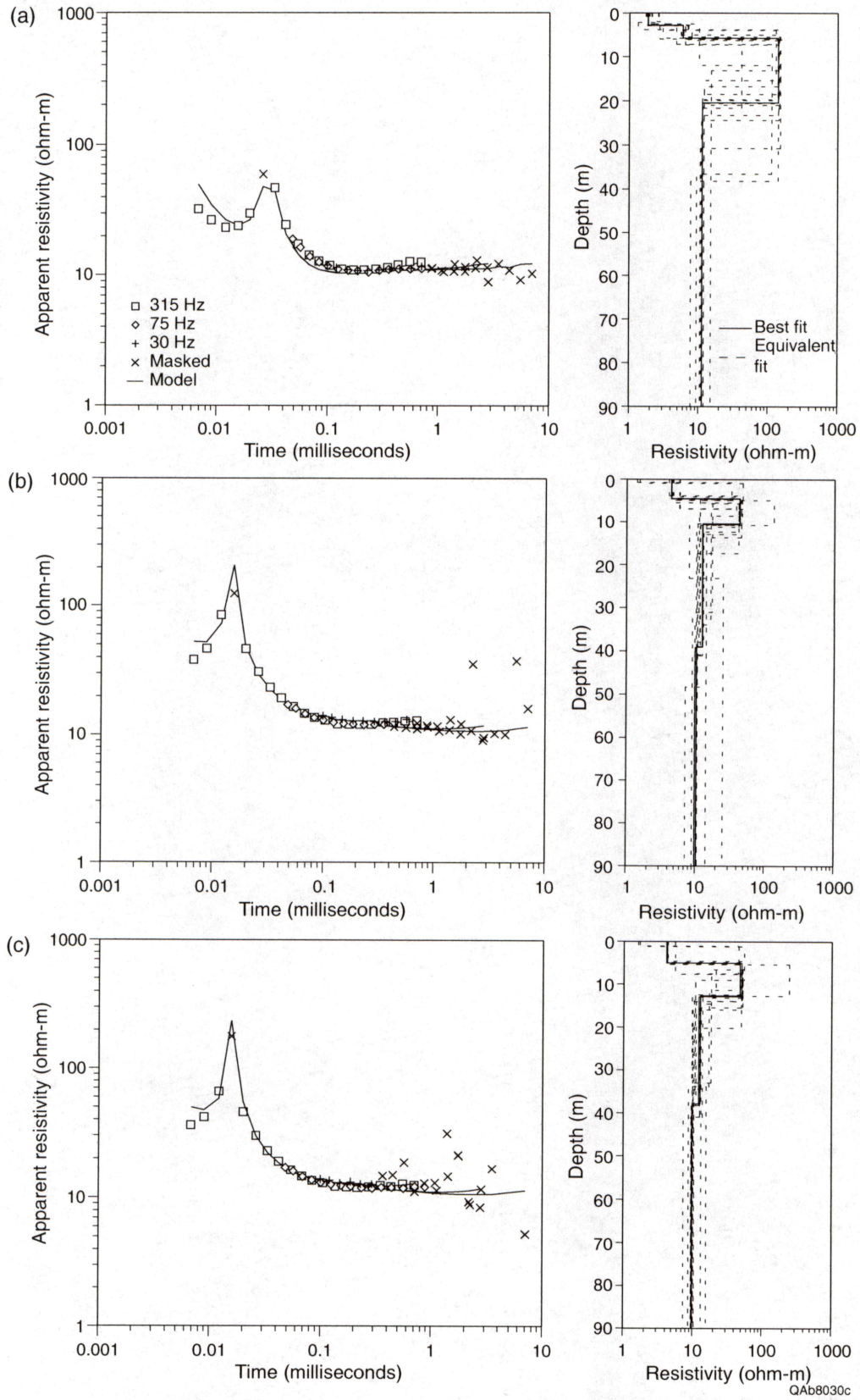

Figure 51. Transient decay curve (left) and resistivity models (right) at time domain sounding sites 17A (a), 17B (b), and 17C (c). Resistivity model with solid line represents the model with the lowest fitting error; dashed lines represent models that have fitting errors within 10 per cent of the best model.

Ground conductivity is not anomalously high on the deeper exploring 900 Hz map (fig. 20). Many magnetic anomalies are located on or near site 25 (fig. 17).

The conductive area that includes site 25 is on the hill top, hill slope, and alluvium east of Elm Creek. Soils on the hill are mapped as Talpa clay loam and Kavett silty clay (fig. 3), both of which are very shallow and grade downward into limestone and marl of the Clear Fork Group (fig. 2). On the valley floor, deep Tobosa clay soil has formed on Quaternary alluvial deposits. At least four wells were located at site 25 (fig. 52): the Beddo B #4, drilled and plugged in 1951; the Beddo A #3, drilled and abandoned in 1956; the Beddo #2, drilled and plugged in 1947; and the Beddo #1, drilled in 1938 and plugged in 1946. Records are insufficient to determine the adequacy of plugging in these wells.

Three reconnaissance conductivity profiles were acquired that passed near the known wells. Line 25A (fig. 53a) began on the eastern hill slope at the B #4 well, extended over the hill top near the A #3 well, turned westward toward the #2 well on the western hill slope, and ended at the base of the hill at the eastern edge of the Elm Creek valley floor. This line shows background horizontal dipole conductivity values near the #4 well that increase to about 110 mS/m in a barren hill top area near the A #3 well (fig. 53a). Down the hill slope, conductivities are near background values at the #2 well, but increase downslope to about 120 mS/m in a barren area on the lower parts of the hill. Lowest conductivities (below 50 mS/m) are observed at the base of the hill.

Line 25B, which begins at the hill top and extends downslope and northwestward past the #1 well (fig. 53b), shows no conductivity peak at the well. Horizontal dipole conductivity gradually increases downslope and reaches a peak of about 120 mS/m at a hill slope level near that of the hill slope peak on line 25A. Line 25C begins at the hill top, passes well A #3 and a barren area at an old tank battery site, and extends down the hill slope to the south. Highest horizontal dipole conductivities, nearly 150 mS/m, are found at the barren tank battery, not the A #3 well.

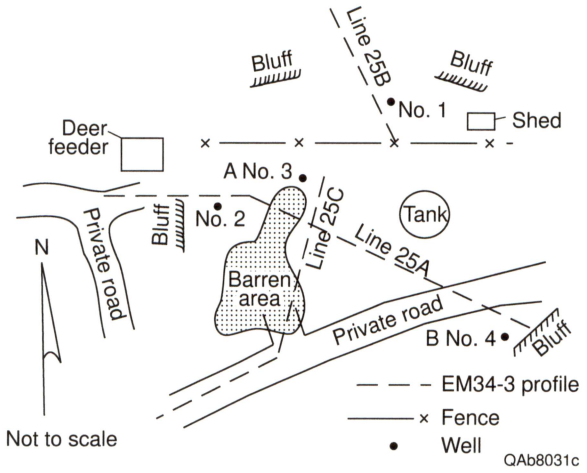

Figure 52. Sketch map of site 25. Three reconnaissance conductivity profiles (25A, 25B, and 25C) pass near the four known wells at this site.

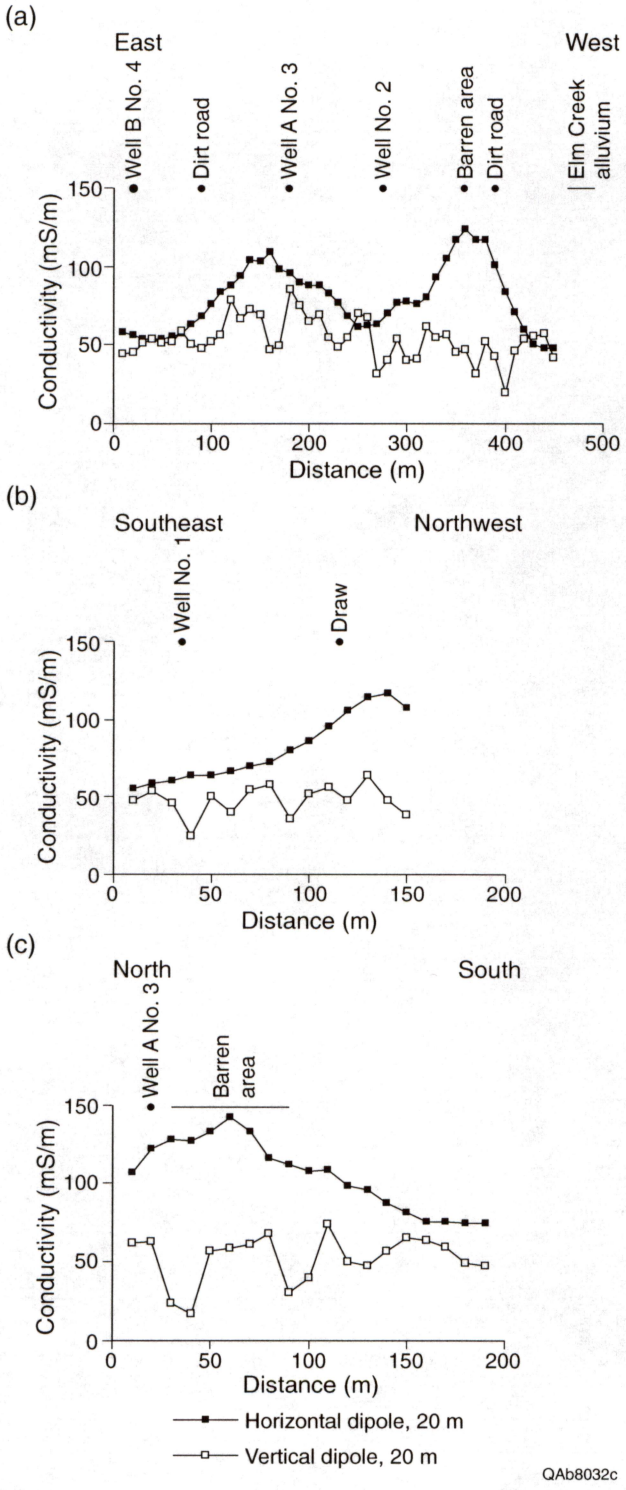

Figure 53. Apparent ground conductivity at site 25 using 20 m coil separation and horizontal and vertical dipole orientations. Line 25A (a) crosses abandoned wells B #4, A #3, and #2, line 25B (b) crosses well #1, and line 25C (c) crosses well A #3 and an adjacent barren area.

The four wells examined at site 25, with the possible exception of well A #3, are probably not leaking significant volumes of brine. The conductivity peak at the top of the hill is most likely related to brine discharge from storage batteries or into surface pits. The conductivity peak observed on the lower part of the hill slope on lines 25A and 25B may represent lateral leakage through relatively permeable bedrock units that intercept brine moving upward along either natural conduits or unplugged well bores. Alternatively, these peaks may represent natural conductivities of clay-rich marl units within Clear Fork Group strata.

Site 61

This site, located on the Waller farm south of Hatchel, extends from the banks of Coyote Creek to the middle of a cultivated field east of the creek. Airborne data show a high conductivity anomaly on the 56,000 Hz map (fig. 18), high conductivities that decrease eastward from the creek on the 7,200 Hz map (fig. 19), and high but not anomalous conductivities on the 900 Hz map (fig. 20). Magnetic anomalies are present at the site but are associated with power lines or structures and not wells (fig. 17).

Two reconnaissance conductivity profiles were acquired at the site. Line 61A began on bottomland at the creek and extended eastward into a cultivated field (fig. 54), passing from deep Colorado loam and Yahola fine sandy loam soils on Quaternary alluvial deposits into shallow Mereta clay loam soils on the valley wall and ending in deep Rowena clay loam and Tobosa clay in the cultivated field (fig. 3). Both the soils and the Quaternary alluvial deposits overlie Clear Fork Group strata (fig. 2), which are closest to the surface on the Coyote Creek valley wall.

Ground conductivities along line 61A generally decrease eastward (fig. 55a) in a pattern similar to that visible on the 7,200 Hz airborne map. Highest horizontal dipole conductivities of about 90 mS/m were measured nearest the creek and remained at 80 mS/m across the valley floor and wall west of the fence. Conductivities decreased to about 60 mS/m in the clay and clay loam soils on the cultivated field. Line 61B, located farther east in the field where the landowner

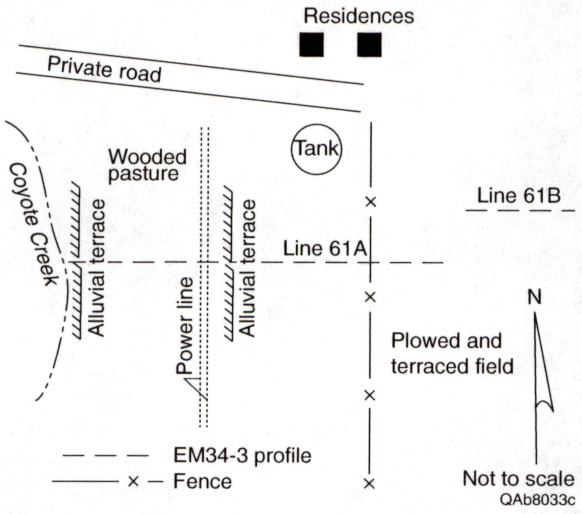

Figure 54. Sketch map of site 61. Reconnaissance conductivity profile 61A extends eastward from Coyote Creek across alluvial terraces. Profile 61B is in a plowed field.

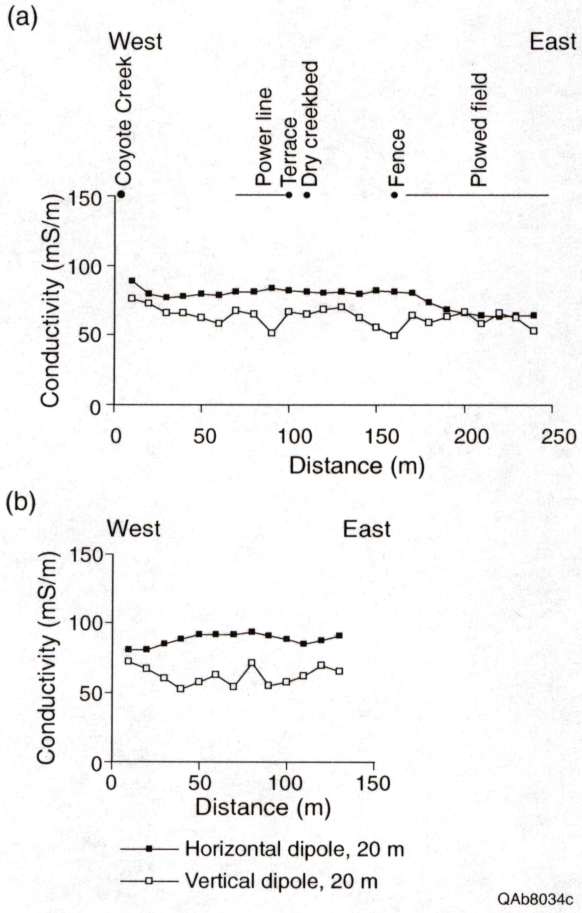

Figure 55. Apparent ground conductivity at site 61 using 20 m coil separation and horizontal and vertical dipole orientations. Line 61A (a) crosses Coyote Creek alluvial terraces and a plowed field from east to west and line 61B (b) crosses a plowed field from west to east.

reported stunted crop growth related to soil salinity (fig. 54), does show higher horizontal dipole ground conductivities of 80 to 100 mS/m (fig. 55b).

There are no wells mapped on this site and no surface evidence of unknown or mislocated wells. High ground conductivities on line 61B were found adjacent to a field terrace and are probably related to enhanced recharge at the terrace, a water table that is locally rising, and evaporative concentration of dissolved salts near the surface. Elevated conductivities measured in the Coyote Creek valley on ground and deeper airborne surveys are probably the combined effects of infiltrating saline creek water and brine migrating upward into Coyote Creek alluvium along natural fracture or pore space conduits.

Site 71

Site 71 is located near an abandoned homestead southeast of Hatchel. An anomaly at the site is visible on the shallow (56,000 Hz) conductivity map (fig. 18) and the magnetic field map (fig. 17). Maps of ground conductivity at deeper levels show slightly anomalous values at 7,200 Hz (fig. 19) and background values at 900 Hz (fig. 20). No nearby wells are mapped. Thin Mereta clay loam and thicker Portales clay loam soils cover the area (fig. 3), which is cultivated in places. These soils grade downward into thin Quaternary deposits that cover Clear Fork Group strata.

Two reconnaissance conductivity profiles cross the site in an east-west (line 71A) and north-south (line 71C) direction (fig. 56). Line 71A shows low, background conductivities (less than 50 mS/m) on the grassland at the east end of the line, a horizontal dipole conductivity peak of about 125 mS/m in the middle of the cultivated field, and a return to background conductivity values westward across the homestead (fig. 57a). Northward from the county road on line 71C (fig. 57b), horizontal dipole conductivities again increase to a peak of 125 mS/m and decline northward to background values of 50 to 60 mS/m. Peak conductivity values on both lines were found in an area barren of vegetation. A magnetometer survey by RRC staff at and adjacent to

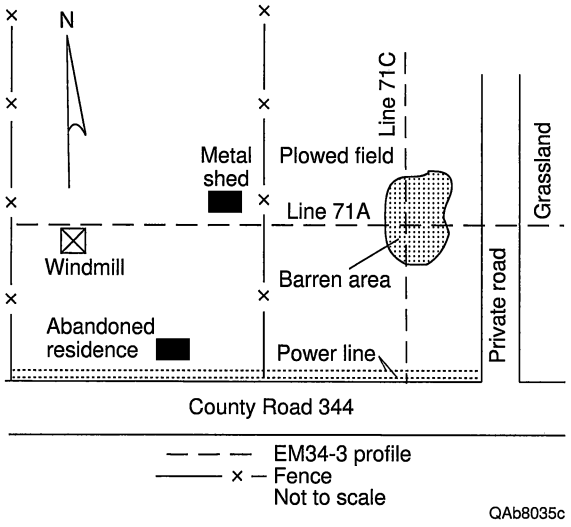

Figure 56. Sketch map of site 71. Reconnaissance conductivity profiles 71A and 71C cross a barren area in a cultivated field near an abandoned homestead.

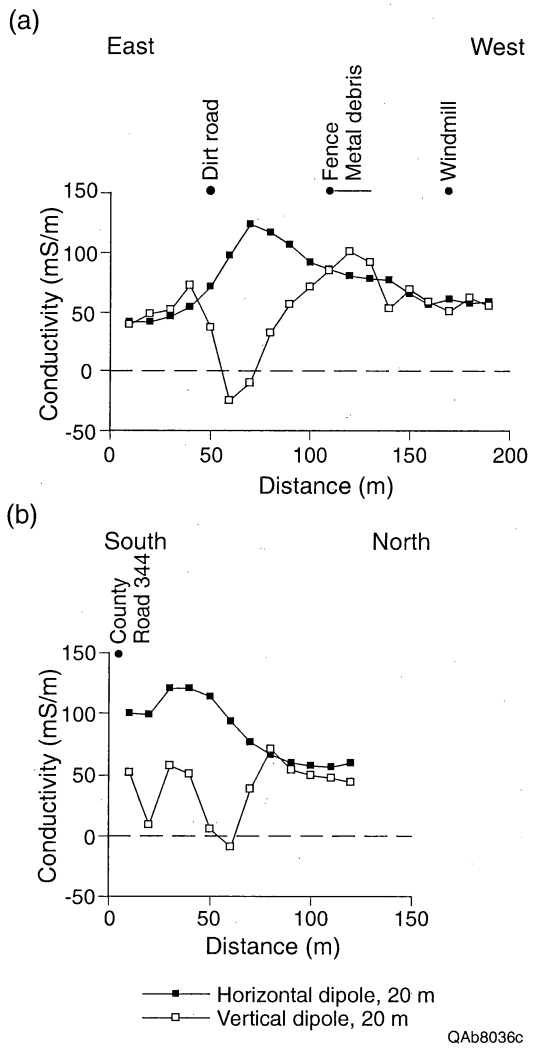

Figure 57. Apparent ground conductivity at site 71 using 20 m coil separation and horizontal and vertical dipole orientations. Line 71A (a) crosses an abandoned oilfield facility, homestead, and windmill from east to west. Line 71B (b) crosses the abandoned oilfield facility from south to north.

the barren area (fig. 9) failed to locate buried well casing, but did locate numerous scattered metallic objects.

On airborne and ground-based geophysical evidence alone, one might conclude that there is an unlocated buried well near the barren area. Aerial photographs show that oilfield tanks were installed at this site between 1940 and 1970 and have since been removed. No evidence of a well was found, either on aerial photographs or during inspections at the site. Brine has probably entered the shallow subsurface from spillage or leakage from the tanks while they were in operation.

Type CW Sites

Type CW sites are those where a conductivity anomaly (C) and a known well location (W) coincide, but there is no magnetic anomaly. These sites are potentially important because their airborne signature combined with the knowledge that there is a well at the site could be interpreted to mean that the well has no casing and may be likely to leak. Ground-based reconnaissance conductivity profiles were acquired at five of the 14 CW sites identified to determine the cause of the airborne signatures.

Site 12

Located in the northeast part of the study area, site 12 was chosen for reconnaissance profiling because it has two known wells with no associated magnetic anomaly (fig. 17) and high conductivity anomalies on the 56,000 Hz and 7,200 Hz airborne maps (figs. 18 and 19). No 900 Hz anomaly is apparent (fig. 20). Soils at the site are classified as Portales clay loam and Potter clay loam (fig. 3), which consist of thin clay loam overlying pedogenic carbonate. These soils grade downward into Permian Clear Fork Group rocks (fig. 2).

Two reconnaissance geophysical profiles were acquired at site 12 (fig. 58). Line 12A extends east-west across the abandoned McMillan #7 well. Line 12B extends north-south across

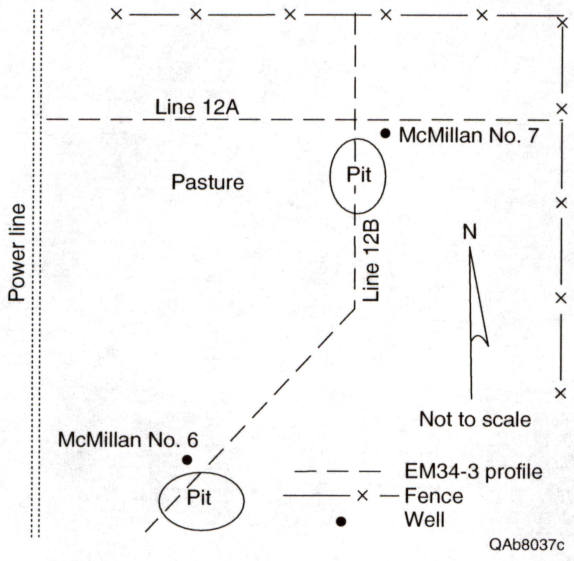

Figure 58. Sketch map of site 12. Two reconnaissance conductivity profiles (12A and 12B) cross the abandoned McMillan #6 and #7 wells and adjacent surface pits.

the #7 well and an adjacent disposal pit, then turns southwestward to cross the abandoned McMillan #6 well and its adjacent disposal pit. RRC records indicate that the #6 well was drilled in 1934 and plugged in 1942 and that the #7 well was drilled in 1935.

No conductivity peaks were found centered on either of the two wells at site 12 (fig. 59). For the horizontal dipole data at 20 m coil separation, the highest conductivities were just above 100 mS/m in two areas: 30 m east of well #7 on line 12A (fig. 59a) and 35 to 45 m south of well #7 on line 12B (fig. 59b). The broad conductive zone south of well #7 extends 90 m downslope (south) of the well. Highest conductivities in this zone are located adjacent to the well #7 disposal pit. Horizontal dipole ground conductivities near the McMillan #6 well are relatively low (50 to 60 mS/m) both near the well and across the adjacent disposal pit (fig. 59b).

Neither well has surface evidence of brine leakage. Well #6, which RRC records show to have been plugged, has no ground-based geophysical evidence of leakage and is probably not leaking. Elevated conductivities near well #7, which are visible in both airborne and ground-based geophysical data, suggest that there is salt water in the ground near this well. The presence of a conductivity peak adjacent to the associated disposal pit rather than at the well implies that brine discharged into the pit is the likely source of elevated conductivities at this site.

Site 13

Site 13 is located in the northeast part of the study area (fig. 18) and is on the north side of Mud Creek. Two old wells fall within the site: the McMillan #1 well, drilled in 1932 and plugged in 1936, and the McMillan #4 well, drilled in 1934 and plugged in 1936 (fig. 60). The #1 well is situated on a slope above the creek that has thin Portales clay loam soil grading downward into Clear Fork Group strata (figs. 2 and 3). The #5 well is nearer the creek, where Colorado loam and Yahola fine sandy loam soils are mapped on Quaternary alluvium.

A conductivity anomaly is visible at the site on the shallow 56,000 Hz map (fig. 18). This anomaly diminishes greatly on the deeper 7,200 Hz map (fig. 19) and is absent on the deepest 900 Hz map (fig. 20). Despite the presence of the two wells, no magnetic anomaly coincides with

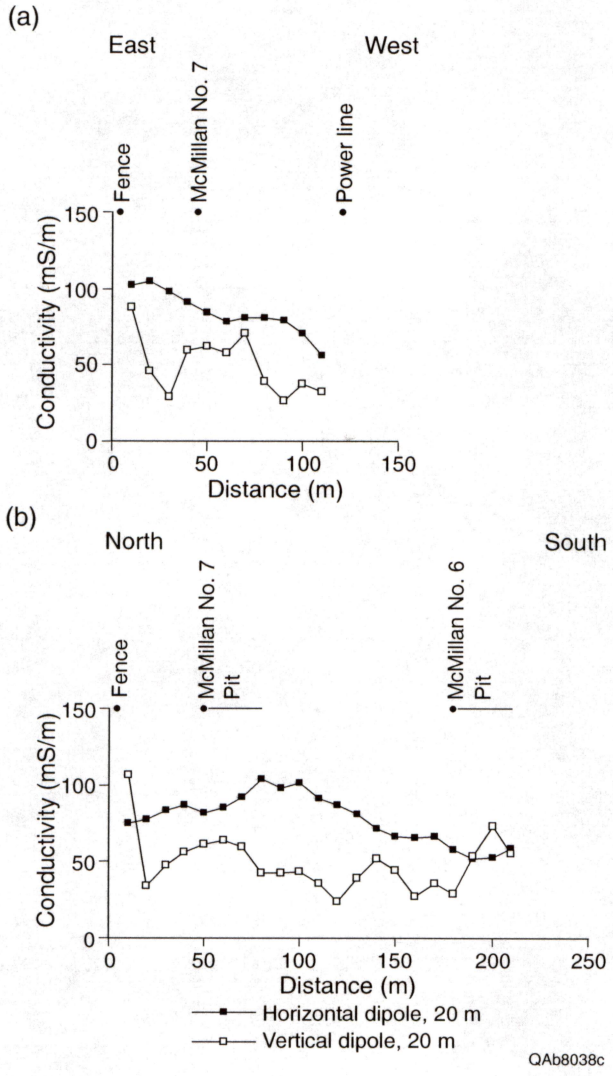

Figure 59. Apparent ground conductivity at site 12 using 20 m coil separation and horizontal and vertical dipole orientations. Line 12A (a) crosses abandoned McMillan #7 well from east to west and line 12B (b) crosses McMillan #7 and #6 wells from north to south.

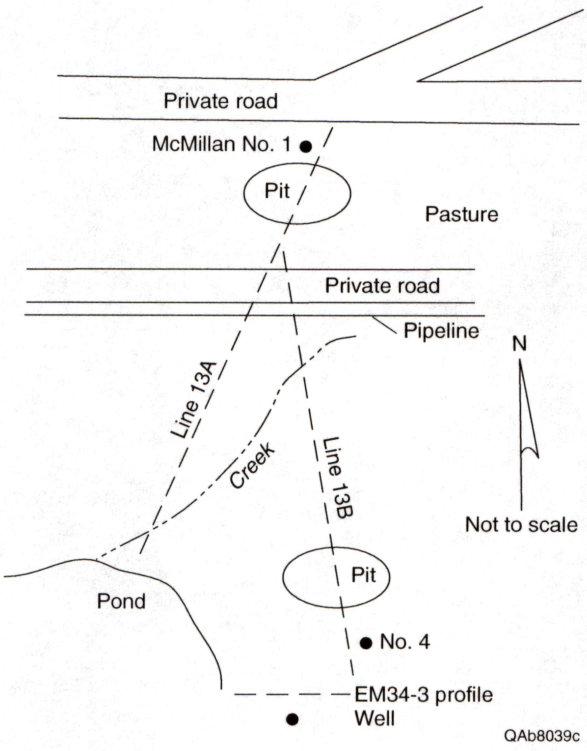

Figure 60. Sketch map of site 13. Reconnaissance conductivity profiles 13A and 13B pass near the McMillan #1 and #4 wells in rangeland on the north side of Mud Creek.

the well locations (fig. 17). On-the-ground magnetometer surveys of the two abandoned well sites did locate buried well casing.

Line 13A, a ground-based conductivity profile that passes from upslope of the McMillan #1 well to the edge of a pond on Mud Creek, measured relatively low horizontal dipole ground conductivities of 50 to 70 mS/m (fig. 61a). No peak was found near the #1 well or its adjacent pit. Horizontal dipole conductivities were also relatively low (45 to 60 mS/m) along line 13B, which crossed the #4 well and an adjacent pit. Large fluctuations in the vertical dipole measurements were recorded near a buried pipeline on both lines.

Ground conductivity profiles that show no peaks at the wells, no surface evidence of brine leakage, and airborne conductivity maps that show decreasing conductivities with depth all suggest that these two wells are not leaking brine. This site is one where the importance of ground surveys is evident. The site was interpreted from the airborne signature to be one where existing old wells might have no casing, yet ground-based magnetometer and electromagnetic surveys located the well casings and established that the wells are not leaking.

Site 16

Site 16 encompasses an old abandoned well in a cultivated field on the south side of Mud Creek. The airborne signature of this site consisted of a strong shallow anomaly on the 56,000 Hz map (fig. 18) that weakens on the 7,200 Hz map (fig. 19) and is absent on the 900 Hz map (fig. 20). There is no magnetic anomaly at the site, although ground investigations revealed the presence of concrete blocks and well debris associated with the McMillan #3 well. This well was drilled in 1928. Deep Olton clay loam soil covers the site and overlies Clear Fork Group strata.

Two conductivity profiles were acquired across the field that both pass near the abandoned well casing (fig. 62), which was located by RRC staff during a magnetometer survey of the site. A horizontal dipole conductivity peak that is more than 100 m wide is present on north-south line 16A (fig. 63a). The peak, which reaches conductivities of 100 mS/m, is centered within a few meters of well #3. The east-west line 16B reveals a slightly broader peak that reaches similar

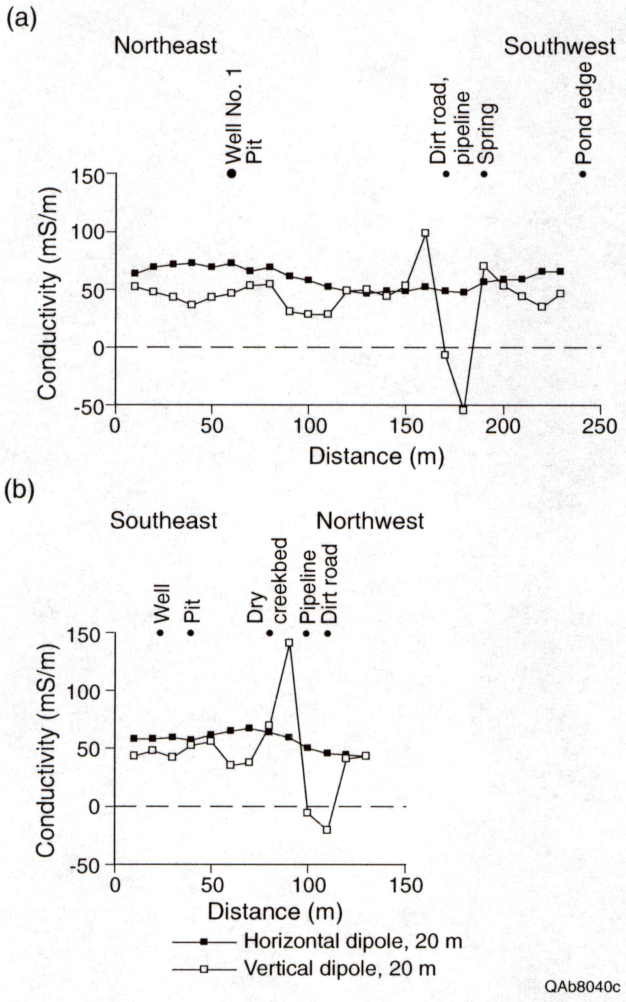

Figure 61. Apparent ground conductivity at site 13 using 20 m coil separation and horizontal and vertical dipole orientations. Line 13A (a) crosses abandoned McMillan #1 well from northeast to southwest and line 13B (b) crosses abandoned #4 well from southeast to northwest.

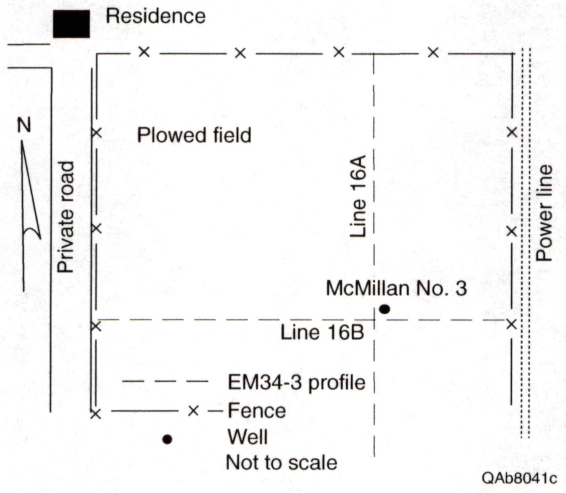

Figure 62. Sketch map of site 16. Reconnaissance conductivity profiles 16A and 16B pass near the abandoned McMillan #3 well in a cultivated field south of Mud Creek.

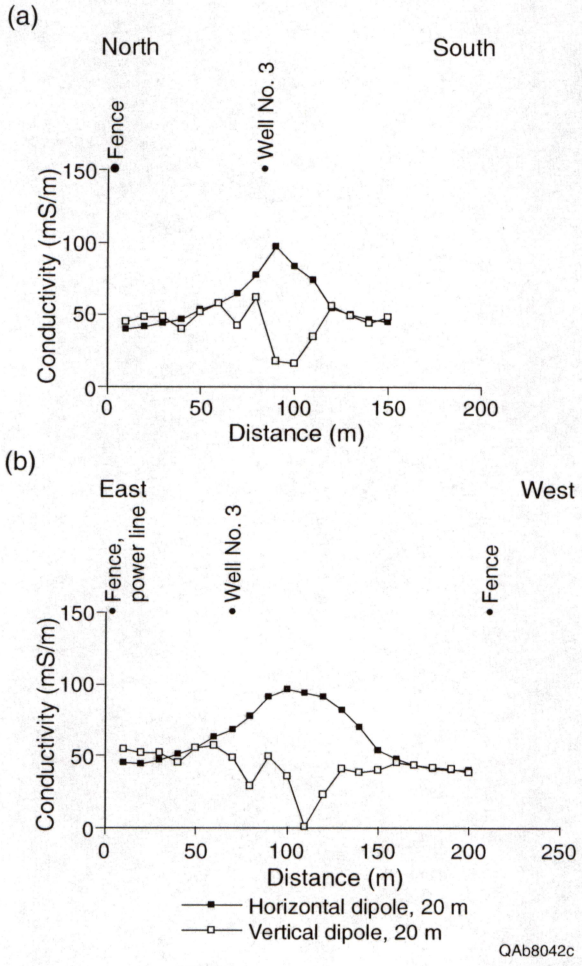

Figure 63. Apparent ground conductivity at site 16 using 20 m coil separation and horizontal and vertical dipole orientations. Line 16A (a) and 16B (b) both cross the abandoned McMillan #3 well.

peak values, but the highest values are centered 20 to 50 m west (downslope) from the well (fig. 63b). Background conductivities of 40 to 50 mS/m are reached within a distance of 160 m west of the well.

The airborne conductivity and magnetic signature of this site suggested an uncased well that might be leaking. Well casing was detected at the site during the ground surveys despite the lack of a magnetic anomaly in the airborne survey. Nevertheless, there is clearly salt water in the shallow surface near the well that was detected by both the airborne and ground-based surveys. Conductivity profiles across the well site suggest that either (a) the well is leaking brine that is preferentially migrating to the west (downslope), or (b) the surface pit was located west of the well and brine that was discharged into it has infiltrated the subsurface. This well should be viewed as one that may be leaking.

Site 70

Just east of Hatchel is site 70 (fig. 18), where the conductivity anomaly is located in a plowed and terraced field. Soils belong to either the moderately deep Portales clay loam or the shallower Mereta clay loam (fig. 3). These soils grade downward into Clear Fork strata (fig. 2).

The conductivity anomaly, which measures 160 m east-west by 240 m north-south, is most apparent on the shallow (56,000 Hz) conductivity map (fig. 18) and progressively diminishes on the deeper penetration conductivity maps (figs. 19 and 20). There is a known well nearby, but no associated magnetic anomaly (fig. 17). The site is disturbed and barren of vegetation on 1940 aerial photographs.

East-west conductivity profile 70A (fig. 64) shows a broad conductivity high that is about 180 m wide (fig. 65), similar to the anomaly width on the 56,000 Hz map. Conductivity increases from background values of about 50 mS/m on the flanks of the high to about 90 mS/m. The peak roughly coincides with an area of stony and sandy soil at and upslope from the two terraces that are crossed by line 70A.

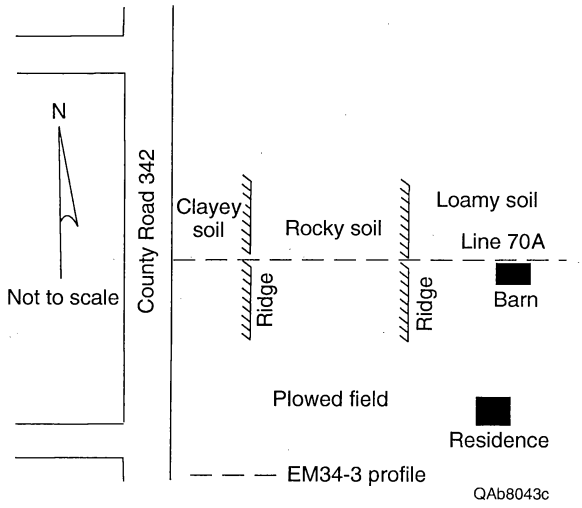

Figure 64. Sketch map of site 70. Reconnaissance conductivity profile 70A crosses a plowed and terraced field on the D. Workman farm.

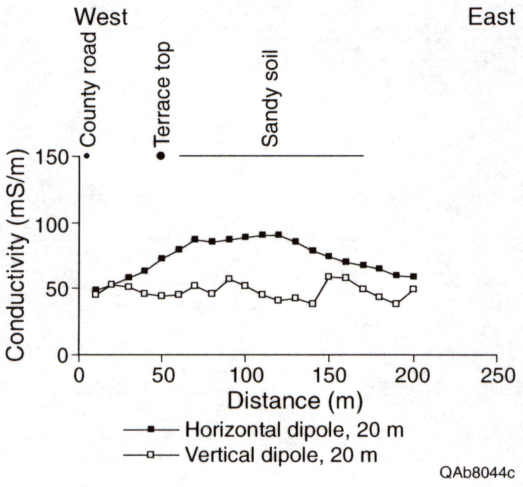

Figure 65. Apparent ground conductivity at site 70 using 20 m coil separation and horizontal and vertical dipole orientations. Line 70A is oriented east-west across a plowed and terraced field at the D. Workman farm.

Progressively lower ground conductivities at deeper penetration depths on the airborne maps suggest that there is no leaking well at this site. The relatively near-surface conductivity peak could be caused by enhanced water infiltration in the loamy soil upslope from the terrace. Alternatively, perhaps the disturbed area evident on the 1940 aerial photographs was the site of an old well where no production occurred but brine encountered during drilling was discharged in a surface pit.

Site 73

This site surrounds the Russell #1 well, which was drilled and abandoned in 1928. The site is located on the western valley of Flag Creek in the southwest corner of the study area and has thin Potter clay loam soil over Clear Fork Group strata. Conductivities are high and slightly anomalous on the shallow 56,000 Hz airborne map (fig. 18). The deeper maps do not have anomalously high conductivities at the site (figs. 19 and 20), nor is there a magnetic anomaly evident (fig. 17). A ground-based magnetometer survey by RRC staff located the buried well casing.

Two orthogonal conductivity profiles were acquired across the site (fig. 66). Line 73A reveals the presence of a conductivity peak in the horizontal dipole mode that is 110 m wide (fig. 67a). Conductivities on this line increase from background values of 50 mS/m to nearly 100 mS/m. The peak is centered beneath a surface pit 10 to 20 m southeast (downslope) of the well casing. Line 73B, which passes between the well and the pit (fig. 66), measured conductivities as high as 80 mS/m near the well and pit (fig. 67b).

The location of peak conductivities at the pit rather than the well casing and the lack of anomalously high conductivities on the 7,200 Hz and 900 Hz maps support the interpretation that this well is not leaking brine. The source of brine in the shallow subsurface at this site appears to be brine disposal into the surface pit during well drilling or operation.

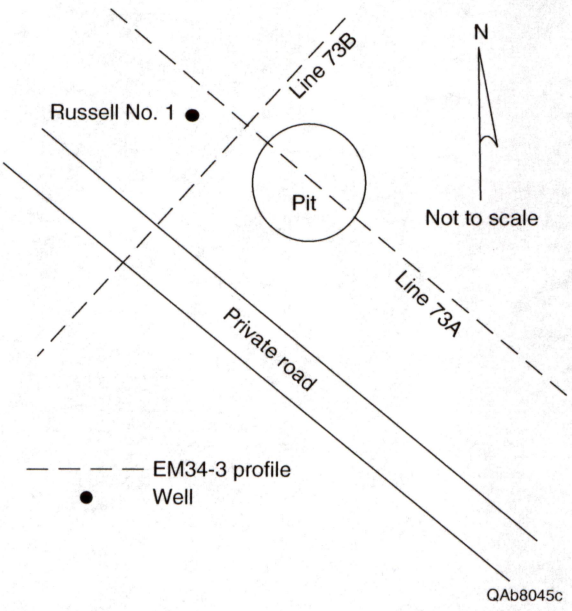

Figure 66. Sketch map of site 73. Reconnaissance conductivity profiles 73A and 73B pass near the abandoned Russell #1 well and adjacent surface pit.

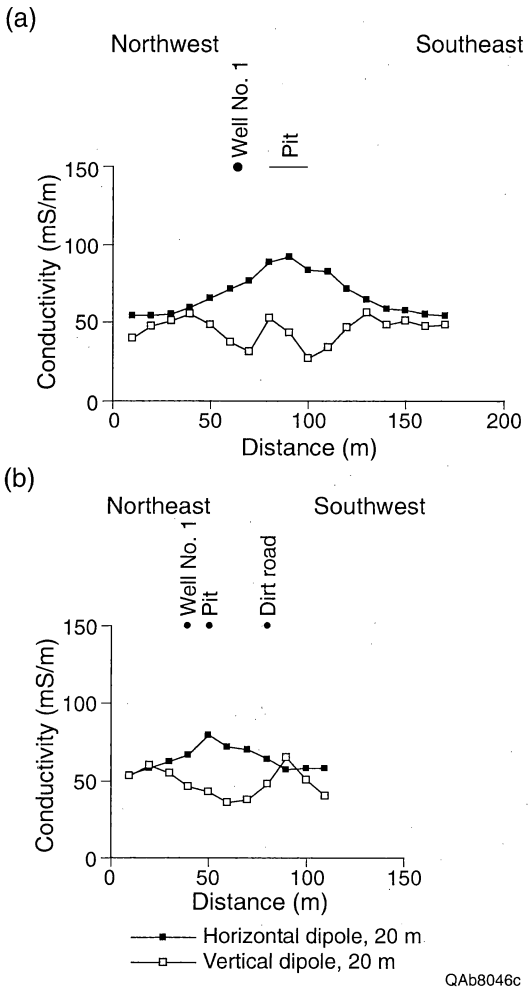

Figure 67. Apparent ground conductivity at site 73 using 20 m coil separation and horizontal and vertical dipole orientations. Line 73A (a) crosses the abandoned Byler #1 well and surface pit from northwest to southeast. Line 73B (b) crosses the well and pit from northeast to southwest.

Other Site Types

In the course of field investigation, a few other site types were examined. There are numerous type C sites, for example, where conductivity anomalies (C) are visible on the airborne maps that do not coincide with magnetic anomalies (M) or well locations (W). There are also many type MW sites, where magnetic anomalies associated with known wells have no coincident conductivity anomaly. Most of the wells in the study area would fall into this category.

Sites 65 and 67

These are type MW sites that are located adjacent to each other in the northeastern part of the study area (fig. 18). Site 65 consists of a magnetic anomaly associated with the Early #1 well, which is a recently abandoned oil well that was drilled in 1982. Site 67 is a separate magnetic anomaly that encircles the Early A #2 well, which is another recently abandoned oil well that was also drilled in 1982. Both wells recently began leaking brine at the surface (fig. 68) and were plugged in 1996 during the field investigation. These wells are in a cultivated field on deep Miles sandy loam soil just upslope from Bluff Creek (fig. 69). On the western part of the site, the soil grades downward into Clear Fork Group strata. Closer to the creek on the eastern side of the site are Quaternary alluvial deposits.

Although magnetic anomalies are associated with the wells (fig. 17) and the wells have been leaking brine, the airborne surveys show no conductivity anomalies. On the 56,000 Hz map, conductivities are generally low and decrease eastward toward the creek (fig. 18). On the deeper 7,200 Hz and 900 Hz maps, conductivities are high and they increase toward the creek, but show no anomalies at the wells (figs. 19 and 20).

Ground-based conductivity profiles verify the absence of major conductivity anomalies at the wells. Line 6567A, which passes near both wells (fig. 69), shows a gradual increase in ground conductivity (horizontal dipole mode) eastward and a modest increase in ground conductivity near the Early A #2 well (fig. 70a). There is no evidence of any increase in

Figure 68. Abandoned Early A #2 well leaking brine at site 67.

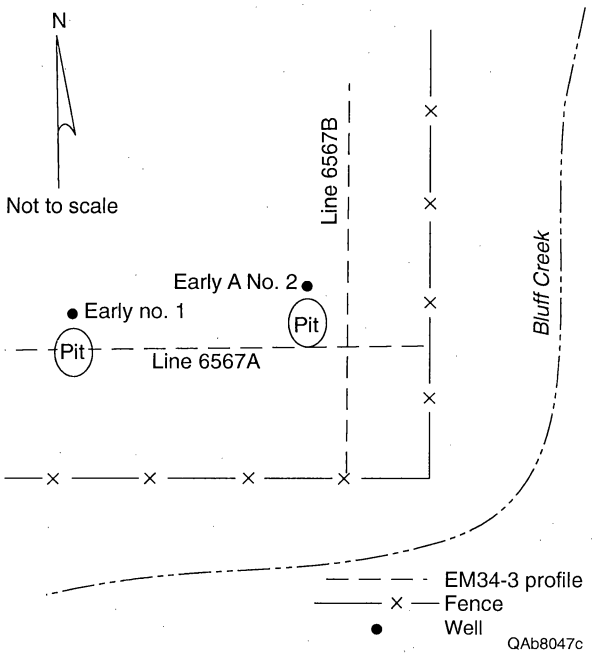

Figure 69. Sketch map of sites 65 and 67. Reconnaissance conductivity profiles 6567A and 6567B pass near the leaking Early #1 and Early A #2 wells in a cultivated field upslope from Bluff Creek.

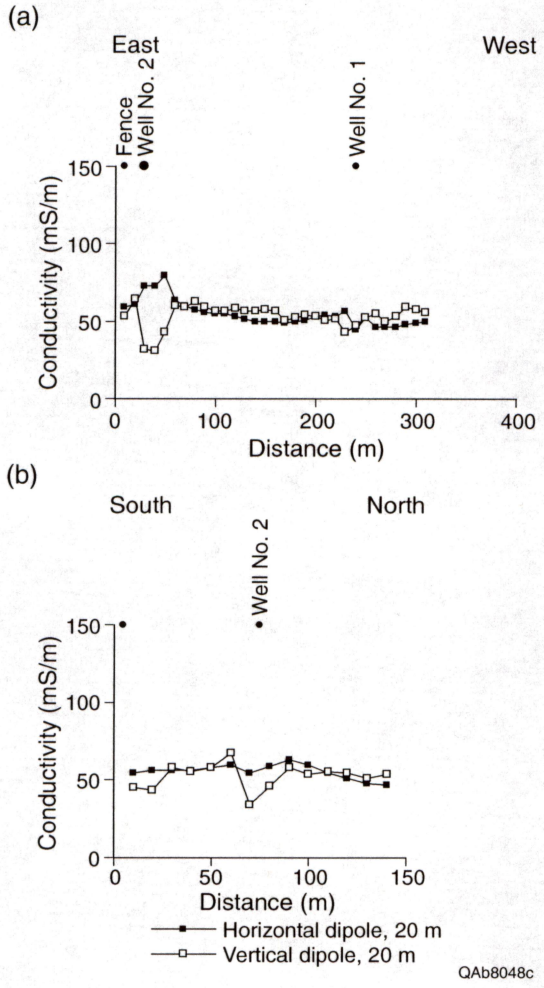

Figure 70. Apparent ground conductivity at site 65 using 20 m coil separation and horizontal and vertical dipole orientations. Line 65A (a) crosses the abandoned and leaking Early A #1 and #2 wells from east to west and line 65B (b) crosses well #2 from south to north.

conductivity near the #1 well. The modest peak near the #2 well is about 50 m across and reaches peak values of 80 mS/m. Line 6567B passes near the #2 well along a north-south line and shows only a small ground conductivity increase near the well (fig. 70b).

Surface evidence proves that these wells are leaking, but ground-based and airborne geophysical data show that a relatively small brine volume has entered the subsurface at these sites. Leakage probably began recently and has occurred only at relatively low rates through the top of the surface casing.

Time-Domain Electromagnetic (TDEM) Soundings

Site geophysical surveys and soil and water samples were designed to help interpret the conductivity patterns relatively near the surface on the shallow 56,000 Hz and intermediate 7,200 Hz conductivity maps. Conductivity patterns on the deep 900 Hz map (compare figs. 18, 19, and 20) are fundamentally different from the shallower maps and have a northeasterly trend that resembles the regional geologic map (Kier and others, 1976). To help interpret the 900 Hz map, thirteen TDEM soundings were acquired at nine sites across the study area. These soundings detected vertical conductivity changes to maximum depths of 80 to 100 m, comparable to the 30 to 60 m exploration depth of the 900 Hz airborne coils (fig. 21) and greater than depths reached by the EM34-3 in any of its configurations (fig. 11). TDEM sounding sites (fig. 20) were representative of large areas with similar conductivities on the 900 Hz map; local anomalies such as those investigated with the EM34-3 were avoided. For sounding purposes, the study area was divided into a low conductivity zone in the northwest part of the study area, a highly conductive band trending north-northeast across the central part of the study area, and another low conductivity zone in the east and southeast part of the study area.

Northwest low conductivity zone

A wedge-shaped zone of relatively low conductivity on the 900 Hz survey is located in the northwest part of the study area (fig. 20). Typical mapped conductivities in this zone are 130 to 180 mS/m. Four TDEM soundings were acquired at two sites within this area: three at site 76 as part of its detailed survey, and one at site 82 near the upstream end of Turkey Creek.

Mapped deep conductivity at site 76 is about 140 mS/m (fig. 20). The deeper parts of all three best-fit conductivity models for site 76 TDEM soundings are similar (fig. 26), showing a 7.8 ohm-m (128 mS/m) layer extending from 10 m to 41 m below the surface that is underlain by a more conductive (2.3 ohm-m or 430 mS/m) layer below 41 m depth. The 900 Hz airborne coils, which sense to depths of 40 to 50 m in this area, measure conductivity that is very close to that of the 10 to 41 m layer in the sounding models and do not fully detect the conductive layer that begins at 41 m and extends to an unknown depth. The top of the conductive layer is calculated to be 497 m above sea level.

Mapped 900 Hz conductivity for the TDEM sounding at site 82 is about 150 mS/m (fig. 20). The best-fit conductivity model for the transient recorded in sounding S82A (fig. 71) has similar deeper layering to that at site 76: a relatively resistive (8.5 ohm-m or 118 mS/m) layer at depths of 15 to 37 m overlies a more conductive (2.6 ohm-m or 384 mS/m) layer below 37 m depth. The conductive layer is modeled at a shallower depth than at site 76, which probably accounts for the slight increase in conductivity sensed by the 900 Hz airborne coils. The top of the conductive layer at site 82 is calculated to be 493 m above sea level.

Relatively low conductivities sensed by the 900 Hz airborne coils largely reflect conductivities characteristic of a stratigraphic interval that extends to a depth of about 40 m in this area. The stratigraphic interval does not contain large volumes of salt water. TDEM soundings detected a more conductive stratigraphic zone deeper than about 40 m that is likely to carry a larger volume of brine. This zone is likely to follow regional geologic trends of west-northwestward deepening into the Permian Basin.

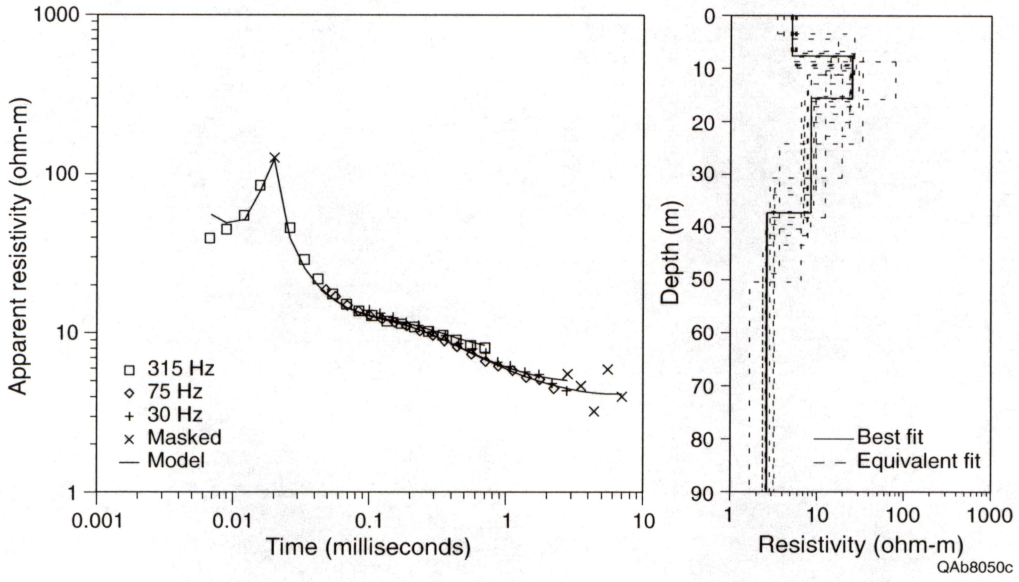

Figure 71. Transient decay curve (left) and resistivity models (right) at TDEM sounding site S82A.

Central conductive zone

The central conductive zone, as depicted on the 900 Hz airborne map (fig. 20), trends north-northeastward from the southwestern corner of the study area. Conductivities in this zone are high and range from 175 to 350 mS/m. These conductivities imply a slightly shallower 900 Hz exploration depth of 30 to 40 m. Two TDEM sounding sites were located within two of the most conductive parts of this trend: site 81, located in a cultivated field west of Hatchel, and site 83, near Bluff Creek at the northern edge of the study area (fig. 20).

At site 81, conductivity measured by the 900 Hz airborne coils is about 340 mS/m. TDEM sounding S81A indicated the presence of a conductive (2.7 ohm-m or 365 mS/m) layer at a depth of 11 m that extends to 61 m (fig. 72). This thick layer encompasses most of the effective exploration depth of the 900 Hz airborne coils and provides a good conductivity match. A more resistive (8.2 ohm-m or 123 mS/m) layer of unknown thickness is below 61 m depth. The top of the 50-m thick conductive layer is at 509 m above sea level.

The conductivity profile that best fits the TDEM sounding data at site 83 also has the conductive layer close to the land surface (fig. 73). At this site, conductivity measured by the 900 Hz airborne coils is about 300 mS/m, slightly lower than at site 81 (fig. 20). The conductive layer detected by the sounding is also slightly less conductive (3.2 ohm-m or 313 mS/m) than the corresponding conductive layer at site 81 and again provides a good match to the airborne measurements. The conductive layer extends from 10 to 71 m below the surface and is underlain by a more resistive (13.5 ohm-m or 74 mS/m) layer of unknown thickness. The top of the conductive layer is estimated to be 514 m above sea level.

The main differences between best-fit conductivity models constructed for TDEM soundings in this zone and those in the northwest low conductivity zone are that (a) the conductive layer is detected at shallower depths, and (b) the base of the conductive layer is detected. Soundings in the central conductive zone are consistent with the interpretation that the conductive layer is a brine-bearing stratigraphic unit that is shallowing east-southeastward away

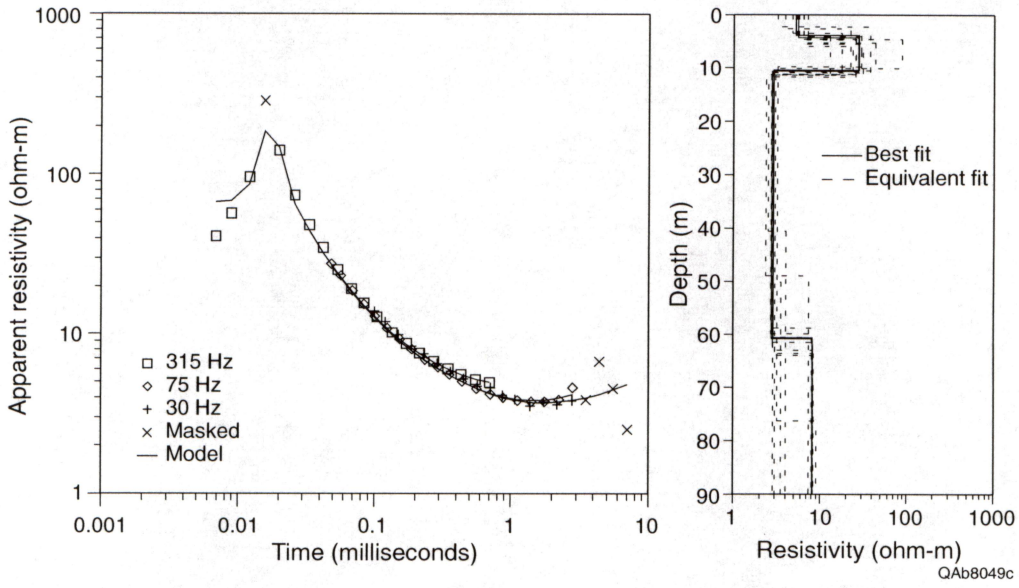

Figure 72. Transient decay curve (left) and resistivity models (right) at TDEM sounding site S81A.

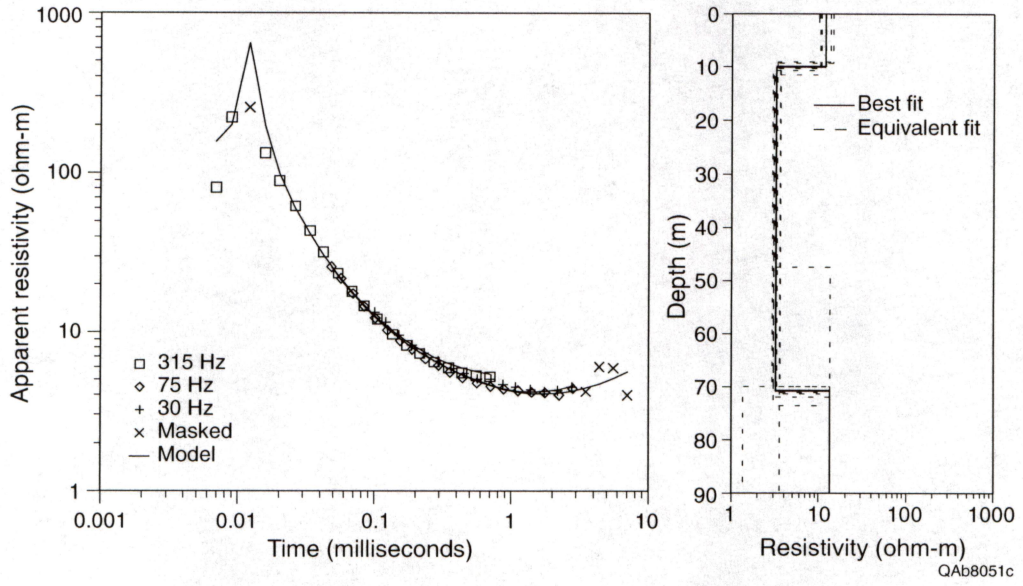

Figure 73. Transient decay curve (left) and resistivity models (right) at TDEM sounding site S83A.

from the Permian Basin. This unit is 50 to 60 m thick and its top approaches the land surface on the southeast margin of the central conductive zone.

East and southeast low conductivity zone

This zone is the largest of the three and covers the eastern and southeastern part of the study area. Ground conductivities measured with the 900 Hz airborne coils are lowest here, ranging from 60 to 150 mS/m (fig. 20). Consequently, maximum exploration depths are greatest (45 m in 150 mS/m terrain and 70 m in 60 mS/m terrain, fig. 21).

Seven soundings were acquired at five sites in this zone. At site 84 in the northeast corner of the study area (fig. 20), conductivity measured by the 900 Hz airborne coils is 120 mS/m. A best-fit conductivity model constructed for sounding S84A (fig. 74) includes a layer with similar conductivity (7.4 ohm-m or 136 mS/m) between 19 and 52 m depth, an interval that covers most of the exploration depth range of the 900 Hz airborne coils. Significantly, no highly conductive layer was detected in the TDEM sounding.

Soundings at sites 85 and 86 (figs. 75 and 76) are located at the base (S85A) and the top (S86A) of a hill along reconnaissance conductivity profile 25A (figs. 20 and 50). Sounding S85A was acquired at lower elevation and thus explores the deepest. Conductivity measured using the 900 Hz airborne coils is 100 mS/m. This value falls between those of two relatively resistive layers modeled for the sounding (fig. 75). The more resistive (86.8 ohm-m or 12 mS/m) layer is between the depths of 5 and 20 m and is underlain by a 7.5 ohm-m (133 mS/m) layer below 20 m. The 900 Hz airborne coils are sensing both of these layers. Again, no highly conductive layer was detected in either TDEM sounding.

Of the five sounding sites in this low conductivity zone, conductivities measured by the 900 Hz airborne coils are the lowest (about 80 mS/m) at site 17 (fig. 20). The deeper parts of three soundings acquired as part of the brine pit investigation are similar (fig. 49). Representative sounding S17B (fig. 49b) shows the presence of a relatively resistive (12.4 ohm-m or 81 mS/m) layer between the depths of 11 and 39 m that corresponds well with observed 900 Hz airborne

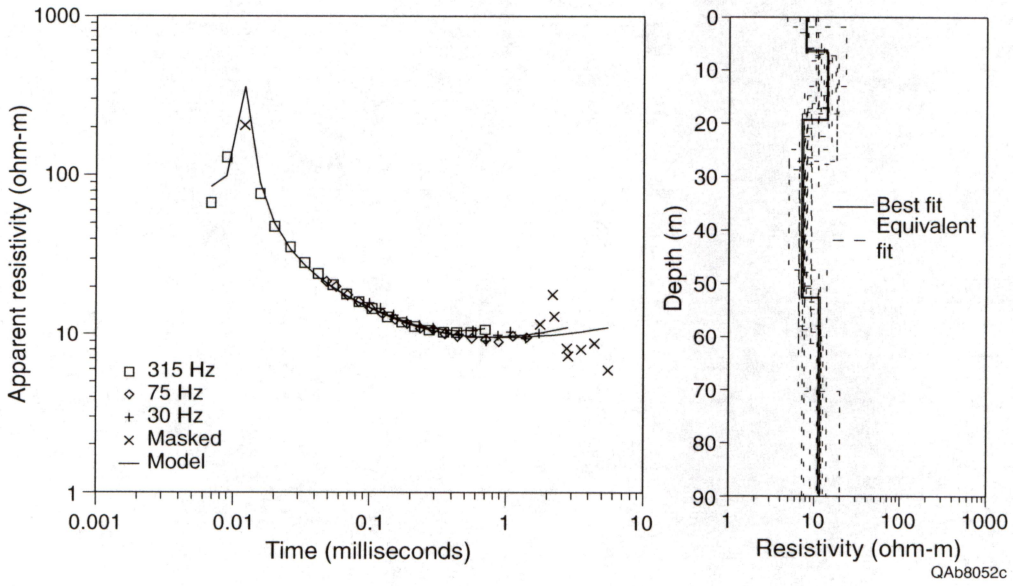

Figure 74. Transient decay curve (left) and resistivity models (right) at TDEM sounding site S84A.

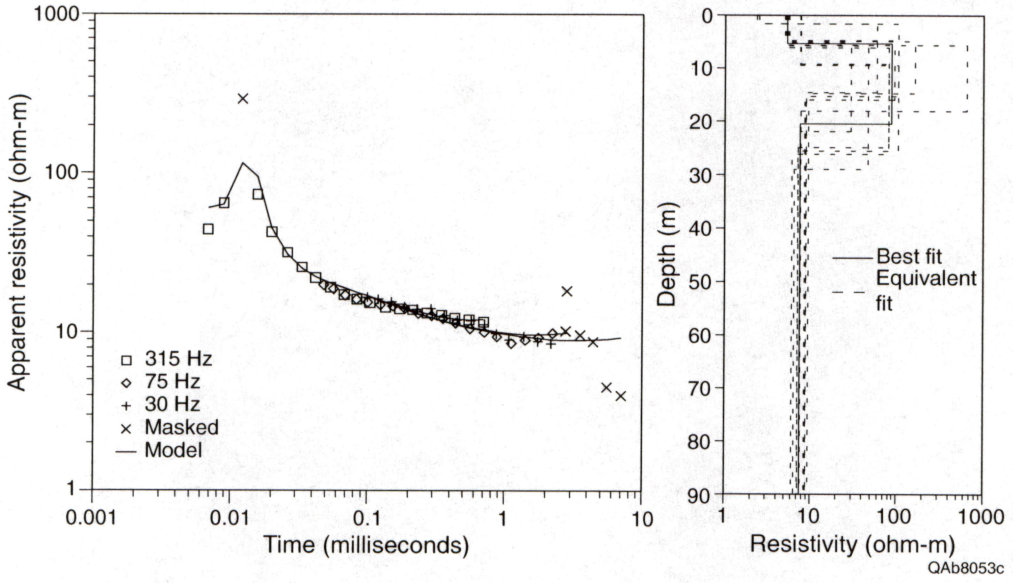

Figure 75. Transient decay curve (left) and resistivity models (right) at TDEM sounding site S85A.

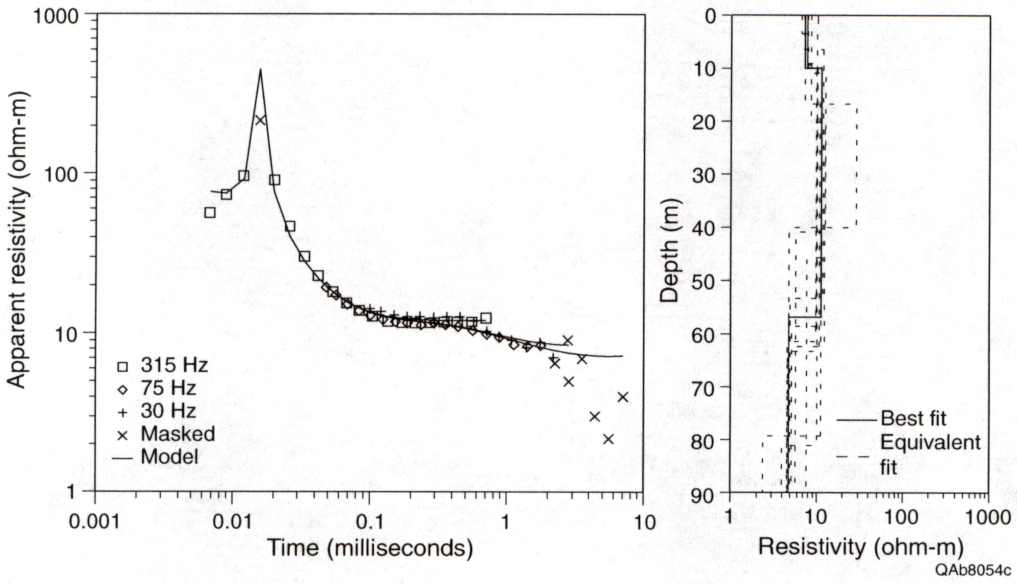

Figure 76. Transient decay curve (left) and resistivity models (right) at TDEM sounding site S86A.

coil measurements. No highly conductive layer other than the surface layer was detected in any of the three soundings at this site. The conductive layer at the surface is related to brine disposal in a surface pit.

Site 87 is located in the southeast corner of the study area where conductivity measured by the 900 Hz airborne coils is about 100 mS/m (fig. 20). The best-fit conductivity model constructed for sounding S87A (fig. 77) indicates that there are three relatively thick layers that fall within the depth range sensed by the airborne coils. The most conductive (6.2 ohm-m or 161 mS/m) of the three layers extends from 14 to 24 m depth and is underlain by a more resistive (17.5 ohm-m or 57 mS/m) layer between 24 and 42 m depth. Below 42 m is a layer of intermediate resistivity (9.4 ohm-m or 107 mS/m). These three layers combined produce a composite resistivity that is consistent with the airborne data. No highly conductive interval was detected in this sounding.

The highly conductive brine-bearing stratigraphic unit that was detected at progressively shallower depths to the east and southeast across the northwest low conductivity zone and the central conductive zone appears to be either absent or too shallow to be detected by the 900 Hz airborne coils in the southeast low conductivity zone. Considering the flatness of the study area and the west-northwestward dip of Permian strata, it is likely that part of the brine-hosting unit reaches the surface and either has been removed by erosion or has discharged brine. Further, this section is shallow enough in the eastern part of the study area to be detected by the shallower-exploring 7,200 Hz (fig. 19) and 56,000 Hz (fig. 18) airborne coils. It is also within reach of infiltrating surface water, which along with brine discharge serves to reduce the salinity and conductivity of the section.

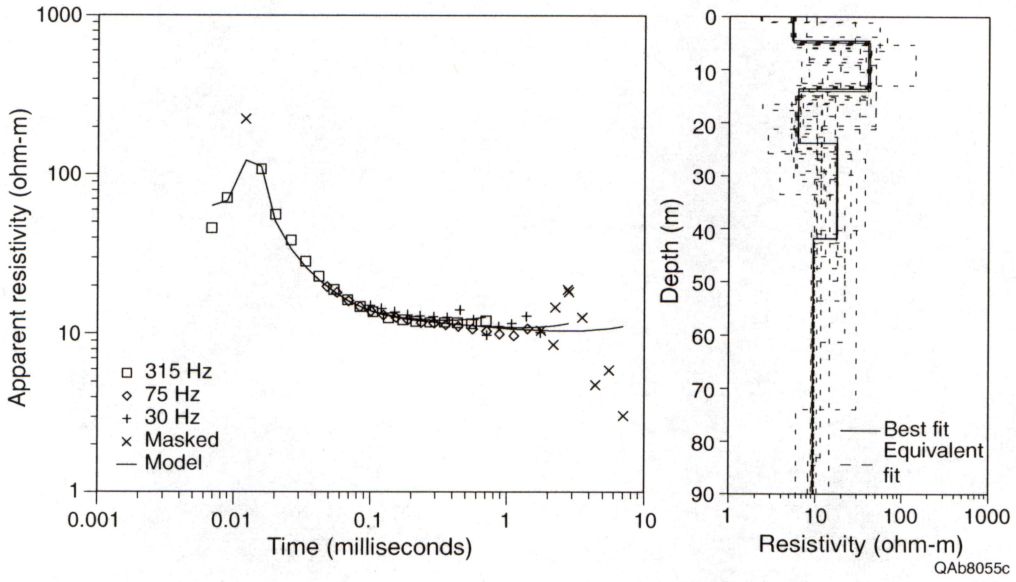

Figure 77. Transient decay curve (left) and resistivity models (right) at TDEM sounding site S87A.

Chemical Composition of Water Samples

Water Salinity

Ground waters sampled in the study area (appendix A) range in total dissolved solids (TDS) from 480 to 7,620 mg/L; the average of the logarithm-transformed variable is 1,746 mg/L (fig. 78). Salinity of water in general follows a logarithmically normal statistics distribution. The best estimate of average TDS, therefore, is based on the logarithm of TDS values. TDS does not significantly differ with well depth. Surface waters sampled during this study have nearly the same range and mean in TDS (fig. 78; appendix A).

The three samples from oilfields have markedly higher salinity. TDS of the two samples from abandoned oil wells were approximately 66,000 mg/L (table 2). Water collected from the seeping core hole had a TDS of more than 10,200 mg/L.

TDS of water samples (fig. 79a) and chloride content of soil (fig. 79b, table 3) correlates with electrical conductivity.

Chemical Composition

Ground and surface waters in the study area have similar chemical compositions that include calcium-bicarbonate, calcium-sulfate, mixed-cation–mixed-anion, and sodium-chloride types of hydrochemical facies (Back, 1966) (fig. 80). In the Runnels County area, it is reasonable to assume that the calcium-bicarbonate type of hydrochemical facies is derived from the reaction of ground water flowing through limestone and that the calcium-sulfate type results from ground water encountering beds of gypsum. The Permian bedrock formations are dominated by limestone, gypsum, and shale. A change from calcium- to sodium-dominated cations can take place along a flow path because of ion exchange or because of mixing with a sodium-chloride water. The water samples in which no single cation or anion is dominant most likely reflect

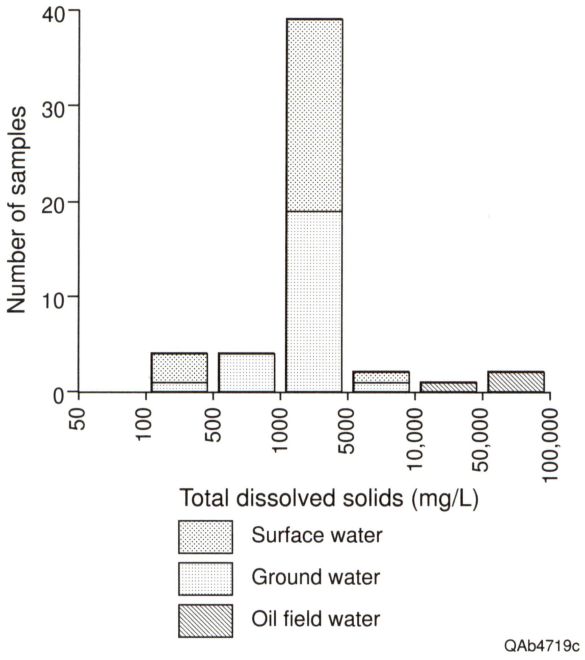

Figure 78. Histogram of total dissolved solids in ground-water, surface-water, and oilfield-water samples in the Runnels County study area. Mean values of surface and ground waters are approximately the same.

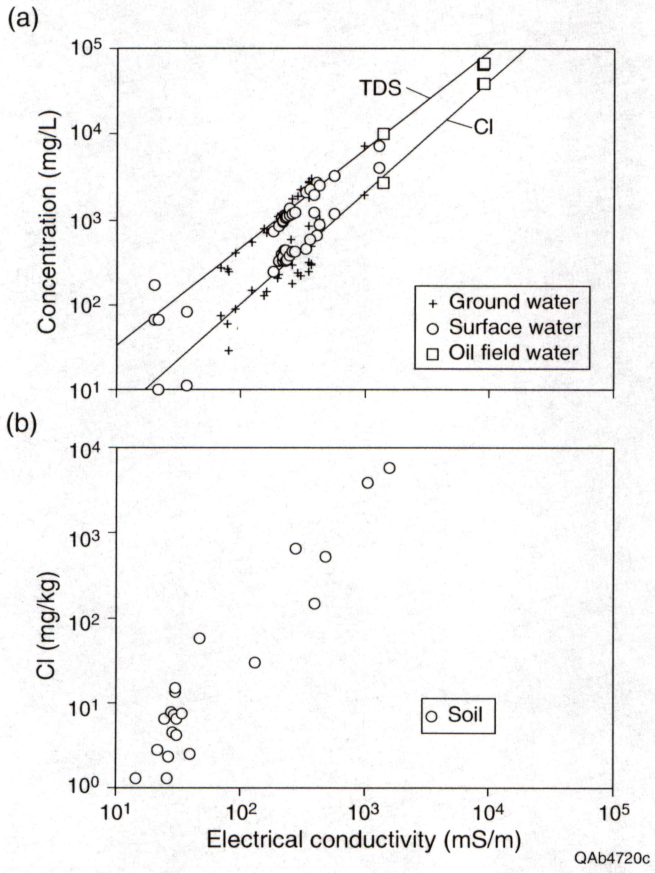

Figure 79. Relation between electrical conductivity and (a) total dissolved solids (TDS) and chloride (Cl) content of water samples and (b) Cl content of soil samples with linear least-squares regression lines. Electrical conductivity is a good predictor of Cl and TDS.

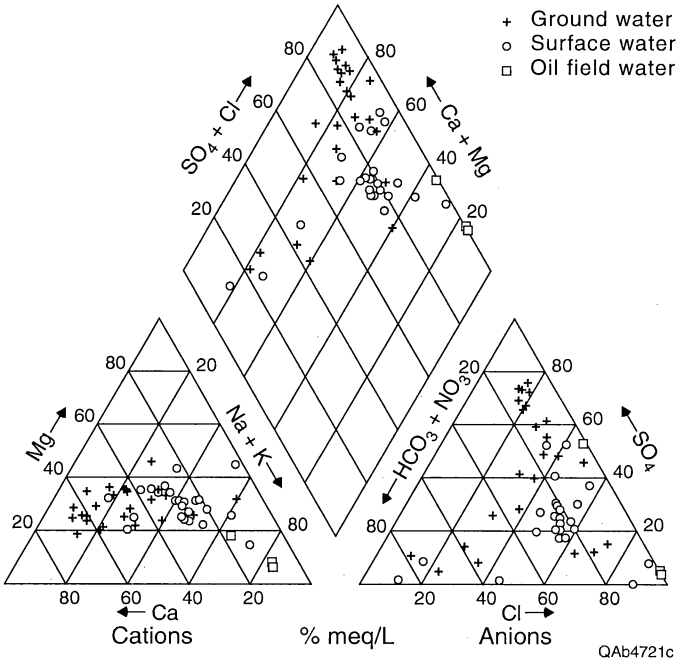

Figure 80. Trilinear diagram showing chemical composition of different hydrochemical facies in ground-water, surface-water, and oilfield-water samples in the Runnels County study area.

mixtures of waters of different hydrochemical facies, movement of water from one lithology to another, or samples taken at an intermediate position along a flow path.

The samples from the two abandoned oil wells have a sodium-chloride hydrochemical facies, as is typical of oilfield waters. The somewhat more dilute water from the unplugged core hole has higher proportions of calcium and sulfate (fig. 80).

Comparison to Regional Trends

Dutton and others (1989) and Richter and others (1990) studied the sources of salinity affecting ground-water quality in Runnels County and adjacent areas. The ground- and surface-water samples collecting in this study do not differ from ground waters described in the earlier regional study. For example, the ratio of bromide to chloride (Br/Cl) of the new samples from Runnels County overlaps that of the older ground- and surface-water samples (fig. 81). The new samples also overlap the regional samples on a cross plot of the chloride to sulfate (Cl/SO_4) ratio and the sodium to calcium (Na/Ca) ratio (fig. 82). Dutton and others (1989) and Richter and others (1990) identified these graphical techniques as particularly effective in distinguishing between different sources of water in the study area. Note that the surface- and ground-water samples lie along a well-defined trend on the Cl/SO4 versus Na/Ca graph (fig. 82). The trend "points" toward the Permian formation end member of the oilfield waters defined by Dutton and others (1989) and Richter and others (1990). The new oilfield waters collected in this study plot at that Permian formation end member (figs. 81 and 82).

Comparison of Soil and Water Salinity to Measured Conductivity

Ground conductivity measured by the airborne geophysical survey appears to directly correspond to total dissolved solids of ground-water samples (fig. 83), although the relationships for the 7,200 and 56,000 Hz surveys are not statistically significant, perhaps because of the large amount of data variance compared to sample size. The 56,000 Hz ground-conductivity survey

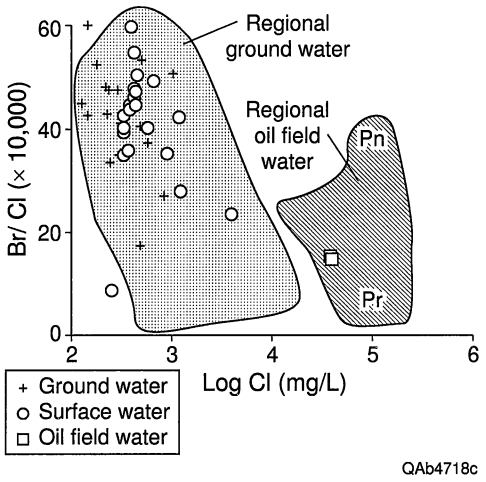

Figure 81. Variation of Br/Cl ratio with Cl concentration in water samples collected during this study in Runnels County (pluses, circles, and squares), compared with regional data presented by Richter and others (1990). Ground and surface waters collected in the study area are similar to other ground waters in the region. The oilfield waters collected in this study more closely resemble the Permian (Pr) than Pennsylvanian (Pn) end member of oilfield brine defined by Richter and others (1990).

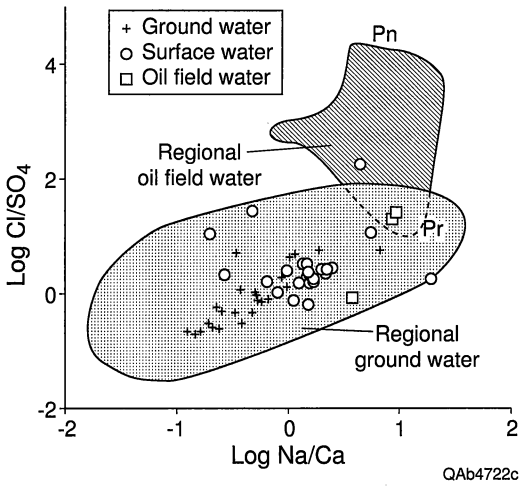

Figure 82. Variation of Cl/SO4 ratios with Na/Ca ratios in water samples collected during this study in Runnels County (pluses, circles, and squares), compared with regional data presented by Richter and others (1990). Ground and surface waters collected in the study area are similar to other ground waters in the region. The oilfield waters collected in this study more closely resemble the Permian (Pr) than Pennsylvanian (Pn) end member of oilfield brine defined by Richter and others (1990). Some surface-water samples have a high Na and Cl content similar to the Permian brine end member.

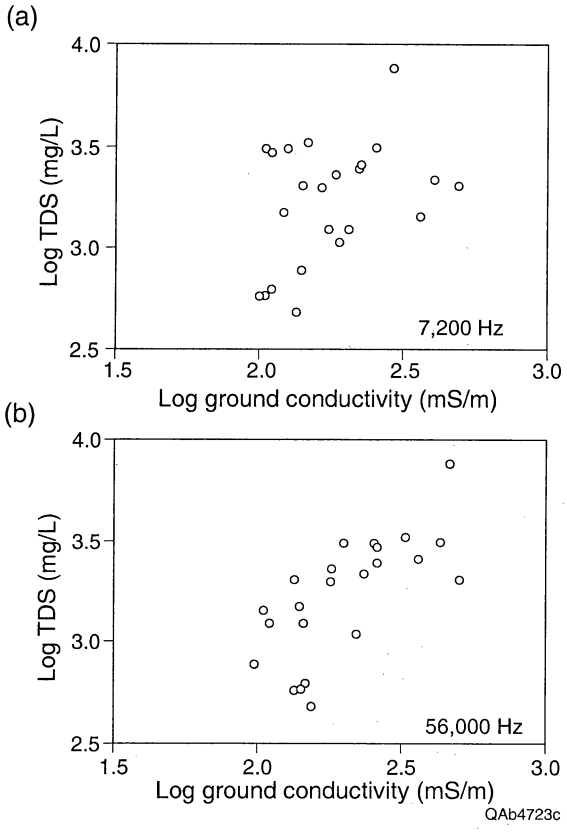

Figure 83. Comparison of total dissolved solids (TDS) of ground-water samples and ground conductivity measured by (a) 7,200 Hz survey and (b) 56,000 Hz survey.

does not correspond well to chloride content or electrical conductivity measured in soil samples (fig. 84).

DISCUSSION

High resolution airborne geophysical measurements, when combined with detailed ground-based geophysical surveys, water and soil sampling and chemical analyses, and high quality background information on soil type, rock type, and oil and gas well distribution, provide an unprecedented opportunity to understand ground conductivity changes and their causes. Specifically, these data from the Hatchel area allow us to examine the relative importance of oilfield-related and non-oilfield sources of salinization, assess the merits of ground-based and airborne geophysical methods in the search for salinity sources of all types, determine the usefulness of the method in locating leaking wells, and develop a geophysical "profile" of a potentially leaking well.

Effectiveness of the Airborne Geophysical Survey

As the ground surveys at anomalies detected by the airborne survey show, the effectiveness of the airborne geophysical methods employed in this study depends on the survey objective. If the goal is to locate areas of potential ground salinization for focused, ground-based study, then the airborne method obviously is successful. If the goal is to locate cased oil and gas wells with an airborne magnetometer, success is more limited and could be improved by employing shorter line spacings. If the goal is to distinguish leaking wells from other salinity sources, both oilfield and non-oilfield, then the airborne method alone has limitations.

The airborne conductivity data combined with a knowledge of oilfield history, qualitative plume migration rates, and land use patterns allow us to distinguish conductivity anomalies related to agricultural practices, soil and rock types, and topography-related soil moisture changes from those that might be oilfield-related. With little ground-truth effort, we can infer that

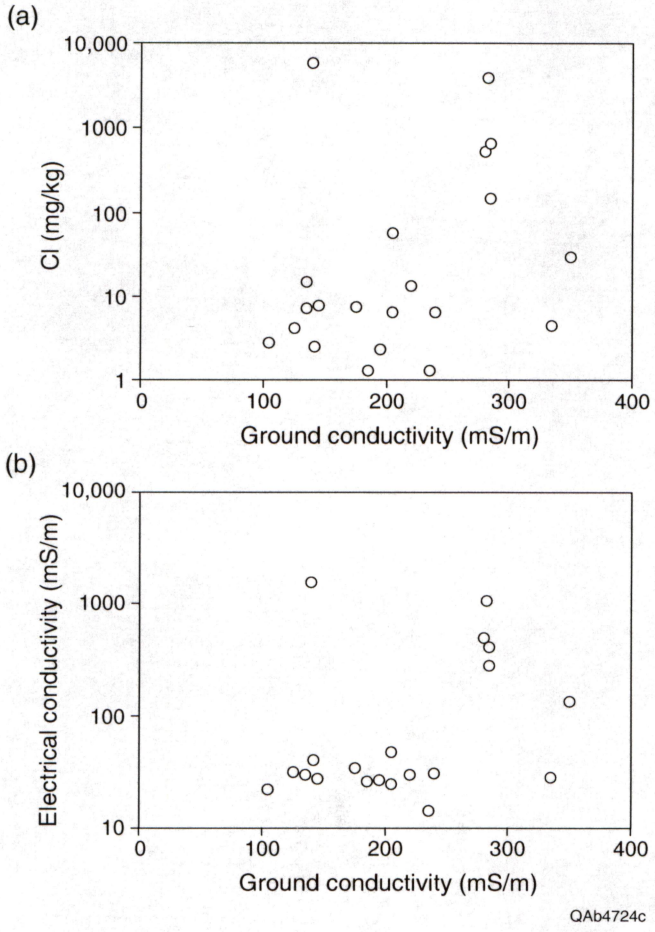

Figure 84. Comparison of ground conductivity measured by airborne geophysical survey (56,000 Hz) and measurement of (a) chloride content and (b) electrical conductivity of soil samples.

most oilfield-related salinity sources will be point sources that show limited lateral migration (typically tens of meters). Conversely, long curvilinear conductivity anomalies that follow topography are likely to be related to agricultural practices, natural hillside seeps, or water-saturated alluvium near flowing creeks. Large conductivity anomalies covering several square kilometers are most likely related to changes in soil or rock type, not oilfield sources. The airborne method is quite successful in identifying these broad source types.

Ground-based investigations are required to help the airborne method distinguish common oilfield-related salinity sources from each other. Airborne signatures of leaking tank batteries, surface brine pits, and leaking wells are similar and require follow-up work to verify the source type. In the Hatchel area, where more than 700 known wells have been drilled, 103 conductivity anomalies (table 2) were identified in the airborne data that were consistent with oilfield-related salinity sources. Ground-based surveys at 23 representative sites suggest that most of these sites are oilfield-related, but relatively few are suspected to be leaking wells.

Most (94) of the airborne conductivity anomalies were identified on the 56,000 Hz conductivity map (table 2), which is the map that shows the shallowest exploration depth. Many of these anomalies appear to be related to surface salinity sources such as brine pits or tank batteries. As exploration depth increases, fewer of the sites have anomalous conductivities. Only 54 of the 103 sites show anomalous conductivities on the 7,200 Hz map, only 46 show anomalous conductivities on both the 7,200 and 56,000 Hz maps, and only 9 show anomalous conductivities at all three frequencies (table 2). Ground-based surveys indicated that anomalies visible on both the 56,000 and 7,200 Hz maps were more likely to be leaking wells than anomalies that are visible on the 56,000 Hz map alone.

Geophysical Profile of a Leaking Well

Ground investigation of several types of airborne geophysical signatures allows development of a "profile" of a typical well that may be leaking brine. Sites with a suspicious airborne signature were those that (a) have either a magnetic anomaly or a known well location,

and (b) have anomalously high ground conductivity on both the shallow-exploring 56,000 Hz airborne coils and the deeper-exploring 7,200 Hz coils (table 2 and appendix A). The suspicious site might or might not have a conductivity high on maps produced from the deeply-penetrating 900 Hz coils.

In the Hatchel study area, 46 of the 103 sites fit the refined airborne profile of a potentially leaking well (table 2). On-the-ground geophysical surveys at 11 of these sites that have conductivity anomalies on both the 56,000 and 7,200 Hz maps have shown that at least eight of them have significant oilfield-related salinization and that five might be leaking wells. If these proportions can be verified by re-entering the wells and then extrapolated to the 46 sites that fit the airborne part of the leaking well profile, then about 20 wells might be expected to be leaking in the Hatchel area. The five wells that are interpreted to be leaking are either CMW (four) or CW (one) sites. The two surveyed sites that had conductivity and magnetic anomalies but no known well location (a potentially leaking unknown well) proved to be tank or pit sites with no associated leaking well.

Ground investigations are intended to reduce the number of suspicious sites to a list of wells that might be leaking or might have had significant leaks in the past. These investigations should include precise location of the well through surface evidence or a magnetometer survey and reconnaissance ground conductivity profiles that cross the well site and any other potential brine sources, such as surface pits or tank batteries.

If a well has been leaking brine into the shallow subsurface, measured ground conductivities will increase by a factor of two or three from background levels to maximum levels recorded within a few meters of the well site. Wells that have begun to leak recently may show only a small anomaly at the shallowest investigation depths; conversely, wells that have been leaking for an extended period will generally have the highest conductivity peaks and the broadest areas of influence. Further information on the lateral extent and infiltration depth of a brine plume can be obtained using more sophisticated geophysical surveys, such as those that employ multiple coil separations and TDEM sounding techniques.

Utility of Airborne and Ground-Based Geophysical Methods

The airborne geophysical survey contributed information on the variations in magnetic field strength and ground conductivity that allowed us to locate key sites for more detailed ground-based investigation. The airborne magnetometer located many, but not all, well casings in the study area. The magnetic data thus serve best as a reconnaissance tool in areas where well locations are unknown or inaccurate. Typical measured magnetic anomaly widths of 80 to 200 m suggest that, as flight line spacing lengthens beyond the 100 m used in this study, progressively more well-casing-related magnetic anomalies will be missed. The 100 m spacing was a compromise between survey cost, which is roughly proportional to line length flown, and the percentage of wells detected.

Airborne conductivity data provided information on the lateral and vertical conductivity distribution to depths of a few to a few tens of meters. The conductivity data acquired at multiple frequencies allowed us to discriminate between near-surface causes of elevated conductivity such as brine pits and deeper causes of elevated conductivity such as brine-bearing geological formations. Used alone, each coil frequency had limitations. Data collected with the 56,000 Hz airborne coils showed the most detail, but most of the conductivity anomalies were related to causes other than wells leaking brine. Conversely, the deep data collected with the 900 Hz coils showed conductivity changes that are probably related to the subsurface distribution of geologic units, but clear anomalies were not visible near wells that ground surveys suggest are leaking. The single most useful coil frequency was 7,200 Hz, which filtered most shallow conductivity anomalies related to soils, soil moisture, brine pits, and surface water bodies as well as deeper geology-related patterns. When data from each of the coil frequencies are combined, they provide a powerful method of visualizing conductivity changes in the subsurface.

The ground-based geophysical surveys complemented the airborne data and form a critical component in the understanding of ground conductivity changes in general and in the search for leaking wells in particular. On-the-ground magnetometer surveys of suspected well sites that

were chosen from the airborne geophysical signature allowed precise location of buried well casings of abandoned wells. Rapid reconnaissance conductivity profiles across these well sites using a ground conductivity meter allowed us to determine whether the airborne conductivity anomaly was likely to be related to a well leaking brine or to brine that entered the subsurface through a nearby disposal pit. More detailed multiple-coil-separation surveys and TDEM soundings acquired at suspect sites enabled us to delineate lateral and vertical extents of salt water plumes. The TDEM soundings also extended the maximum exploration depth of the airborne survey, located a subsurface salt-water-bearing unit, and allowed a better understanding of conductivity patterns visible on the deeper 7,200 Hz and 900 Hz conductivity maps.

Without the ground-based geophysical surveys and soil and water sampling, the airborne geophysical data would be difficult to interpret reliably. Without the airborne data, ground-based surveys can help determine whether known wells are leaking and may find wide usage as a relatively inexpensive method of testing whether a well is leaking brine into the shallow subsurface. However, unknown wells and unsuspected brine leaks likely would be missed and conductivity profiles and soil and water samples would lack a regional ground conductivity context.

No matter how successful the airborne method is judged, its wide application is inhibited by the current high costs of helicopter-based geophysical surveys. High mobilization costs and minimum airborne survey charges preclude the use of this method in small areas of a few tens of square kilometers or less. Ground-based methods are a more cost-effective approach for these small areas. Similarly, tight flight line spacings required to locate relatively small conductivity and magnetic anomalies make the method uneconomical in excessively large areas as well. A realistic upper limit might be a typical oilfield size of a few tens to a few hundreds of square kilometers. Areas larger than a given oilfield would involve needless, expensive surveying of non-oilfield land for sources of oilfield-related salinity. In addition to the survey cost, the airborne data require follow-up, ground-based measurements to verify salinity source types and distinguish likely leaking wells from other oilfield-related sources.

In summary, ground-based surveys of prioritized known wells would be a relatively inexpensive technique for determining wells that should be plugged in small areas (a few tens of square kilometers or less) where well locations are reasonably well known. Over large areas (oilfield size) where well locations are uncertain or the extent of brine leakage is unknown, an airborne survey should be considered because it improves the efficiency of labor-intensive ground investigations.

Interpretation of Salinity Sources

Dutton and others (1989) and Richter and others (1990) hypothesized that there are several sources and mechanisms affecting salinity of ground water in Runnels County and adjacent areas:

- natural discharge of subsurface brines moving across the Permian Basin (Bein and Dutton, 1993),
- upward movement of brine across confining beds through oil wells and deep, unplugged water wells,
- seepage of saline water from rocks beneath former brine-disposal pits,
- evaporative concentration of ground water from shallow water tables that have risen in response to agricultural landscaping and increased recharge, and
- evaporation of irrigation water in the soil zone.

It is most likely that at least one of these sources or mechanisms can explain the salinity and ground conductivity pattern for different specific areas. For example, areas of elevated conductivity with a small radius and centered on the magnetic anomaly that marked an oil well might reflect the presence of a well that is leaking saline water. The small anomaly might instead reflect the location of the former brine-disposal pits located next to the well. It also is possible that a high-conductivity anomaly is centered around a steel-cased water well that was deepened and abandoned during the 1950s (Richter and others, 1990) and that now might be a conduit for saline water.

The correspondence of topographic features with patterns of ground conductivity might be a clue to identifying the role of other sources or mechanisms of salinization. For example, one area of high conductivity (56,000 Hz) underlies the upland area east of highway 83 between ground-surface elevations of 515 and 530 m (fig. 18). Aerial photographs and field inspection show this area to be extensively terraced to prevent erosion. The correspondence of the terracing with the high ground conductivity at shallow depth suggests that soil salinity is being affected by evaporative concentration of shallow ground water or of applied irrigation waters.

High ground conductivity was also detected over a broad area along the valley of Coyote Creek west of highway 83. Superimposed on this are numerous small-radius areas of especially high conductivities. In these more low-lying areas the effects of terracing and irrigation can most likely be eliminated. Other possible explanations include:

- discharge of ground water recharged locally east and west of Coyote Creek and converging on the valley as its discharge zone, with the water picking up salinity along its flow path;
- discharge of ground water moving eastward from the Permian Basin, as described by Dutton and others (1989) and Richter and others (1990).

The local ground-water flow system most likely discharges in the low-lying areas along Coyote Creek where hydraulic head is low. It might be more likely to account for the loading of salinity by discharge of the Permian Basin brine than having the short local flow system pick up much salinity. The area of low hydraulic head in the local, shallow ground-water flow system, however, also is an area of low hydraulic head in the regional flow system heading up to the west in the Permian Basin. Saline water moving eastward through permeable formations would diverge from its predominant lateral flow path and take a direct upward path through fractures to discharge into the local shallow aquifer. In addition, the potential for unplugged, abandoned wells to leak saline water is greater in the low-lying area than in upland areas, which might account for the numerous small-radius areas of elevated conductivity.

The deeply penetrating survey (900 Hz) indicates that conductivity at depth decreases from west to east across the study area. This survey frequency probably is detecting a fundamental hydrogeologic characteristic of the formations that underlie the study area. Dutton and others (1989) and Richter and others (1990) showed that the Permian bedrock formations differ in their ability to transport saline water. Ground-water salinity differs between the outcrops of the various formations. As is apparent from the TDEM soundings, it might be that the lithologic unit that underlies the western half of the study area naturally contains more saline water than the underlying unit that crops out beneath the eastern half of the study area. The low-lying areas of Coyote Creek might have greater ground conductivity and higher ground-water salinity than comparable areas along Elm Creek because of the different hydrogeology of the bedrock units.

The local area of high conductivity coinciding with part of the Beddo Field east of Elm Creek is an upland area. Discharge of subsurface saline water beneath the upland area should be different from its discharge beneath the valley. The high-conductivity zone appears to consist of numerous small-radius areas of high conductivity. It seems most likely, therefore, that this feature is related to some combination of abandoned oil wells, brine-disposal pits, and unplugged core holes.

CONCLUSIONS

Properly designed airborne and ground-based geophysical surveys have proven useful in the search for near-surface concentrations of saline water in general and oilfield-related saltwater sources in particular. Airborne surveys offer the advantages of rapid coverage of large areas, broader context for potential salinity sources, and knowledge of the shape and change with depth of conductivity anomalies. The Cesium magnetometer used in this study was sensitive enough to detect subtle magnetic field changes related to well casings, but not every magnetic anomaly was a well casing and not every well casing was detected. Nevertheless, the magnetometer was helpful in locating unknown or mislocated wells and in identifying oilfield-related salinity

sources where magnetic and conductivity anomalies coincided. The magnetometer would be more useful in areas that have incomplete records or poorly located wells.

Conductivity maps produced from the airborne data indicate a wide range in ground conductivity both laterally and vertically. The high frequency (56,000 Hz), shallow penetration coils detected a large number of conductivity anomalies across the study area. Many of these conductivity highs are not caused by leaking wells, but rather are related to changes in soil type, soil moisture content, or surface features such as brine pits, stock tanks, and streams. The low frequency (900 Hz), deep penetration coils detected only a small number of conductivity anomalies, but were useful in determining (a) whether anomalies at shallower depths had surface or subsurface sources and (b) where brines are most likely to naturally infiltrate the near-surface environment. The most useful frequency for locating potential leaking wells was 7,200 Hz. Maps produced with the 7,200 Hz coils had less land-surface related detail than maps produced from the high frequency coils, yet contained the conductivity anomalies that were most likely to represent leaking wells.

Ground-based geophysical methods proved valuable in locating actual well sites and determining whether the salinity source was likely to be a leaking well, a storage tank, or a brine pit. Ground methods included magnetometer surveys to locate buried well casings, reconnaissance conductivity profiles to determine whether there was evidence for a near-surface leak, multiple-coil-separation surveys to establish the lateral and vertical dimensions of saltwater infiltration, and time-domain electromagnetic soundings to determine plume thickness, explore deeper conductivity changes, and identify subsurface brine-bearing stratigraphic units. The ground-based surveys also helped verify the accuracy of the airborne conductivity data and greatly aided in interpreting the deepest (900 Hz) conductivity map patterns.

Despite the success of the airborne method in locating most wells and in identifying types and areas of near-surface salinization, widespread application of the method is hindered by the current high costs of helicopter-based geophysical surveys and the need for follow-up ground investigations to discern salinity source types. Mobilization charges and minimum survey fees

preclude its use in small areas that are less than a few tens of square kilometers. In these areas, ground-based geophysical surveys alone represent a cost-effective technique. In addition, tight line spacings required to locate small magnetic anomalies associated with well casings and relatively small salt water plumes make surveys of very large areas excessively expensive. The optimum survey size for an airborne survey is thus on the order of a typical oilfield size and ranges from a few tens to a few hundred square kilometers. Areas larger than a given oilfield would involve expensive airborne surveying over non-oilfield areas that have no oilfield-related salinization.

Chemical analyses of soil and water provided ground truth for the geophysical data and helped differentiate between natural, agricultural, and oilfield-related causes of near-surface salinization. Salinization related to a brine pit and that related to evaporative concentration can be difficult to distinguish using only geophysical surveys, but chemical composition of the saline water has been shown to differ enough to enable us to distinguish the two sources. The data for the study area suggests a general relation between ground conductivity and ground-water salinity, although the correlation is not statistically valid. Perhaps the failure of the statistical test was due to a small sample size and the complication of other unaccounted for variables. This relation needs to be proven for there to be more confidence in correct identification of salinity anomalies related to abandoned wells. On the other hand, soil conductivity measured on the scale of hand samples did not correlate statistically with ground conductivity measured in the 56,000 Hz frequency.

Multiple sources of salinity appear to affect ground and surface waters and soil in the study area:

- discharge of subsurface brine along natural pathways in the valley of Coyote Creek;
- seepage of brine into the subsurface through brine disposal pits;
- discharge of subsurface brine along coreholes and abandoned wells that are either unplugged or not plugged in compliance with present standards; and
- evaporation of shallow ground water and irrigation water, especially in terraced land.

ACKNOWLEDGMENTS

This project was funded by the Railroad Commission of Texas (RRC) under Contracts IAC 94-0443 and IAC 96-0034, Jeffrey G. Paine, Principal Investigator. The Lower Colorado River Authority (LCRA) contributed financially to the project. Staff from the Lower Colorado River Authority and the Colorado River Municipal Water District (CRMWD) sampled surface and ground water during the airborne survey and provided chemical analyses.

Geoff Saunders of LCRA, Okla Thornton of CRMWD, and Bruce Smith of the U.S. Geological Survey made many suggestions that contributed to the success of the project. Jose Mayorga, Randall Ross, and Isack Ramirez of the RRC provided invaluable assistance in searching well records, locating wells, contacting landowners, and facilitating project progress in many other ways.

REFERENCES

Abilene Geological Society, 1992, The stratigraphic distribution of hydrocarbon production from 19 counties in the Abilene area: Abilene, Texas, not consecutively paginated.

American Association of Petroleum Geologists, 1973, Geological highway map of Texas: U. S. Geological highway map of Texas: U.S. Geological Highway Map Series, Map No. 7, scale 1:500:000.

Back, W., 1966, Hydrochemical facies and ground-water flow patterns in the northern part of the Atlantic coastal plain: U.S. Geological Survey Professional Paper 498-A, 42 p.

Bein, Amos, and Dutton, A. R., 1993, Origin, distribution, and movement of brines in the Permian Basin (U.S.A.): a model for connate brine displacement: Geological Society of America Bulletin, v. 105, no. 6, p. 695-707.

Brown, E., Skougstad, M. W., and Fishman, M. J., 1970, Methods for collection and analysis of water samples for dissolved minerals and gases: U.S. Geological Survey Techniques of Water-Resources Investigations, book 5, chapter A1, 160 p.

Brown, L. F., Jr., Goodson, J. L., and Harwood, Peggy, 1972, Abilene sheet: The University of Texas at Austin, Bureau of Economic Geology, Geologic Atlas of Texas, scale 1:250,000.

Core Laboratories, Inc., 1972, A survey of subsurface saline water in Texas: Texas Water Development Board Report 157, v. 1, 113 p.

Dutton, A. R., Richter, B. C., and Kreitler, C. W., 1989, Brine discharge and salinization, Concho River watershed, West Texas: Ground Water, v. 27, no. 3, p. 375-383.

Eifler, G. K., Jr., 1975, San Angelo sheet: The University of Texas at Austin, Bureau of Economic Geology, Geologic Atlas of Texas: scale 1:250,000.

Fitzgerald, N. D., 1952, The Beddo Field, Runnels County, Texas: Abilene Geological Society Contributions, p. 7-8.

Frischknecht, F. C., Labson, V. F., Spies, B. R., Anderson, W. L., 1991, Profiling using small sources: in Nabighian, M. N., ed., Electromagnetic methods in applied geophysics—Applications, part A and part B: Tulsa, Oklahoma, Society of Exploration Geophysicists, p. 105–270.

Gardner, F. J., and Phifer, R. L., 1953, The oil and gas fields of west Texas, Part 1: Railroad Commission District 7-C: Five Star Oil Report, p. 148-198.

Garrie, D. G., 1996, DIGHEMV survey for Bureau of Economic Geology, University of Texas, Hatchel study area, Runnels County, Texas: Dighem, Mississauga, Canada, Report 625, not consecutively paginated.

Geonics Limited, 1992, PROTEM 47 operating manual 2.1: Mississauga, Canada, 115 p.

Jorgensen, D. G., Downey, Joe, Dutton, A. R., and Maclay, R. W., 1988, Regional hydrogeology of the Nonglaciated Great Plains, in Back, William, Rosenshein, J. S., and Seaber, P. R., eds., Hydrogeology: Geological Society of America, Geology of North America v. O-2, p. 141-156. Kaufman, A. A., and Keller, G. V., 1983, Frequency and transient soundings: Elsevier, Amsterdam, Methods in geochemistry and geophysics, no. 16, 685 p.

Kaufman, A. A., and Keller, G. V., 1983, Frequency and transient soundings: Amsterdam, Elsevier, Methods in Geochemistry and Geophysics, no. 16, 685 p.

Keller, G. R., Unpublished aeromagnetic map of Texas.

Kier, R. S., Brown, L. F., Jr., Harwood, P., and Goodson, J. L., 1976, Brownwood sheet: Geologic atlas of Texas: The University of Texas at Austin, Bureau of Economic Geology, Geologic Atlas of Texas, scale 1:250,000.

Lee, J. N., 1986, Shallow ground-water conditions, Tom Green County, Texas: U.S. Geological Survey, Water Resources Investigations Report 86-4177, 88 p.

McNeal, R. P., 1965, Hydrodynamics of the Permian Basin: American Association of Petroleum Geologists, Memoir 4, p. 308-326.

McNeill, J. D., 1980a, Electrical conductivity of soils and rocks: Geonics Limited, Mississauga, Ontario, Technical Note TN-5, 22 p.

McNeill, J. D., 1980b, Electromagnetic terrain conductivity measurement at low induction numbers: Geonics Limited, Mississauga, Ontario, Technical Note TN-6, 15 p.

McNeill, J. D., 1980c, EM34-3 survey interpretation techniques: Geonics Limited, Mississauga, Ontario, Technical Note TN-8, 16 p.

Parasnis, D. S., 1973, Mining geophysics: Elsevier, Amsterdam, 395 p.

Rhoades, J. D., 1981, Predicting bulk soil electrical conductivity versus saturation paste extract electrical conductivity calibrations from soil properties: Soil Science Society of America Journal, v. 45, p. 42-44.

Richter, B. C., Dutton, A. R., Kreitler, C. W., 1990, Identification of sources and mechanisms of salt-water pollution affecting ground-water quality: a case study, West Texas: The University of Texas at Austin, Bureau of Economic Geology Report of Investigation 191, 43 p.

Richter, B. C., and Kreitler, C. W., 1986, Geochemistry of salt water beneath the Rolling Plains, north-central Texas: Ground Water Monitoring Review, v. 7, no. 4, p. 75-84.

Spies, B. R., and Frischknecht, F. C., 1991, Electromagnetic sounding: in Nabighian, M. N., ed., Electromagnetic methods in applied geophysics—Applications, part A and part B: Tulsa, Oklahoma, Society of Exploration Geophysicists, p. 285-386.

Tóth, J., 1962, A theory of groundwater motion in small drainage basins in central Alberta: Journal of Geophysical Research, v. 67, no. 11, p. 4375-4387.

West, G. F., and Macnae, J. C., 1991, Physics of the electromagnetic induction exploration method: in Nabighian, M. N., ed., Electromagnetic methods in applied geophysics—Applications, part A and part B: Tulsa, Oklahoma, Society of Exploration Geophysicists, p. 5-45.

Wiedenfeld, C. C., Barnhill, L. J., Novosad, C. J., 1970, Soil survey of Runnels County, Texas: Soil Conservation Service, U. S. Department of Agriculture, 60 p.

Wood, W. W., 1976, Guidelines for collection and field analysis of ground-water samples for selected unstable constituents: U.S. Geological Survey, Techniques of Water-Resources Investigations, book 1, chapter D2, 24 p.

APPENDIX A. Hatchel Area Geophysical Sites

List of 113 geophysical sites (figs. 18 to 20) in the Hatchel study area. CMW sites are those where conductivity and magnetic anomalies were identified from airborne data, and there is a known well at the site; CM sites are those where airborne conductivity and magnetic anomalies are present, but there is no record of a well nearby; CW sites are those where a conductivity anomaly is present at a known well, but there is no associated magnetic anomaly; C sites are those with a conductivity anomaly but neither a known well nor a magnetic anomaly; MW sites are those with a magnetic anomaly and a known well, but no conductivity anomaly.

CMW sites (n=71)

Site	Conductivity Anomaly 56 kHz	7.2 kHz	0.9 kHz	Magnetic Anomaly	RRC Well[1]	Fits Profile?[2]	Geophysical Surveys[3]	Likely Source[4]	Notes
2	Yes	No	Yes	Yes	Yes				Could be same site as 3; weak 900
3	Yes	No	No	Yes	Yes				Could be same site as 2
4	Yes	Yes	No	Yes	Yes	Yes			Leaking?
5	Yes	Yes	Yes	Yes	Yes	Yes			7200 north of site; slight 900 to north
8	Yes	Yes	No	Yes	Yes	Yes			
9	Yes	Yes	No	Yes	Yes	Yes			Weak 7200
14	Yes	Yes	No	Yes	Yes	Yes	2P	Pit or leak?	
15	Yes	Yes	No	Yes	Yes	Yes			
18	Yes	No	No	Yes	Yes		1P		
19	Yes	Yes	No	Yes	Yes	Yes			Weak 7200
20	Yes	Yes	No	Yes	Yes	Yes			Leaking?
21	Yes	No	No	Yes	Yes				
22	Yes	Yes	No	Yes	Yes	Yes			Weak 7200
26	Yes	No	No	Yes	Yes				
30	Yes	Yes	Yes	Yes	Yes	Yes			Leaking?
31	Yes	No	No	Yes	Yes				
32	Yes	No	No	Yes	Yes				
33	Yes	No	No	Yes	Yes		1P	Pit	2 wells
34	Yes	No	No	Yes	Yes		1P	No source found	Weak M
36	Yes	Yes	No	Yes	Yes	Yes			Slight 7200
39	Yes	No	No	Yes	Yes				
40	Yes	Yes	No	Yes	Yes	Yes			C anomaly NW of M
41	Yes	No	No	Yes	Yes				
43	Yes	No	No	Yes	Yes		1P	Leak?	Along stream
46	Yes	Yes	No	Yes	Yes	Yes	1P	No source found	Weak 7200
47	Yes	Yes	No	Yes	Yes	Yes			Weak 7200
48	Yes	No	No	Yes	Yes				
49	Yes	No	No	Yes	Yes				
50	Yes	No	No	Yes	Yes				Along stream

51	Yes	No	No	Yes	Yes		1P	No source found	Near Coyote Creek
52	Yes	Yes	No	Yes	Yes	Yes			2 M; weak 7200
53	Yes	No	Yes	Yes	Yes				Weak 900
54	Yes	No	No	Yes	Yes				
55	Yes	No	No	Yes	Yes				
56	Yes	Yes	Yes	Yes	Yes	Yes	1P	Leak?	Abandoned water well; metal barn
59	Yes	Yes	Yes	Yes	Yes	Yes	2P	Leak?	Weak 7200; moderate 900
63	Yes	Yes	No	Yes	Yes	Yes			Part of curvilinear 56K; weak 7200
64	Yes	No	No	Yes	Yes				
68	Yes	Yes	No	Yes	Yes	Yes			Leaking?
69	Yes	No	No	Yes	Yes				Near high conductivity water well
74	Yes	Yes	No	Yes	Yes	Yes	2P		Weak 7200; mislocated well
75	Yes	No	No	Yes	Yes		1P	Pit	C southeast of M
76	Yes	Yes	No	Yes	Yes	Yes	1P;2MCP;3S	Leak?	Soundings (3); multicoil EM
80	Yes	Yes	Yes	Yes	Yes	Yes			Injection well
88	Yes	Yes	Yes	Yes	Yes	Yes			Linear 900
89	No	Yes	Yes	Yes	Yes				
90	Yes	No	No	Yes	Yes				
93	Yes	No	No	Yes	Yes				
94	Yes	Yes	No	Yes	Yes	Yes			
95	Yes	Yes	No	Yes	Yes	Yes			Weak 7200
96	Yes	No	No	Yes	Yes				
97	Yes	Yes	Yes	Yes	Yes	Yes			
98	Yes	No	No	Yes	Yes				
99	Yes	Yes	No	Yes	Yes	Yes			
100	Yes	Yes	No	Yes	Yes	Yes			M weak
101	Yes	Yes	No	Yes	Yes	Yes			M weak
102	No	Yes	No	Yes	Yes				
103	No	Yes	No	Yes	Yes				
105	Yes	Yes	No	Yes	Yes	Yes			Leaking?
106	No	Yes	No	Yes	Yes				
107	Yes	No	No	Yes	Yes				Weak 7200
108	Yes	Yes	No	Yes	Yes	Yes			M weak
109	No	Yes	No	Yes	Yes				
110	Yes	Yes	Yes	Yes	Yes	Yes			Leaking?
111	No	Yes	No	Yes	Yes				
112	No	Yes	Yes	Yes	Yes				At farm house and barn
113	Yes	No	No	Yes	Yes				
114	Yes	No	No	Yes	Yes				
115	Yes	No	No	Yes	Yes				
116	Yes	Yes	No	Yes	Yes	Yes			
117	Yes	No	No	Yes	Yes				

CM sites (n=15)

Site	Conductivity Anomaly 56 kHz	7.2 kHz	0.9 kHz	Magnetic Anomaly	RRC Well[1]	Fits Profile?[2]	Recon Surveys[3]	Likely Source[4]	Notes
1	Yes	No	No	Yes	No				
17	Yes	No	No	Yes	No		2P;2MCP;3S	Pit	
24	Yes	Yes	No	Yes	No	Yes			No RRC wells; well on topo; weak 7200
25	Yes	Yes	No	Yes	No	Yes	3P	Tanks/pits	No plotted wells nearby
28	Yes	No	No	Yes	No				Weak M
29	Yes	Yes	No	Yes	No	Yes			Along stream; slight 7200
35	Yes	No	No	Yes	No				
44	Yes	Yes	Yes	Yes	No	Yes			C anomaly NW of M; weak 7200
45	Yes	No	No	Yes	No				Well nearby
61	Yes	No	No	Yes	No		2P	No source found	
62	Yes	Yes	No	Yes	No	Yes			Weak 7200
71	Yes	Yes	No	Yes	No	Yes	2P	Tanks/pits?	At windmill; v. weak 7200
78	Yes	No	No	Yes	No				
104	No	Yes	No	Yes	No				
118	No	No	Yes	Yes	No				Leaking?

CW sites (n=14)

Site	Conductivity Anomaly 56 kHz	7.2 kHz	0.9 kHz	Magnetic Anomaly	RRC Well[1]	Fits Profile?[2]	Recon Surveys[3]	Likely Source[4]	Notes
6	Yes	No	No	No	Yes				
7	Yes	No	No	No	Yes				
10	Yes	Yes	No	No	Yes	Yes			
11	Yes	Yes	No	No	Yes	Yes			
12	Yes	Yes	No	No	Yes	Yes	2P	Pit	
13	Yes	No	No	No	Yes		2P	No source found	M nearby
16	Yes	Yes	No	No	Yes	Yes	2P	Leak or pit?	Weak 7200
27	Yes	No	No	No	Yes				Along stream
37	Yes	Yes	No	No	Yes	Yes			Weak 7200
38	Yes	Yes	No	No	Yes	Yes			Weak 7200
42	Yes	No	No	No	Yes				
58	Yes	No	No	No	Yes				
70	Yes	Yes	No	No	Yes	Yes	1P	No source found	Workman well; weak 7200
73	Yes	No	No	No	Yes		2P	Pit	

C sites (n=3)

Site	Conductivity Anomaly 56 kHz	7.2 kHz	0.9 kHz	Magnetic Anomaly	RRC Well[1]	Fits Profile?[2]	Recon Surveys[3]	Likely Source[4]	Notes
72	Yes	No	No	No	No				
91	Yes	No	No	No	No				
92	Yes	No	No	No	No				

MW sites (n=3)

Site	Conductivity Anomaly 56 kHz	7.2 kHz	0.9 kHz	Magnetic Anomaly	RRC Well[1]	Fits Profile?[2]	Recon Surveys[3]	Likely Source[4]	Notes
65	No	No	No	Yes	Yes		1P	Leak	Leaking well
66	No	No	No	Yes	Yes				Core hole leaked; plugged well
67	No	No	No	Yes	Yes		2P	Leak	Leaking well

Sounding only sites (n=7)

Site	Conductivity Anomaly 56 kHz	7.2 kHz	0.9 kHz	Magnetic Anomaly	RRC Well[1]	Fits Profile?[2]	Recon Surveys[3]	Likely Source[4]	Notes
81	No	No	No	No	No		1S		Sounding
82	No	No	No	No	No		1S		Sounding
83	No	No	No	Yes	No		1S		Sounding
84	No	No	No	No	No		1S		Sounding
85	No	No	No	Yes	Yes		1S		Sounding
86	No	No	No	No	Yes		1S		Sounding; recently plugged well
87	No	No	No	Yes	Yes		1S		Sounding

1 RRC records show well at site.

2 Site fits geophysical profile of oilfield-related saltwater source.

3 Types of reconnaissance, ground-based surveys completed at site. P = EM34 profile at 20 m coil separation; MCP = EM34 profiles at 10, 20, and 40 m coil separation; S = TDEM sounding.

4 Likely saltwater source deduced from airborne and ground-based surveys.

APPENDIX B.

Chemical composition of ground-water, surface-water, and oilfield-water samples. CRMWD data provided by the Colorado River Municipal Water District. Figure 16 gives sample location referenced by ID number.

ID	Sample ID	Sample date	Well depth (ft)	Temp (°C)	DO (mg/L)	pH	HCO3 (mg/L)	EC (mS/m)	Cl (mg/L)	Br (mg/L)
					Ground waters					
1	RUN-011	4/18/96	22.8	17.7	4	7.93	275	992	1952	nd
2	CRMWD-12	1/17/96	66.5	20	2.8	6.73	227	374	300	1.1
3	CRMWD-10	1/17/96	48.8	19.4	4.9	6.9	257	354	314	1.3
4	RUN-003	4/04/96	90.0	19.5	1.4	7.25	317	368	308	nd
5	CRMWD-16	1/17/96	20.8	14.2	3	7.75	669	435	1,032	5.2
6	RUN-002	4/03/96	75.0	20.2	0.2	7.17	309	352	246	0.8
7	CRMWD-11	1/17/96	80.0	20.1	4.5	6.77	240	370	483	0.9
8	CRMWD-2	1/16/96	25.7	19	0.4	6.75	249	305	218	1.1
9	RUN-013	4/19/96		21	0.7	6.84	372	337	478	1.9
10	CRMWD-5	1/16/96	40.6	19.7	3	6.7	269	323	448	2.1
11	CRMWD-3	1/16/96	45.0	19.7	3.6	6.85	238	369	500	2.7
12	CRMWD-19	1/29/96	51.9	20.5	3.6	6.83	264	288	234	1.1
13	CRMWD-1	1/15/96	26.4	18.9	5.8	6.73	248	259	179	0.9
14	CRMWD-13	1/17/96	35.0	18.5	nr	7.22	230	357	841	2.3
15	CRMWD-7	1/16/96	57.0	20.3	5.1	7.14	240	261	295	1.4
16	CRMWD-9	1/16/96	36.9	17.8	8.3	7.27	253	254	581	2.2
17	RUN-001	4/02/96	27.0	20	5.3	7.03	307	197	204	nd
18	CRMWD-4	1/16/96	64.8	20.2	3.7	6.85	249	204	232	1
19	CRMWD-6	1/16/96	69.0	20.8	4.7	6.95	535	164	145	0.9
20	CRMWD-8	1/16/96		19.7	2.3	7.03	273	154	129	0.6
21	CRMWD-17	1/17/96	36.1	19.5	nr	7.57	222	122	146	0.6
22	CRMWD-14	1/17/96	94.4	19.1	6.1	7.43	215	90	88	0.5
23	CRMWD-18	1/17/96		19.5	nr	7.18	333	80	29	0.2
24	CRMWD-15	1/17/96	27.0	15.5	2.7	7.47	309	79	59	0.4
25	RUN-014	4/19/96	12.8	17.1	0.6	7.53	207	69	73	nd

Appendix B (cont.)

ID	Sample ID	Sample date	Well depth (ft)	Temp (°C)	DO (mg/L)	pH	HCO3 (mg/L)	EC (mS/m)	Cl (mg/L)	Br (mg/L)
					Oilfield waters					
26	RUN-009	4/12/96		18.3	3.2	7.59	104	1,415	2,698	21.6
27	RUN-010	4/12/96		nm	0.1	6.5	42.7	8,924	39,190	57.7
28	RUN-012	4/18/96		24.9	nm	6.26	30.5	8,763	38,740	60.1
					Surface waters					
29	RUN-005	4/10/96		20.4	8.3	8.1	299	335	457	2.3
30	RUN-006	4/10/96		22	9.5	8.27	268	225	444	2.1
31	RUN-007	4/10/96		20.5	8.2	8.11	323	216	401	2.4
32	RUN-008	4/11/96		18.9	7.1	8.07	323	223	425	2.3
33	CRMWD-S1	1/15/96		8.01	10.8	8.14	263	248	377	1.7
34	CRMWD-S2	1/15/96		8.74	10.2	7.94	251	235	338	1.4
35	CRMWD-S3	1/15/96		8.77	10.1	7.87	248	232	335	1.4
36	CRMWD-S4	1/15/96		9.48	11	8.13	250	218	329	1.3
37	CRMWD-S5	1/15/96		8.99	10.9	8.02	308	261	419	1.9
38	CRMWD-S6	1/15/96		10.31	10.9	7.9	342	272	421	2
39	CRMWD-S7	1/15/96		11.75	12.6	8.17	241	204	333	1.2
40	CRMWD-S8	1/15/96		12.98	10.5	8.07	294	186	249	0.2
41	CRMWD-S9	1/16/96		10.3	9.2	7.94	289	220	363	1.3
42	CRMWD-S10	1/16/96		11.72	10	7.44	250	228	441	2
43	CRMWD-S11	1/16/96		11.9	17.8	8.02	185	1,309	3,990	9.4
44	CRMWD-S12	1/17/96		10.89	6.4	7.74	241	251	376	1.7
45	CRMWD-S13	1/17/96		11.08	11.2	7.78	193	410	656	3.2
46	CRMWD-S14	1/15/96		12.93	8.9	7.27	269	391	1,233	3.5
47	CRMWD-S15	1/16/96		10.88	9.7	8.9	519	573	1,199	5.1
48	CRMWD-S16	1/16/96		11.52	11.5	8.44	78	22	10	0.2
49	CRMWD-S17	1/16/96		14.68	9.7	7.85	196	431	896	3.2
50	CRMWD-S18	1/16/96		12.49	9.4	8.49	144	37	11	0.1
51	CRMWD-S19	1/16/96		15.76	8.6	8.25	137	20	67	0.3
52	CRMWD-S20	1/17/96		9.07	8.8	8.35	613	361	586	2.4
53	CRMWD-S21	1/17/96		12.13	7.9	8.52		36		

Appendix B (cont.)

Sample ID	NO3 (mg/L)	SO4 (mg/L)	Na (mg/L)	K (mg/L)	Mg (mg/L)	Ca (mg/L)	Ba (mg/L)	SiO2 (mg/L)	TDS (mg/L)	Ground conductivity 7200 Hz (mS/m)	Ground conductivity 56000 Hz (mS/m)
					Ground waters						
RUN-011	789	2,410	719	2.4	705	752	<0.01	15.4	7,620	290	465
CRMWD-12	dnt	1,815	114	4.9	222	595	0.03	17.3	3,295	147	325
CRMWD-10	dnt	1,617	158	3.6	111	653	<0.01	13.6	3,129	255	430
RUN-003	212	1,350	134	2.8	151	598	0.02	22.9	3,096		
CRMWD-16	dnt	246	790	12	222	103	0.06	10.2	3,088	105	200
RUN-002	0.4	1,630	104	4.6	139	620	0.01	12.1	3,066	125	255
CRMWD-11	dnt	1,340	180	3.5	211	463	0.01	18.2	2,939	110	260
CRMWD-2	3.2	1,326	75	4.2	143	520	0.02	17.5	2,556	225	360
RUN-013	3.7	883	241	1.3	135	358	0.02	15.6	2,489		
CRMWD-5	dnt	1,003	123	3.5	115	464	0.04	17	2,444	222	260
CRMWD-3	13.5	806	273	4.1	98	351	0.03	19.7	2,307	185	182
CRMWD-19	4.5	1,003	153	5	142	343	0.02	25.5	2,175	405	235
CRMWD-1	dnt	990	110	4	90	390	0.01	24.9	2,036	490	135
CRMWD-13	dnt	234	309	4.5	150	234	0.05	20.6	2,025	142	500
CRMWD-7	dnt	851	152	6.6	135	276	0.03	15.8	1,973	165	180
CRMWD-9	dnt	137	283	1.8	78	129	0.05	27.2	1,493	122	140
RUN-001	124	363	128	3.1	65	206	0.01	19.4	1,419	360	105
CRMWD-4	4.3	334	112	2.4	92	186	0.03	19.5	1,232	175	145
CRMWD-6	dnt	102	168	<1.00	89	168	0.09	23.8	1,232	205	110
CRMWD-8	dnt	340	54	7.5	58	183	0.03	16.8	1,062		
CRMWD-17	dnt	146	96	3.1	56	85	0.06	17.9	772	140	98
CRMWD-14	dnt	98	48	1.4	25	112	0.07	35.7	624	110	147
CRMWD-18	dnt	35	46	<1.00	39	79	0.19	16.5	578	95	150
CRMWD-15	dnt	16	42	4.1	21	106	0.18	15.4	574	100	135
RUN-014	31.5	23	61	3.3	20	52	0.1	9.8	481	135	155

Appendix B (cont.)

Sample ID	NO3 (mg/L)	SO4 (mg/L)	Na (mg/L)	K (mg/L)	Mg (mg/L)	Ca (mg/L)	Ba (mg/L)	SiO2 (mg/L)	TDS (mg/L)	Ground conductivity 7200 Hz (mS/m)	Ground conductivity 56000 Hz (mS/m)
					Oilfield waters						
RUN-009	nd	4,130	2,378	3.4	348	553	1	1.2	10,237		
RUN-010	nd	2,720	21,210	11.1	1,001	2,124	<0.01	30.6	66,387		
RUN-012	nd	2,080	21,840	94.8	893	2,014	0.49	62.6	65,816		
					Surface waters						
RUN-005	nd	933	307	7.2	205	175	0.07	3.6	2,388		
RUN-006	13.7	247	222	6.1	81	127	0.11	5.3	1,415		
RUN-007	9.5	207	236	5.1	84	101	0.11	6.8	1,376		
RUN-008	5.4	221	235	3.3	83	92	0.1	2.9	1,393		
CRMWD-S1	1.1	277	256	3.5	79	129	0.1	8.5	1,395		
CRMWD-S2	4.9	290	238	3	66	133	0.08	9.2	1,335		
CRMWD-S3	4.3	272	247	3.1	64	127	0.08	9.5	1,312		
CRMWD-S4	1.1	191	254	3	56	102	0.09	9.1	1,197		
CRMWD-S5	2.6	263	248	3.5	93	136	0.11	10.8	1,487		
CRMWD-S6	3.9	290	255	3.6	102	148	0.11	12.3	1,581		
CRMWD-S7	2.2	134	198	2.8	59	114	0.09	10.3	1,096		
CRMWD-S8	0.8	136	133	3	75	119	0.08	26.4	1,037		
CRMWD-S9	4.4	152	204	2.7	84	128	0.06	28.2	1,256		
CRMWD-S10	dnt	209	269	12.2	78	92	0.43	0.7	1,354		
CRMWD-S11	dnt	484	2,143	8.4	225	338	0.15	2.4	7,385		
CRMWD-S12	dnt	481	174	20.5	117	185	0.48	2.4	1,599		
CRMWD-S13	dnt	1,151	378	5.9	217	294	0.04	3.5	2,901		
CRMWD-S14	dnt	9	492	15.9	110	97	0.72	1.5	2,231		
CRMWD-S15	dnt	870	781	13.3	353	35	0.14	1.3	3,778		
CRMWD-S16	dnt	7	6	14.7	10	18	0.19	<0.3	144		
CRMWD-S17	dnt	798	390	10.1	193	272	0.25	0.7	2,759		
CRMWD-S18	dnt	1	8	11.8	14	36	0.3	<0.3	226		
CRMWD-S19	dnt	3	29	9.4	13	51	0.3	0.4	311		
CRMWD-S20	dnt	479	434	10	198	586	0.07	3.2	2,912		
CRMWD-S21											

APPENDIX C

Chloride content and electrical conductivity of soils collected in this study in Runnels County. Figure 16 gives sample location referenced by ID number.

ID	Sample	Date	Ground conductivity (mS/m)	Electrical conductivity (mS/m)	Chloride (mg/kg)
54	RUN-100	4/03/96	285	283	654
55	RUN-101	4/03/96	280	492	519
56	RUN-102	4/03/96	335	28.4	4.5
57	RUN-103	4/04/96	185	26.0	1.3
58	RUN-104	4/04/96	175	34.5	7.3
59	RUN-105	4/04/96	195	26.6	2.3
60	RUN-106	4/11/96	105	21.9	2.8
61	RUN-107	4/11/96	135	30.0	14.6
62	RUN-108	4/12/96	240	30.7	6.4
63	RUN-109	4/12/96	205	24.4	6.5
64	RUN-110	4/12/96	205	47.7	57.8
65	RUN-111	4/11/96	220	29.8	13.2
66	RUN-112	4/11/96	235	14.4	1.3
67	RUN-113	4/12/96	140	1,580	5,857
68	RUN-114	4/12/96	142	39.9	2.5
69	RUN-115	4/12/96	125	31.3	4.1
70	RUN-116	4/12/96	350	132	29.9
71	RUN-117	4/12/96	135	29.7	7.1
72	RUN-118	4/12/96	145	27.7	7.6
73	RUN-119	4/19/96	282	1,078	3,846
74	RUN-120	4/19/96	285	405	144